TURUN
YLIOPISTO
UNIVERSITY
OF TURKU

HYDROPHOBICITY AND LIPID INTERACTIONS OF HYDROLYSABLE TANNINS

Valtteri Virtanen

TURUN YLIOPISTON JULKAISUJA – ANNALES UNIVERSITATIS TURKUENSIS
SARJA – SER. AI OSA – TOM. 699 | ASTRONOMICA – CHEMICA – PHYSICA – MATHEMATICA | TURKU 2023

TURUN
YLIOPISTO
UNIVERSITY
OF TURKU

HYDROPHOBICITY AND LIPID INTERACTIONS OF HYDROLYSABLE TANNINS

Valtteri Virtanen

TURUN YLIOPISTON JULKAISUJA – ANNALES UNIVERSITATIS TURKUENSIS
SARJA – SER. AI OSA – TOM. 699 | ASTRONOMICA – CHEMICA – PHYSICA – MATHEMATICA | TURKU 2023

University of Turku

Faculty of Science
Department of Chemistry
Natural Chemistry Research Group
Doctoral programme in Exact Sciences

Supervised by

Adjunct professor, Maarit Karonen
Department of Chemistry
University of Turku
Turku, Finland

Adjunct professor, Petri Tähtinen
Department of Chemistry
University of Turku
Turku, Finland

Reviewed by

Professor, Hideyuki Ito
Department of Nutritional Science
Okayama Prefectural University
Okayama, Japan

Professor, Perttu Permi
Department of Chemistry
University of Jyväskylä
Jyväskylä, Finland

Opponent

Dr, Ana Reis
Department of Chemistry and Biochemistry
University of Porto
Porto, Portugal

ISBN 978-951-29-9430-4 (Print)
ISBN 978-951-29-9431-1 (PDF)
ISSN 0082-7002 (Print)
ISSN 2343-3175 (Online)
Painosalama, Turku, Finland 2023

UNIVERSITY OF TURKU
Faculty of Science
Department of Chemistry
Natural Chemistry Research Group
VALTTERI VIRTANEN: Hydrophobicity and lipid interactions of hydrolysable tannins
Doctoral Dissertation, 236 pp.
Doctoral Programme in Exact Sciences
October 2023

ABSTRACT

This thesis work focused on a specialized plant metabolite group called hydrolysable tannins with the aim of expanding the knowledge on their hydrophobicity, interactions with lipid membranes and antibacterial capacity. Hydrolysable tannins are known to possess many nutritionally and pharmacologically beneficial properties, which is why it is important to find the effective structures and unravel the mechanisms behind these activities.

Initially, the hydrophobicities of 47 chromatographically purified and spectrometrically characterized hydrolysable tannins were determined with octanol/water partitioning measurements. These results revealed that increased flexibility of the structure and larger molecular weight increased the hydrophobicity of the compounds while rigid substituent groups and macrocyclicity decreased it.

In the second and third study, the lipid interactions of hydrolysable tannins were studied with nuclear magnetic resonance (NMR) spectroscopy and isothermal titration calorimetry (ITC) using a phospholipid extract of *Escherichia coli*. The NMR results revealed how some hydrolysable tannins were able to penetrate to lipid moieties that reside inside the lipid bilayer structures thus verifying that hydrolysable tannins are able to perturb surface structures of lipid bilayers. Again, the more flexible structures proved to be more effective but the larger tannins were not able to perturb deep into the lipid bilayers most probably due to their bulkier structures. The thermodynamic results obtained with ITC corroborated the NMR results by showing increased interaction from the same compounds.

In the final part of this work, the antibacterial capacity of selected hydrolysable tannins was evaluated against *Escherichia coli* and *Staphylococcus aureus* cultures using an untargeted NMR metabolomics approach and plated inhibition results. All the tested hydrolysable tannins showed antibacterial activity and were able to influence the bacterial metabolome of the bacterial cultures. The altered bacterial metabolome results correleted with the plated inhibition results confirming that the NMR based method was able to reveal inhibition results directly from the culture medium.

KEYWORDS: antibacterial, *E. coli*, hydrolysable tannin, hydrophobicity, lipid, *S. aureus*

TURUN YLIOPISTO
Matemaattis-luonnontieteellinen tiedekunta
Kemian laitos
Luonnonyhdistekemian tutkimusryhmä
VALTTERI VIRTANEN: Hydrolysoituvien tanniinien hydrofobisuus ja lipidivuorovaikutukset
Väitöskirja, 236 s.
Eksaktien tieteiden tohtoriohjelma
Elokuu 2023

TIIVISTELMÄ

Tämä väitöskirjatyö keskittyi erikoistuneiden metaboliittien yhdisteryhmään nimeltään hydrolysoituvat tanniinit tavoitteena laajentaa tietämystä niiden hydrofobisuudesta, vuorovaikutuksista lipidikalvojen kanssa ja antibakteerisesta kapasiteesta. HT:lla tiedetään olevan useita ravitsemuksellisesti ja farmakologisesti hyödyllisiä ominaisuuksia, minkä vuoksi onkin tärkeää löytää tehokkaat rakenteet ja selvittää niiden aktiivisuuteen liittyvät mekanismit.

Aluksi 47 kromatografisesti puhdistetun ja spektrometrisesti karakterisoidun hydrolysoituvan tanniinin hydrofobisuudet määritettiin oktanoli/vesi-jakaantumiskerroin mittauksilla. Nämä tulokset osoittivat lisääntyvän rakenteen joustavuuden ja suuremman molekyylipainon kasvattavan yhdisteen hydrofobisuutta, kun taas jäykkien substituenttiryhmien ja makrosyklisyyden havaittiin alentavan sitä.

Työn toisessa ja kolmannessa osassa tutkittiin hydrolysoituvien tanniinien lipidivuorovaikutuksia ydinmagneettisen resonanssispektroskopian (NMR) ja isotermisen titrauskalorimetrian (ITC) avulla käyttäen *Escherichia coli*:sta eristettyä lipidiuutetta. NMR-tulokset paljastivat, miten jotkut hydrolysoituvat tanniinit pystyivät tunkeutumaan lipidikaksoiskalvojen sisäosiin siten varmistaen näiden yhdisteiden kyvyn häiritä lipidikaksoiskalvojen pintarakenteita. Jälleen joustavammat hydrolysoituvat tanniinit osoittautuivat tehokkaiksi rakenteiksi, kun taas suuremmat tanniinit eivät kyenneet tunkeutumaan syvälle kaksoiskalvoon johtuen tilaavievistä rakenteistaan. ITC:n avulla saadut termodynaamiset tulokset tukivat NMR-tuloksia osoittaen vuorovaikutuksen kasvavan samoilla yhdisteillä.

Lopuksi arvioimme valittujen hydrolysoituvien tanniinien antibakteerista kapasiteettia *Escherichia coli* ja *Staphylococcus aureus* -viljelmiä vastaan käyttäen kohdistamatonta NMR-metabolomiikkaa ja bakteerimaljausta. Kaikki testatut hydrolysoituvat tanniinit osoittivat antibakteerista aktiivisuutta ja kykenivät vaikuttamaan näiden bakteeriviljelmien metabolomiin. Muuttuneet bakteerimetabolomit korreloivat maljattujen inhibitiotulosten kanssa varmistaen NMR-pohjaisen menetelmän pystyvän paljastamaan inhibition suoraan viljelmän elatusaineesta.

ASIASANAT: antibakteerisuus, *E. coli*, hydrofobisuus, hydrolysoituvat tanniinit, lipidit, *S. aureus*

Table of Contents

Abbreviations **7**

List of Original Publications **8**

List of Related Publications not Included in the Thesis **9**

1 Introduction **10**
1.1 Structures and classification of hydrolysable tannins 11
1.2 Bioactivities of hydrolysable tannins 14
1.3 Antimicrobial activities of hydrolysable tannins 17
1.4 Main aims of the thesis 18

2 Materials and Methods **19**
2.1 General Instrumentation 19
2.1.1 NMR Spectroscopy 19
2.1.2 UHPLC-DAD–MS 20
2.1.3 Partition coefficient measurements 21
2.1.4 HR-MAS NMR sample preparation 21
2.1.5 Isothermal titration calorimetry 21
2.1.6 Dynamic light scattering 22
2.2 Extraction, purification and characterization of hydrolysable tannins 22
2.2.1 Extraction of plant material 22
2.2.2 Purification of hydrolysable tannins 22
2.2.2.1 Gel chromatography 23
2.2.2.2 Liquid chromatohraphy 23
2.2.3 Characterization of hydrolysable tannins 23
2.3 Data analysis and statistical methods 26

3 Results and Discussion **27**
3.1 Partition coefficients (log $P_{octanol/water}$) of hydrolysable tannins 27
3.2 Interactions of hydrolysable tannins with bacterial lipid membranes 30
3.2.1 HR-MAS NMR measurements 30
3.2.2 ITC measurements 34
3.3 NMR metabolomics of bacterial cultures treated with hydrolysable tannins 36

4 Conclusions **41**

Appendix **43**

Acknowledgements **79**

List of References **82**

Original Publications **93**

Abbreviations

AOA	Antioxidant activity
CT-HMBC	Constant time heteronuclear multiple bond correlation
DAD	Diode array detector
DHHDP	Dehydrohexahydroxydiphenoyl
DLS	Dynamic light scattering
DQF-COSY	Double quantum filtered correlation spectroscopy
E. coli	*Escherichia coli*
ESI	Electrospray ionization
ET	Ellagitannin
GT	Gallotannin
HCD	Higher-energy collisional dissociation
HHDP	Hexahydroxydiphenoyl
HMBC	Heteronuclear multiple bond correlation
HPLC	High-performance liquid chromatography
H. pylori	*Helicobacter pylori*
HR-MAS	High-resolution magic angle spinning
HSQC	Heteronuclear single quantum coherence
HT	Hydrolysable tannin
ITC	Isothermal titration calorimetry
MRM	Multiple reaction monitoring
MS	Mass spectrometry
NHTP	Nonahydroxytriphenoyl
NMR	Nuclear magnetic resonance
NOESY	Nuclear Overhauser effect spectroscopy
PCA	Principal component analysis
PPC	Protein precipitation capacity
ROS	Reactive oxygen species
S. aureus	*Staphylococcus aureus*
TOCSY	Total correlation spectroscopy
UHPLC	Ultrahigh-performance liquid chromatography

List of Original Publications

This dissertation is based on the following original publications, which are referred to in the text by their Roman numerals:

I **Virtanen, V.**, Karonen, M. Partition Coefficients (*logP*) of Hydrolysable Tannins. *Molecules*. 2020; 25: 3691. https://doi.org/10.3390/molecules25163691

II **Virtanen, V.**, Räikkönen, S., Puljula, E., Karonen, M. Ellagitannin–Lipid Interaction by HR-MAS NMR Spectroscopy. *Molecules*. 2021; 26: 373. https://doi.org/10.3390/molecules26020373

III **Virtanen, V.**, Green, R.J., Karonen, M. Interactions Between Hydrolysable Tannins and Lipid Vesicles from *Escherichia coli* with Isothermal Titration Calorimetry. *Molecules*. 2022; 27: 3204. https://doi.org/10.3390/molecules27103204

IV **Virtanen, V.**, Puljula, E., Walton, G., Woodward, M.J., Karonen, M. NMR Metabolomics and DNA sequencing of *Escherichia coli* and *Staphylococcus aureus* Cultures Treated with Hydrolysable Tannins. *Metabolites*. 2023; 13: 320. https://doi.org/10.3390/metabo13030320

List of Related Publications not Included in the Thesis

Engström, M., Arvola, J., Nenonen, S., **Virtanen, V.**, Leppä, M., Tähtinen, P., Salminen, J-P. Structural Features of Hydrolyzable Tannins Determine Their Ability to Form Insoluble Complexes with Bovine Serum Albumin. *Journal of Agricultural and Food Chemistry*. 2019; 67: 6798–6808. https://doi.org/10.1021/acs.jafc.9b02188

Bello, A., **Virtanen, V.**, Salminen, J-P., Leiviskä, T. Aminomethylation of Spruce Tannins and their Application as Coagulants for Water Clarification. *Separation and Purification Technology*. 2020; 242. https://doi.org/10.1016/j.seppur.2020.116765

Grünewald, F., Punt, M. H., Jefferys, E. E., Vainikka, P. A., König, M., **Virtanen, V.**, Meyer, T. A., Pezeshkian, W., Gormley, A. J., Karonen, M., Sansom, M. S. P., Souza, P. C. T., Marrink, S. J. Martini 3 Coarse-Grained Force Field for Carbohydrates. *Journal of Chemical Theory and Computation*. 2022; 18: 7555–7569. https://doi.org/10.1021/acs.jctc.2c00757

Engström, M. T., **Virtanen, V.**, & Salminen, J. P. Influence of the Hydrolyzable Tannin Structure on the Characteristics of Insoluble Hydrolyzable Tannin-Protein Complexes. *Journal of Agricultural and Food Chemistry*. 2022; 70: 13036–13048. https://doi.org/10.1021/acs.jafc.2c01765

1 Introduction

Plants biosynthesize a plethora of metabolites for many different purposes be it for direct growth and development via primary metabolites like carbohydrates, proteins, lipids, vitamins, and nucleic acids or for defense and survival via specialized (formerly secondary) metabolites like terpenoids, phenolics, alkaloids, and sulfur containing compounds.

Hydrolysable tannins (HTs) are a sub-group of phenolic metabolites that exhibit several beneficial activities such as antioxidative[1–5], antimicrobial[6–16], antitumoric[4,17–20], and anti-inflammatory[21,22] activities as isolated compounds but also in plant extracts.[23,24] HTs are widely distributed across the plant kingdom[17,25–28] including many nutritionally important food items such as fruits, berries, nuts, and red wine.[29] The nutritional and health benefits of consuming a diet that includes these polyphenol-rich foods and drinks have been known for a long time[30–32] and these benefits have been partially linked to the antioxidant properties of their phenolic constituents.[33,34] Phenolic compounds are able to relieve oxidative stress in the original plants as well as in humans when ingested by neutralizing reactive oxygen species (ROS) and by suppressing some oxidation reactions that would, if left uninhibited, produce ROS in excess.[35–37] As the name suggests ROS readily react in cells with cell components such as proteins, nucleic acids, and lipids and can in so doing lead to several health problems.[38] Among many active phenolic compounds, several HTs have been reported to have high antioxidative capacity[1,5] even when compared to some flavonoids that are often attributed as the major source of antioxidants in fruits for example.[39]

Another well-known property of HTs is to bind and crosslink with proteins in solution producing complexes that, with high enough concentration, will precipitate.[40–44] This characteristic interaction of tannins has been studied extensively and detailed structure-activity patterns have been observed linking active structural features of individual HT structures to the overall activity of plant species containing them in abundance. Other HT-macromolecule interactions, such as fiber or lipid interactions[45–47], have not been studied as comprehensively even though they might reveal insight into their notable antimicrobial activities.

This thesis focuses on studying a physicochemical property of HTs, which governs the transportation of compounds in biological processes, hydrophobicity, with additional focus on the interactions that HTs have with bacterial lipid membranes and the effect that HTs have to bacterial growth and the bacterial metabolome.

1.1 Structures and classification of hydrolysable tannins

Although some hydrolysable tannins have been purified and their structures characterized by Schmidt and Mayer already in 1956[48] the more detailed classification of this structurally very diverse metabolite group really gained momentum starting from the later characterization of geraniin from *Geranium Thunbergii* by Okuda *et al*., in 1977.[49] The improved instrumentation and modern spectrometric techniques enabled the revision of old structures[50,51] and the characterization of countless new structures ranging in size from small monomers all the way up to undecamers[52,53] as well as the determination of absolute configurations of different HT substructures.[54,55] With this enriched structural knowledge, the classification of HTs (Figure 1) based on their structural features with emphasis also on their suggested biosynthetic route was made possible[26,56] but generally most HTs can be described as gallic acid/HHDP esters of a central polyol, most often glucose.

Thus, HTs are divided into simple galloylglucoses, gallotannins (GTs), and ellagitannins (ETs). The simple galloylglucoses are, as per the name, gallic acid esters of glucose starting from monogalloylglucose all the way to pentagalloylglucose[57]. When additional galloyl groups are bound via *meta*-depside bonds to the galloyls directly bound to the polyol glucose these compounds are classified as GTs[57]. Both groups produce gallic acid when hydrolysed with acidic or alkaline conditions or via enzymatic (tannase or β-glucosidase) ways and produce characteristic fragment ions at *m/z* 169 and 125 in negative ionization mass spectrometry.[58–60]

The third group, ETs, is structurally more diverse than the previous two and is thus further divided into subgroups such as HHDP esters, *C*-glycosidic ETs, dehydro-HHDP esters and other HHDP modifications, flavanoellagitannins, and oligomeric ETs. The biosynthetic precursor for all of these ETs is pentagalloylglucose. The initial structure that can be classified as an ET forms when the spatially adjacent O4 and O6 galloyls in pentagalloylglucose dehydrogenate to form the characteristic biaryl ET structure in tellimagrandin II (Figure 1), i.e., the hexahydroxydiphenoyl (HHDP) group.[61,62] These structures are classified as HHDP esters. Further modifications of this initial structure include the dehydrogenation of

the O2 and O3 galloyls to form another HHDP group or the possible degalloylation of the glucose core.

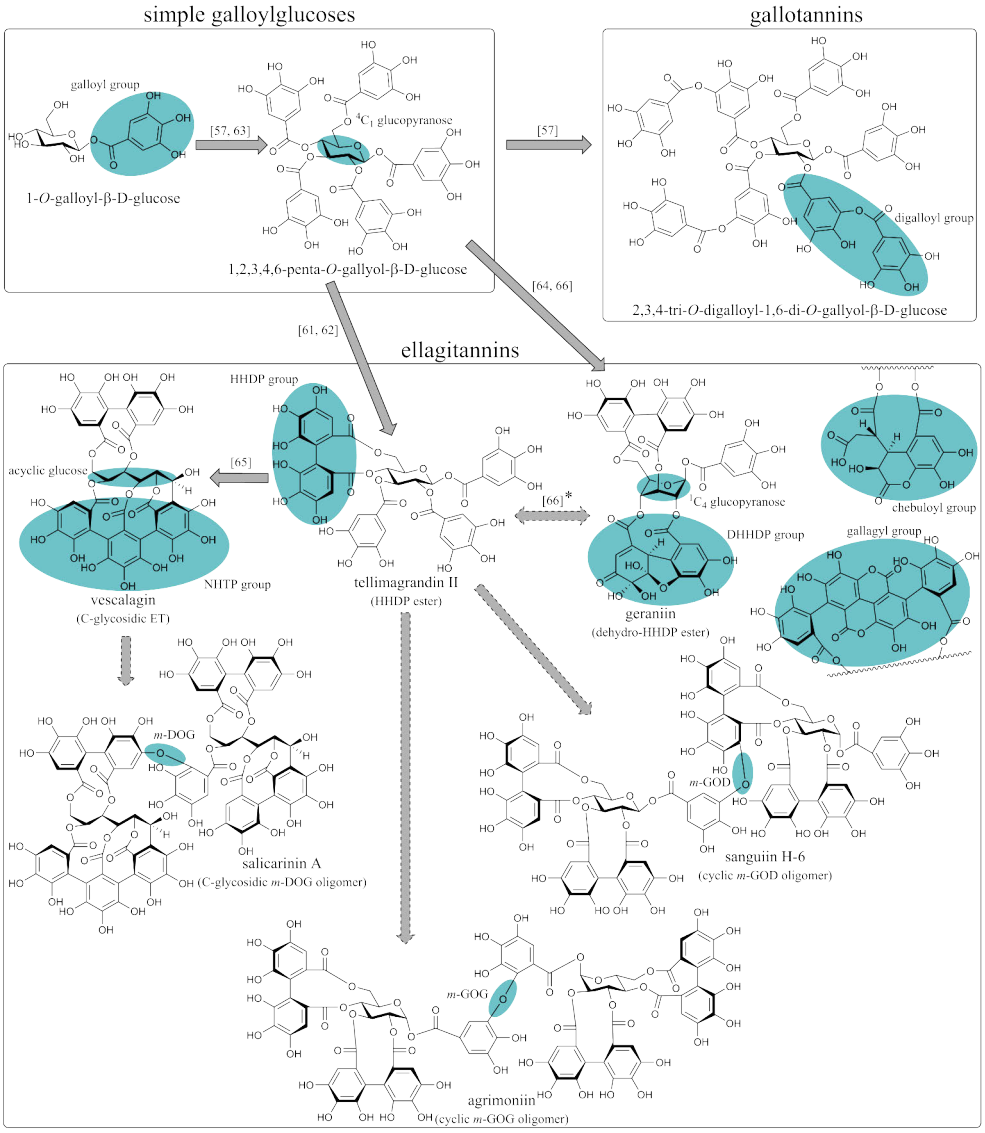

Figure 1. Hydrolysable tannin subgroups and example structures with arrows denoting confirmed and suggested (dashed) biosynthetic pathways.[57,61–66] Characteristic structural features are shown with blue ellipses. *It is speculated, but unproven as of yet, whether DHHDP esters and HHDP esters can interconverse.

The glucose core in most of the HHDP esters is in the energetically favourable $^4C_1$ chair conformation, which also defines the described possible positions (O2~O3

and O4~O6) for the HHDP groups. It is also noteworthy that the HHDP group in ETs with $^4C_1$ glucose is most often in *S* configuration.[54] Due to the HHDP group, most ETs produce ellagic acid when subjected to acidic or alkaline conditions or if hydrolysed enzymatically (tannase or β-glucosidase) and produce the characteristic fragment ion at *m/z* 301 in negative ionization mass spectrometry.[59,60]

From here, the biosynthesis of ETs can go in two different directions. In the route towards *C*-glycosidic ETs, the galloyl in glucose O-1 is cleaved and the galloyls in O-2 and O-3 are oxidatively C-C coupled to form an HHDP-group. Subsequently, the glucopyranose ring opens and the O-5 (i.e., the ring oxygen) is galloylated leaving a reactive aldehyde function in the C-1 and producing the intermediate *C*-glycosidic ET-structure of liquidambin.[65] Next the HHDP that was formed in O-2~O-3 reacts with the aldehyde function in glucose position C-1 to form the C-glycosidic bond. This *C*-glycosidic bond forces the glucose to stay in the open chain (acyclic) form and locks the anomeric glucose position 1 to either α or β conformation. The free galloyl in glucose O-5 can in some cases bind to the 2,3-HHDP to form a nonahydroxytriphenoyl (NHTP) group, which is characteristic to many *C*-glycosidic ETs.[65]

The general consensus on the biosynthetic origin of dehydro-ETs is that they form directly from pentagalloylglucose[64,66] but it has also been suggested that the DHHDP group would form from an already existing HHDP in the structure. There is strong evidence to support the former pathway as the glucose in dehydro-ETs is predominantly in the energetically unfavourable $^1C_4$ chair conformation. And it might be more difficult for the glucose to adopt a conformation where it is also hindered by a rigid HHDP group (which in most HHDP esters are also attached in different positions of the glucose core than the DHHDP group in dehydro-ETs) rather than a conformation where the glucose is only substituted by freely rotating galloyls. However, interestingly in a recent study by Yamashita *et al*., 2021 they were able to show that the DHHDP group can be an intermediate towards the formation of an HHDP group (Figure 2).[66] They also suggested that the formation of tellimagrandin II type HHDP esters, that Niemetz *et al.*, in 2001 showed were formed from pentagalloylglucose, could flow through an intermediate DHHDP structure before reduction to the HHDP group.[61] They rationalized that the strain from the formed macrocyclic structure depending on which glucose galloyls were participating in its formation could be the deciding factor if the process stops at the DHHDP group (O2~O4 or O3~O6) or proceeds through reduction to the HHDP group (O2~O3 or O4~O6). If these ETs with $^1C_4$ glucose core have an HHDP group, it is often found in O3~O6 or sometimes even in O1~O6 positions and most often in *R* configuration but in rare cases also in *S* configuration.[55,67] The DHHDP group can also further oxidize to form a chebuloyl group.

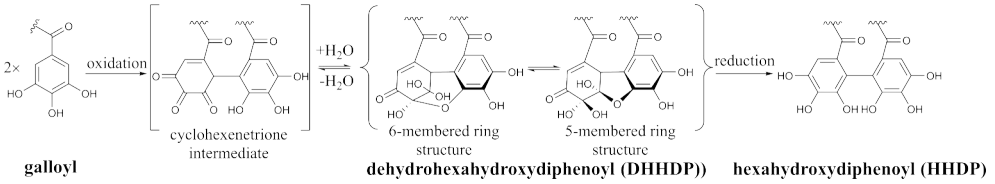

Figure 2. Possible biosynthetic pathway of the dehydrohexahydroxydiphenoyl (DHHDP) and hexahydroxydiphenoyl (HHDP) groups from galloyl groups. Adapted from Yamashita *et al.*, 2021.[66]

Plants often accumulate ETs with mainly one type of polyol glucose whether it be $^4C_1$ cyclic, acyclic or $^1C_4$ cyclic (Figure 1).[34,68] Though some exceptions are also found as is the case with many plants in the genus *Terminalia*, which produce many $^1C_4$ based ETs but also one particular ET, punicalagin, with a $^4C_1$ core.[69,70] This ET is noteworthy also because it has the peculiar gallagyl group in its structure, which in practice is an ellagic acid moiety bound between the O4 and O6 galloyls.

The described monomeric ETs can also oligomerize with different linkages further increasing the structural complexity. Possible links between the monomeric constituents include but are not limited to ones such as *m*-DOG (valoneoyl group), *m*-GOG (dehydrodigalloyl), and *m*-GOD (sanguisorboyl group) and are presented in Figure 1. It is common that oligomers are formed by adding consecutively the same or at least similar monomeric building blocks, but this is not always the case and even a few oligomers with monomeric units from different ET subgroups have been characterized.[71]

1.2 Bioactivities of hydrolysable tannins

The protein precipitation capacity (PPC)[40,43,44,72–74] and antioxidant activity (AOA)[1–5,75] of HTs have been studied extensively with a comprehensive set of HT structures, which have enabled the discovery of nuanced structure-activity relationships. This vast knowledge has also led to the observation that these two HT activities are generally inversely related to each other, i.e., a structure that is very efficient in binding proteins, like pentagalloylglucose, is not very prone to oxidation and might thus not be a very efficient antioxidant. The opposite is also true, like in the case of *C*-glycosidic ETs like vescalagin, which has relatively low PPC but quite high capacity to oxidize. These studies have shown the importance of the different substituents (galloyl, HHDP, DHHDP, chebuloyl, gallagyl, NHTP, and others), the oligomeric linkage types, structural flexibility and the overall size (i.e., molecular weight) of the HT. For example, the effect of the galloyl group was efficiently demonstrated in 2011 by Salminen *et al*. with a series of galloyl glucoses where each subsequent galloylation of the glucose core decreased the compounds capability to

oxidize but at the same time increased its PPC (Figure 3).[53] Similar trends have been reported regarding the more rigid substituent groups (e.g. HHDP and NHTP) where their presence in the ET structure has been observed to decrease PPC but increase their capability to oxidize. These groups decrease the structural flexibility thus decreasing the capability of the compound to bind with proteins with weak interactions such as hydrogen bonding and hydrophobic interactions, which have been reported as the main types of binding mechanisms in tannin-protein interactions in most conditions.[40,76] Previously when the majority of tannin bioactivity research was focused on their PPC it rose into question what was the purpose for plants to evolve in a direction where they produced ETs with more oxidized groups that had much less capacity to bind proteins than the "less evolved" galloylglucoses and gallotannins. This view was however reversed when a new consensus was formed that the capacity of HTs to oxidize under various conditions could be a large source of the defensive capability they offer for the plant whether it be against UV radiation or herbivory insects.

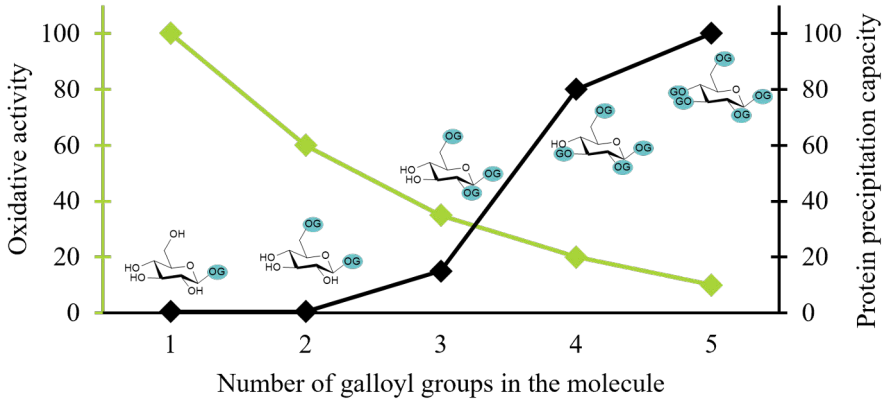

Figure 3. The oxidative activity (green) and protein precipitation capacity (black) of a series of galloyl glucoses displaying the opposite trend of these activities and the degree of galloylation. Activity values are shown as percentages of the most active compound. Adapted from Salminen *et al*., 2011.[53]

Another way of observing the relationship between HT structures and the bioactivities (AOA and PPC) is through the determination of physico-chemical properties such as hydrophobicity.[77] Hydrophobicity is often utilized in drug discovery and development, for example in quantitative structure-activity relationship (QSAR) models[78], to ascertain if a particular compound of interest could be a candidate for further research.[79,80] It is a useful indicator because potential

candidate drugs need to be hydrophobic enough to be transported to their target regions in biological systems, which often involve passing lipid membranes.

Hydrophobicity is most reliably determined via experimental partitioning measurements (e.g. shake-flask method[81,82]) where the concentration of the compound in a two phase system (typically *n*-octanol/H_2O or *n*-hexane/H_2O) is determined in each phase with HPLC-UV (high-performance liguid chromatography-ultraviolet) or other suitable detection method.[80] The acquired partition coefficient between the phases is then typically presented as the decadic logarithm (log $P_{\text{octanol/water}}$ or log $P_{\text{hexane/water}}$) to enable easier visual comparisons. Other alternatives include atomic and fragment-based prediction models which aim to divide the target compound into smaller pieces or functional groups, which have statistically and/or experimentally determined log *P* values which are then used to predict the log *P* of the entire structure. These methods (XLogP[83–85], ALogP[86], CLogP[87], KOWWIN[88,89], and other similar variations) give fairly accurate estimates for compounds that are structurally similar to the training set compounds that were used to validate the method, however for compounds that differ significantly from the training set compounds they offer mixed predictions at best. Another shortcoming of these methods is that they are unable to take into account the actual spatial structures of large molecules with many possible conformers (like HTs) where the weak intramolecular interactions like hydrogen bonding and hydrophobic effects play a significant role with the shape that they reside in solutions. Recently, a much quicker method than the classical shake-flask method was reported by Cumming and Rücker[90], which involved an NMR spectroscopic determination of the analyte's concentration directly from an NMR tube with appropriate 1-octanol-d_{18} and D_2O volumes to enable the excitation and measurement of only the D_2O phase. This method therefore allows the determination of partition coefficients without the laborious work of separating the phases. Theoretically, one could achieve similar analytical results with LC-UV by injecting samples only from the height of corresponding water phase. However, there is a possibility of contamination if the injection needle has to pass through the upper octanol phase, and also, the passing of the needle then disturbs the settled phase equilibrium therefore increasing the unreliability of the measurement.

Linking the physico-chemical property, hydrophobicity, to the actual HT-lipid interactions, and more specifically to the HT-phospholipid interactions, it has been suggested that more hydrophobic compounds should be more prone to interacting with lipid membranes as most hydrophobic compounds are highly lipophilic.[80,91] This, however, might not be a property that is unconditionally desired as there is also evidence which shows that highly hydrophobic compounds are not able to efficiently pass through cell membranes via diffusion as their high affinity towards the membrane itself hinders this transportation.[92,93] Thus, it is probable that when

assessing the real-world roles of HT-lipid interactions, such as their antimicrobial activity, the tannins that display the strongest interaction with membrane lipids are not the best in inhibiting pathogens, and there is already evidence of this phenomenon.[14] Now, similarities in the interactions and dominant structural features involved between the known HT-protein and the lesser known HT-lipid and HT-fiber interactions could be hypothesized as they involve relatively small tannin molecules interacting with macromolecules (proteins, lipid vesicles, and fibers).[45,46] These interaction similarities can include aspects such as the fact that HT-protein interactions are primarily reversible surface phenomena where HTs interact via weak interactions with the outer surface or exposed binding pockets of the protein. And as phospholipids form globular vesicles in aqueous solutions their interactions with small molecules also take place initially via the exterior of the vesicles (polar lipid headgroups), but unlike with proteins, small molecules are also able to perturb and ultimately permeate the lipid bilayers.[91] This perturbation of the originally ordered lipid bilayer structure limits the transportation and distribution of other molecules, including ROS, through the bilayer, and thus, reduces oxidative stress that would have occurred from the reaction of ROS and fatty acids.[94]

1.3 Antimicrobial activities of hydrolysable tannins

Many traditional medicinal plants[68] that have been widely used as herbal remedies are now known to contain many different HTs in addition to other phenolics in high concentrations.[17,34,95] Studies have shown that the HT compositions of these plants are full of compounds with high bioactivities and that they are efficient antimicrobials against several relevant pathogens such as *Herpes simplex* virus[96,97], human immunodeficiency virus[16,98], *Staphylococcus aureus* (*S. aureus*, including methicillin resistant and sensitive strains)[14,15,99,100], *Helicobacter pylori* (*H. pylori*)[9,101], and *Escherichia coli* (*E. coli*)[14,102,103]. There are also studies reporting synergistic effects between HTs and some antibiotics[104,105] which offers ways of counteracting the evergrowing problem of antimicrobial resistant strains and their prevalence.

The mechanisms and modes of action behind HTs antimicrobial activity has been suggested to mainly derive from their protein/peptide interactions and their capacity to reduce oxidative stress[23,24,76] but the ability of HT molecules to perturb lipid membrane structures has also recently seen growing interest[106,107]. The full mechanism is not explained by any one interaction but rather a combination of all of them which explains how HTs with significantly different structures and bioactivities can inhibit pathogens with comparative efficiencies.

As many antimicrobial studies have been performed with plant extracts or semipurified mixtures it makes it hard to differentiate the antimicrobial efficiencies

of different HTs. There are also studies using pure compounds[9,14–16,96,97,99] that have already revealed the significance of several structural features; however, more knowledge is needed on the subject to uncover how and why these compounds display their demonstrated antimicrobial efficacy.

1.4 Main aims of the thesis

The main aims of this thesis can be divided into three categories where the next one is a direct continuation of the findings in the previous one.

i. Determining the hydrophobicity of a wider range of different HT structures than previously reported (**Article I**).

ii. Observing the interactions between bacterial lipid membranes and HTs (**Articles II** and **III**).

iii. Studying the antibacterial capacity of HTs and how they affect bacterial metabolome during bacterial growth (**Article IV**).

In **Article I,** the partition coefficients (log $P_{\text{octanol/water}}$) of 47 purified and characterized HTs were measured to determine and verify the effects that different structural features had on the hydrophobicities of the compounds. The knowledge acquired in the first study was then used to select a more focused group of HTs that had potential to move spatially close to and interact with lipid vesicles in aqueous solution. Specifically, more hydrophobic HTs were hypothesized to be better candidates for this as more hydrophobic compounds are known to better penetrate lipid bilayers.

In **Article II,** we observed with NMR spectroscopy how deep within the lipid bilayer these selected HT structures were able to penetrate and uncover the possible orientation of these HT structures in the bilayers. Furthermore, in **Article III**, we studied the HT-lipid vesicle interaction thermodynamics with ITC and were able to determine that the same HTs that moved spatially close to the lipid vesicles in **Article II** also produced more heat of interaction with the lipids further demonstrating the efficiency of these compounds regarding their lipid-interactions.

In **Article IV,** we observed directly from the culture media the bacterial metabolome changes that HT treatments caused to *E. coli* and *S. aureus* cultures with an untargeted NMR metabolomics approach. The metabolome changes were hypothesized to correlate with growth inhibition which was also investigated with plated bacterial inhibition measurements. Additionally, the impact of the HT treatments on *S. aureus* cultures with donor fecal samples included in the growth medium were assessed with DNA sequencing.

2 Materials and Methods

2.1 General Instrumentation

2.1.1 NMR Spectroscopy

The NMR experiments of the study were performed using three different Bruker spectrometers: i) Bruker Avance-III spectrometer operating at 600.16 MHz for ^{1}H and 150.90 MHz for ^{13}C equipped with a Prodigy TCI inverse CryoProbe cooled with liquid nitrogen, ii) Bruker Avance-III spectrometer operating at 500.08 MHz for ^{1}H and 125.76 MHz for ^{13}C equipped with a broadband Smartprobe (Fällanden, Switzerland), iii) Bruker Avance-III spectrometer operating at 399.75 MHz for ^{1}H and 100.52 MHz for ^{13}C equipped with a high-resolution magic angle spinning (HR-MAS) probe.

Characterization measurements of the hydrolysable tannins were performed either with the 600 MHz or the 500 MHz instrument. Typical experiment set consisted of standard ^{1}H and ^{13}C spectra, DQF-COSY (double quantum filtered correlation spectroscopy), NOESY (nuclear Overhauser effect spectroscopy), multiplicity-edited HSQC (heteronuclear single quantum coherence), HMBC (heteronuclear multiple bond correlation), band-selective CT-HMBC (constant time) and selective 1D-TOCSY (total correlation spectroscopy) experiments. Spectra were recorded at 298.15 K in acetone-d_6 and the residual solvent signal was used as chemical shift reference, δ_H = 2.05 ppm and δ_C = 29.92 ppm.

The HR-MAS measurements of the lipid-hydrolysable tannin interactions in **Article II** were performed with the 400 MHz instrument. The MAS unit was operated at 9 kHz rotational speed with the temperature set at 298.15 K and samples were prepared in D_2O. ^{1}H spectra with water suppression by presaturation and 2D-NOESY with 0.1 s and 0.3 s mixing times (d_8) were recorded. As the residual solvent signal was suppressed the chemical shift of the methyl group ($\delta_H(CH_3)$ =0.94 ppm) in the end of the fatty acid chain of the lipids was used as chemical shift reference. The methyl group resides “deepest” in the lipid bilayer structure (Figure 8) and its chemical shift is the least affected by the possible spatial vicinity of the tannins.

The metabolomics experiments in **Article IV** were performed with the 600 MHz instrument. All spectra in the metabolomics set were acquired with a water

suppressed 1D NOESY pulse sequence (Bruker's pulse program noesygppr1dep) at 298.15 K. All samples included 0.2 mM of TSP (3-(trimethylsilyl)propionic-2,2,3,3-d_4 acid) and 1.0 mM potassium phthalate for chemical shift calibration and metabolite quantitation, respectively. TSP was not used for quantitations as it has been shown to inconsistently bind to proteins thus rendering it not fit as a quantitation standard in this application. For the comprehensive description of the data preprocessing and sample preparation see **Article IV**.

2.1.2 UHPLC-DAD–MS

The UHPLC-DAD instrument used in all analyses was an Acquity UPLC system (Waters Corporation, Milford, MA, USA) which consisted of a binary solvent manager, a column, and a diode array detector. The used column was an Acquity BEH phenyl column (100 × 2.1 mm id., 1.7 μm; Waters Corporation, Wexford, Ireland). The mobile phase consisted of acetonitrile (A) and 0.1% aqueous formic acid (B) with the following elution profile: 0–0.5 min, 0.1% A in B (isocratic); 0.5–5.0 min, 0.1–30% A in B (linear gradient); 5.0–6.0 min, 30–35% A in B; 6.0–9.5 min; column wash and stabilisation. Colum temperature was 40 °C. All samples were filtered (4 mm, 0.2 µm, PTFE; Thermo Fisher Scientific Inc., Waltham, MA, USA), injection volume was 5 μL and flow rate was 0.5 mL min^{-1}. UV data was collected with a wavelength range of 190–500 nm.

The UHPLC system was connected via an ESI (electrospray ionization) source to a Xevo TQ triple quadrupole (Waters Corporation, Milford, MA, USA) mass spectrometer. The mass spectrometer was operated with negative ionization and the source parameters were as follows: capillary voltage 1.8 kV, source temperature 150 °C, desolvation gas temperature 650 °C, desolvation and cone gas (N_2) flow rates 1000 and 100 L/h, respectively, and collision gas was argon. Full scan MS data was collected with an *m/z* range of 150–2000 as well as multiple specific MRMs (multiple reaction monitoring) developed by Engström *et al*., in 2014 and 2015.[60,108]

An identical UHPLC system coupled to a Q Exactive hybrid quadrupole-Orbitrap (Thermo Fisher Scientific GmbH, Bremen, Germany) mass spectrometer via a heated ESI source was also used. The mass spectrometer was operated in negative ion mode and the source parameters were as follows: spray voltage 2.5 kV, capillary temperature 380 °C, auxiliary gas temperature 300 °C, and sheath and auxiliary gas (N_2) flow rates 60 and 20 arbitrary units, respectively. Orbitrap was calibrated with Pierce ESI Negative Ion Calibration Solution (Thermo Fischer Scientific Inc., Waltham, MA, USA). Full Scan MS data was collected with a mass range of *m/z* 150–2250, a resolution of 70 000 and automatic gain of 3×10^6. Product ion spectra were acquired using a data dependent acquisition method termed full scan $ddMS^2$ (TopN) with a resolution of 35 000 and automatic gain of 1×10^5 using

normalized collision energies of 20, 50, and 80 eV in the higher energy collisional dissociation (HCD) cell.

2.1.3 Partition coefficient measurements

The partition coefficient (log $P_{octanol/water}$) measurements were performed with a shake-flask method.[81,82] Briefly, the used *n*-octanol and water were saturated with each other and separated before the measurements. A known amount of analyte was dissolved into the saturated water phase. Then, the saturated octanol was added, and the mixture shaken for 120 min and centrifuged (15 000 g) for 10 minutes. The phases were then separated and analyte concentrations in both phases and in an unpartitioned reference sample were determined UV spectroscopically at 280 nm.

2.1.4 HR-MAS NMR sample preparation

The used lipid material was a commercial *E. coli* phospholipid extract (Avanti Polar Lipids, Alabaster, AL, USA). The extract comprised of L-α-phosphatidylethanolamine (PE, 57.5 wt%), L-α-phosphatidylglycerol (PG, 15.1 wt%), cardiolipin (CA, 9.8 wt%), and unidentified lipid (17.6 wt%) each with various chain lengths and degrees of unsaturation. The NMR sample preparation method was adapted from Grélard *et al*., 2010.[109] Briefly, a known quantity of the lipid extract was hydrated with D_2O and subsequently subjected to four cycles of freeze-thaw treatment where the sample was rapidly cooled with liquid nitrogen, heated in a warmed water bath, and shaken rigorously. The prepared lipid sample formed an emulsion, which prevented us from using traditional liquid NMR probes. However, the HR-MAS probe (see Section 2.1.1) enables the measurement of colloidal samples while still allowing typical liquid NMR experiments including solvent suppression and many 2D correlation experiments.

2.1.5 Isothermal titration calorimetry

The used isothermal titration calorimeter (ITC) was a MicroCal iTC200 (Malvern Panalytical, Malvern, UK). Calorimeters sample and reference cell volumes were 200 μL. The reference cell was filled with ultrapure water in all measurements. Measurements were performed at 298.15 K, and they comprised of an initial injection of 0.4 μL followed by 19 injections of 2.0 μL. An equilibration period of 120 s was employed between injections and the sample was stirred with 750 rpm during the measurement.

2.1.6 Dynamic light scattering

Dynamic light scattering (DLS) measurements were performed with a Zetasizer Nano ZS (Malvern Panalytical, Malvern, UK) instrument. The He-Ne light source was operated at 633 nm and back scattered light was recorded at an angle of 173° at 293.15 K. Final measurements consisted of 10 repetitions each with 13 size runs.

2.2 Extraction, purification and characterization of hydrolysable tannins

2.2.1 Extraction of plant material

The studied hydrolysable tannins were extracted from the following 11 plant species: Norway maple (*Acer platanoides*) leaves, silverweed (*Argentina anserina*) leaves, willowherb (*Chamaenerion angustifolium*) leaves, meadowsweet (*Filipendula ulmaria*) flowers, herb Bennet (*Geum urbanum*) leaves, wood cranesbill (*Geranium sylvaticum*) leaves, sea buckthorn (*Hippophaë rhamnoides*) leaves, purple loosestrife (*Lythrum salicaria*) leaves, raspberry (*Rubus idaeus*) leaves, black myrabolan (*Terminalia chebula*) leaves, and English oak (*Quercus robur*) acorns. 1,2,3,4,6-penta-*O*-galloyl-β-*D*-glucose was prepared from commercial tannic acid (J.T. Baker, Denventer, Holland) via methanolysis.

The extraction and purification of the hydrolysable tannins followed our previously reported methods.[43,44,52,110–112] Extraction of the collected plant material began with maceration in acetone at 4 °C for several days. The plant material was then repeatedly extracted using acetone/water (80/20, v/v) and the different extract batches were combined. Acetone was evaporated from the extracts and the remaining aqueous extracts were filtered and finally lyophilized. The extraction and each subsequent purification step were followed by UHPLC-DAD–MS to select fractions for the following purification steps and to ultimately verify the final product purity.

2.2.2 Purification of hydrolysable tannins

Hydrolysable tannin purification process consisted of four main steps: i) crude Sephadex LH-20 gel fractionation in a Büchner funnel, ii) column gel chromatography with Sephadex LH-20, iii) preparative HPLC fractionation, and iv) semipreparative HPLC fractionation.

2.2.2.1 Gel chromatography

For the initial crude fractionation, dry extract (maximum 50 g) was dissolved in ultrapure water and mixed to slurry of Sephadex LH-20 gel (stabilised in water). The slurry was eluted with water, methanol/water (50/50, v/v), methanol, acetone/water (80/20, v/v) and acetone in a Büchner funnel (⌀ = 240 mm) with vacuum through a filter paper (Grade 3). Fractions were evaporated to water phase and then lyophilized.

Approximately 6–10 g of the initial fractions were dissolved in ultrapure water, filtered (4 mm, 0.2 μm, PTFE; Thermo Fisher Scientific Inc., Waltham, MA, USA) and applied on top of a glass column (40 × 4.8 cm i.d.; Kimble-Chase Kontes Chromaflex), which was loaded with Sephadex LH-20 gel (stabilized in water). A stepwise gradient with a constant flow rate of 5 mL min^{-1} was used with water, aqueous methanol and aqueous acetone as the solvents. The elution profile was modified according to the targeted HT.

2.2.2.2 Liquid chromatohraphy

The preparative and semipreparative HPLC purifications were performed using a system consisting of a Waters 2535 Quaternary Gradient Module, a Waters 2998 PDA Detector, and a Waters Fraction Collector III. For preparative purification, a column (327 × 33 mm i.d.) filled with LiChroprep RP-18 (40–63 μm, Merck KGaA, Darmstadt, Germany) material was used. Gradient elution with a constant flow rate of 8 mL min^{-1} using methanol (A) and 1% aqueous formic acid (B) with the following gradient was used: 0–5 min, 100% B (isocratic); 5–180 min, 0–40% A in B (linear gradient); 180–220 min, 40–60% A in B (linear gradient); 220–240 min, 60–80% A in B (linear gradient), 240–300 min, column wash and stabilisation.

For semipreparative purification, a Gemini 10 µ C18 110 Å column (150 × 21.2 mm i.d., 10 μm; Phenomenex, CA, USA) was used with acetonitrile (A) and 0.1% aqueous formic acid (B). The used gradient profile was modified for different HTs but a typical gradient for a relatively hydrophilic HT was as follows: 0–5 min, 10% A in B (isocratic); 5–51 min, 10–35% A in B (linear gradient); 51–55 min, 35–70% A in B (linear gradient); 55–120 min, column wash and stabilisation.

2.2.3 Characterization of hydrolysable tannins

All 47 purified HTs (Figures 4 and 5) were characterised based on their measured UV, MS and NMR spectra and available literature. MS identifications, ^{1}H-NMR assignations, and UV spectra of the HTs used in the thesis work can be found in the Appendix along with purity at 280 nm and plant origin.

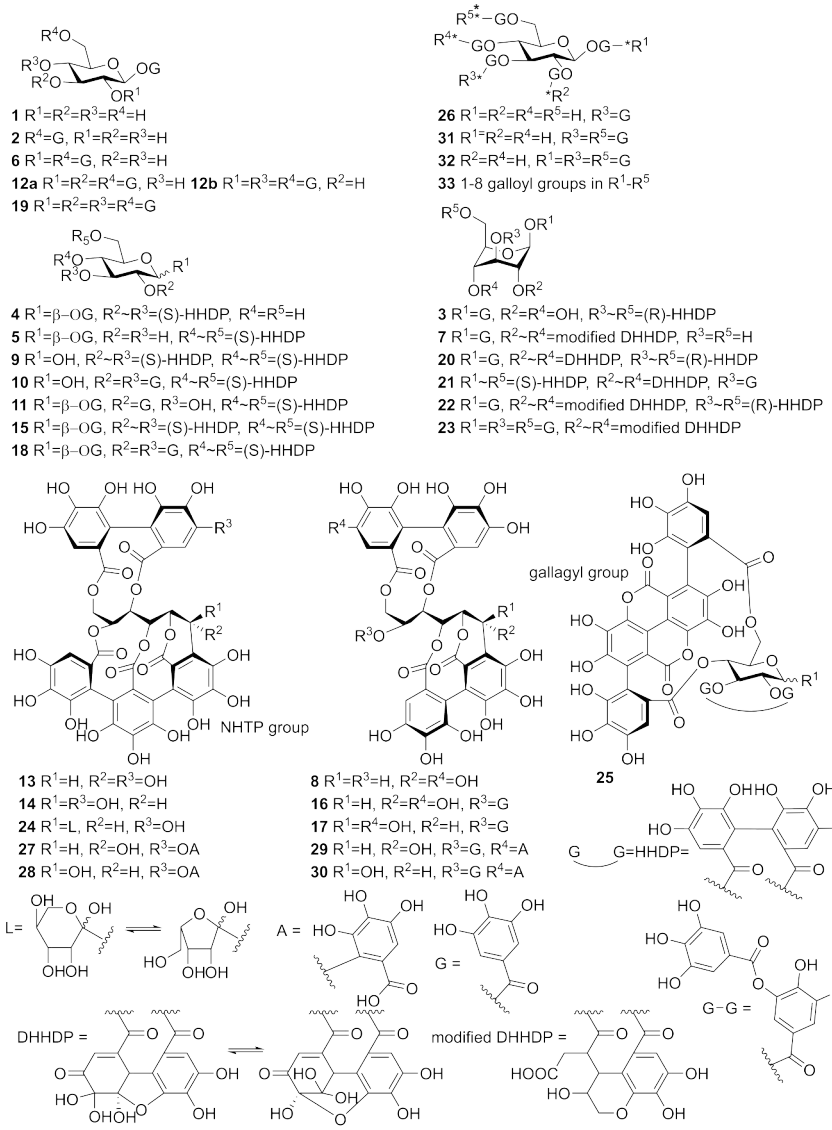

Figure 4. Chemical structures of monomeric hydrolysable tannins studied in the thesis: (**1**) 1-*O*-galloyl-β-*D*-glucose, (**2**) 1,6-di-*O*-galloyl-β-*D*-glucose, (**3**) corilagin, (**4**) isostrictinin, (**5**) strictinin, (**6**) 1,2,6-tri-*O*-galloyl-β-*D*-glucose, (**7**) chebulanin, (**8**) casuariin**,** (**9**) pedunculagin, (**10**) tellimagrandin I**,** (**11**) 1,2,-di-*O*-galloyl-4,6-HHDP-β-*D*-glucose, (**12a**) 1,2,3,6-tetra-*O*-galloyl-β-*D*-glucose, (**12b**) 1,2,4,6-tetra-*O*-galloyl-β-*D*-glucose, (**13**) castalagin, (**14**) vescalagin, (**15**) casuarictin, (**16**) casuarinin, (**17**) stachyurin, (**18**) tellimagrandin II, (**19**) 1,2,3,4,6-penta-*O*-galloyl-β-*D*-glucose, (**20**) geraniin, (**21**) carpinusin, (**22**) chebulagic acid, (**23**) chebulinic acid, (**24**) grandinin, (**25**) punicalagin, (**26**) hexagalloylglucose, (**27**) castavaloninic acid, (**28**) vescavaloninic acid, (**29**) hippophaenin B, (**30**) hippophaenin C, (**31**) heptagalloylglucose, (**32**) octagalloylglucose, and (**33**) gallotannin mixture. DHHDP=dehydrohexahydroxydiphenoyl, A= gallic acid, G=galloyl, HHDP=hexahydroxydiphenoyl, L=lyxose, NHTP=nonahydroxytriphenoyl. *The location of the galloyl groups of compounds **26**, **31**, **32** and **33** were tentatively confirmed. Figure adapted from **Article I**.

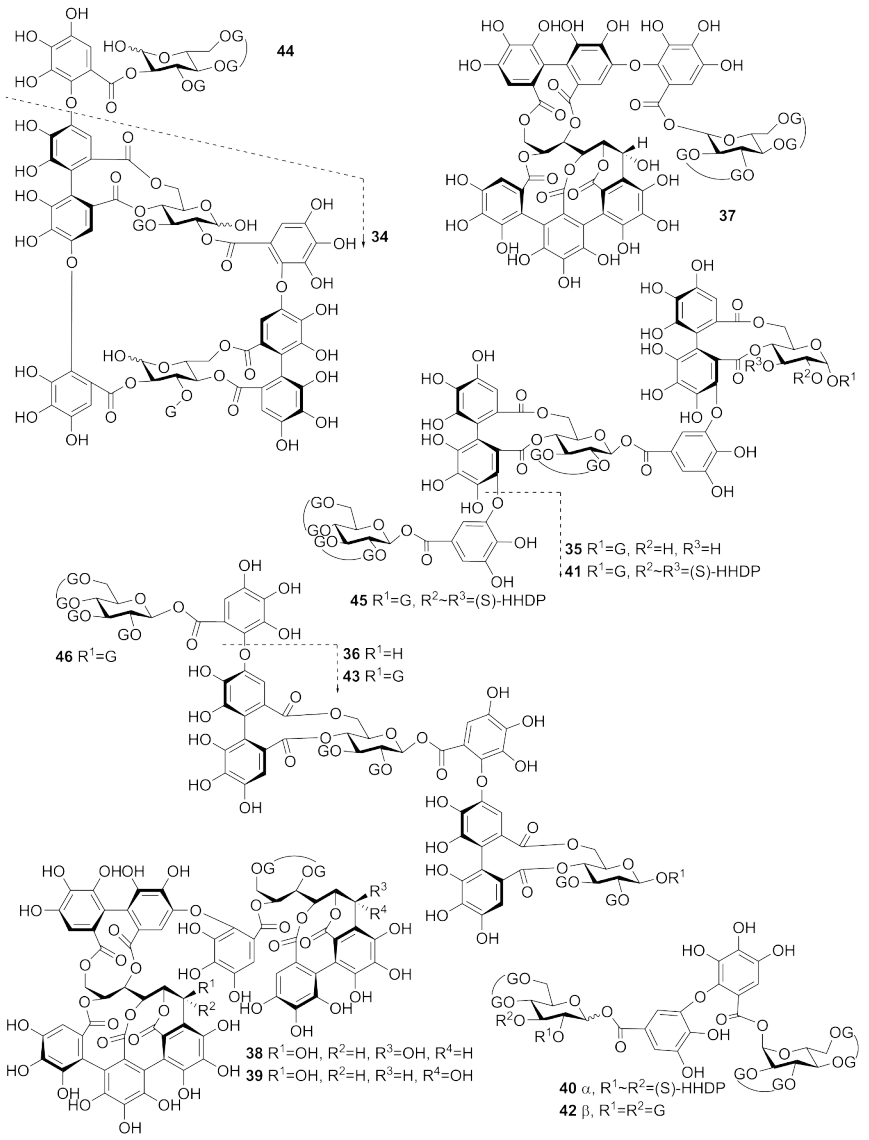

Figure 5. Chemical structures of oligomeric hydrolysable tannins studied in the thesis: (**34**) oenothein B, (**35**) roshenin C, (**36**) rugosin E, (**37**) cocciferin D2, (**38**) salicarinin A, (**39**) salicarinin B, (**40**) agrimoniin, **(41**) sanguiin H-6, (**42**) gemin A, (**43**) rugosin D, (**44**) oenothein A, (**45**) lambertianin C, and (**46**) rugosin G. See Figure 4 for the substituent details. Figure adapted from **Article I**.

2.3 Data analysis and statistical methods

Data visualisations were done with Origin 2016 SR2 b9.3.2.303 (OriginLab, Northampton, MA, USA) and R (version 4.2.1)[113] using RStudio (version 2022.02.0 Build 443)[114] with the following packages: "ggplot2"[115], "ggpubr"[116], and "mdatools"[117]. ChemDraw 20.1.0.110 (PerkinElmer, Waltham, MA, USA) was used for 2D molecular modelling and Blender[118] was used for 3D molecular modelling. LC-MS data was acquired and processed with MassLynx software (version 4.2 SCN982, WatersCorp., Milford, MA, USA) and Xcalibur software (version 4.1.31.9, ThermoFisher Scientific Inc., Waltham, MA, USA). NMR measurements and quantitations were done with TopSpin software (version 3.5 pl 7, Bruker, Billerica, MA, USA). NMR metabolomics data was processed with NMRProcFlow[119] a dedicated NMR metabolomics platform for batch processing of 1D spectra. ITC data was processed with NanoAnalyze software (version 3.12.0, TA instruments, New Castle, DE, USA) and Origin 7 (version 7.0552, OriginLab, Northampton, MA, USA) with a MicroCal ITC add-on. DLS measurements were done with Zetasizer software (version 7.13).

3 Results and Discussion

3.1 Partition coefficients (log $P_{octanol/water}$) of hydrolysable tannins

The partition coefficients (log $P_{octanol/water}$) of 47 purified and characterized HTs (Figures 4 and 5) were determined with the shake-flask method.[81,82] The selected HTs represented the entire HT class reasonably well, i.e., there were compounds from most of the different HT subgroups (see Section 1.1) which allowed us to make detailed observations into i) how the hydrophobicities of the different HT subgroups compare to one another and ii) how individual structural features of HTs have an effect to the hydrophobicities of the compounds.

Figure 6 displays the experimentally determimed log *P* values as a function of the molecular weight of the HTs with different coloured series for different configurations of the polyol glucose with galloyl glucoses and gallotannins further separated from the $^4C_1$ ETs.

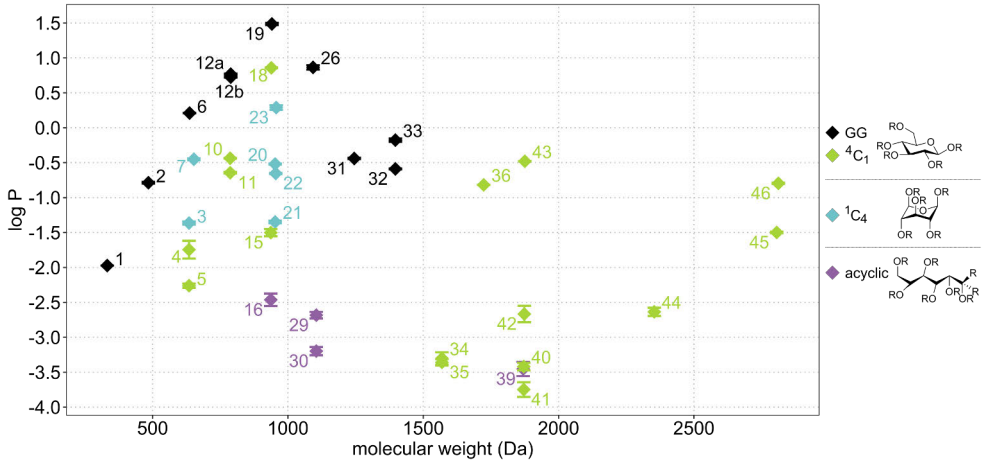

Figure 6. Experimentally determined log *P* values of 47 hydrolysable tannins (n=3, mean ± standard deviation). Numbering of tannins follows Figures 4 and 5. Galloyl glucoses and gallotannins are presented in black series and ellagitannins are divided into three groups based on the configuration of the polyol glucose: green = $^4C_1$ chair, blue = $^1C_4$ chair, and purple = acyclic. Figure Adapted from **Article I**.

This separation also mimicks the HT subgroups as the subgroups in most cases contain compounds with only one specific polyol configuration although there are some exceptions to this guideline. The general order of HT subgroups in the order of descending hydrophobicity is: i) galloylglucoses/gallotannins, ii) dehydro-ETs with $^4C_1$ chair polyol, iii) HHDP-esters with $^1C_4$ chair polyol, and iv) *C*-glycosidic ETs with acyclic polyol.

When the structures, where the polyol glucose is only substituted with galloyl groups were compared to similar sized ETs (i.e., the polyols degree of substitution is the same) it was observed that all galloyl derivatives resulted in lowering the structures hydrophobicity (Figure 7) from their galloyl substituted counterparts. This decrease in hydrophobicity is a result of increased structural rigidity stemming from the biaryl and other flexibility restricting substituents as the substituents themselves are not more hydrophilic than gallic acid. As a comparison, the flexible five-pronged tridimensional structure of pentagalloylglucose (**19**) enables it to self-associate, i.e., it readily stacks with other pentagalloylglucose molecules in aqueous solution leading to exclusion of solvent molecules from its vicinity.[77,120] This has been proposed as the reason for its low water solubility and tendency to form gels in higher concentrations in ambient temperature which is not unlike the self-assembly of phospholipid vesicles in aquoues media from hydrophobic effects to reduce solvent contacting surface area. However, if more galloyl groups are depsidically linked to the glucose bound galloyls these additions lower the hydrophobicity of the compound as seen with **26**, **31**, **32**, and **33**.

Looking at the individual structural differences in the three "series" of similar sized HTs in Figure 7 more closely it can be seen that the inclusion of the first HHDP group (**6** → **4** / **5**; **12a** → **10**; **19** → **18**) lowers the log *P* significantly but the second HHDP group (**10** → **9**; **18** → **15**) has an even larger decreasing effect. Interestingly the comparison of **4** and **5** also showed that the HHDP group in glucose O4~O6 lowers the hydrophobicity more than in O2~O3. Similarly, the comparison of **20** and **21** (see Figure 4 for structures) showed that **20**, which has a free galloyl group in O1 and and HHDP group in O3~O6, is more hydrophobic than **21**, which which has a free galloyl group in O3 and and HHDP group in O1~O6. This comparison does not solely prove that the HHDP group bound to O1~O6 makes the structure more hydrophilic as the galloyl groups position also varies and the hydrophobicity increasing effect of the galloyl group in the anomeric position (like in **20**) versus some other glucose positions has been previously reported by Tanaka *et al*., in 1997.[77]

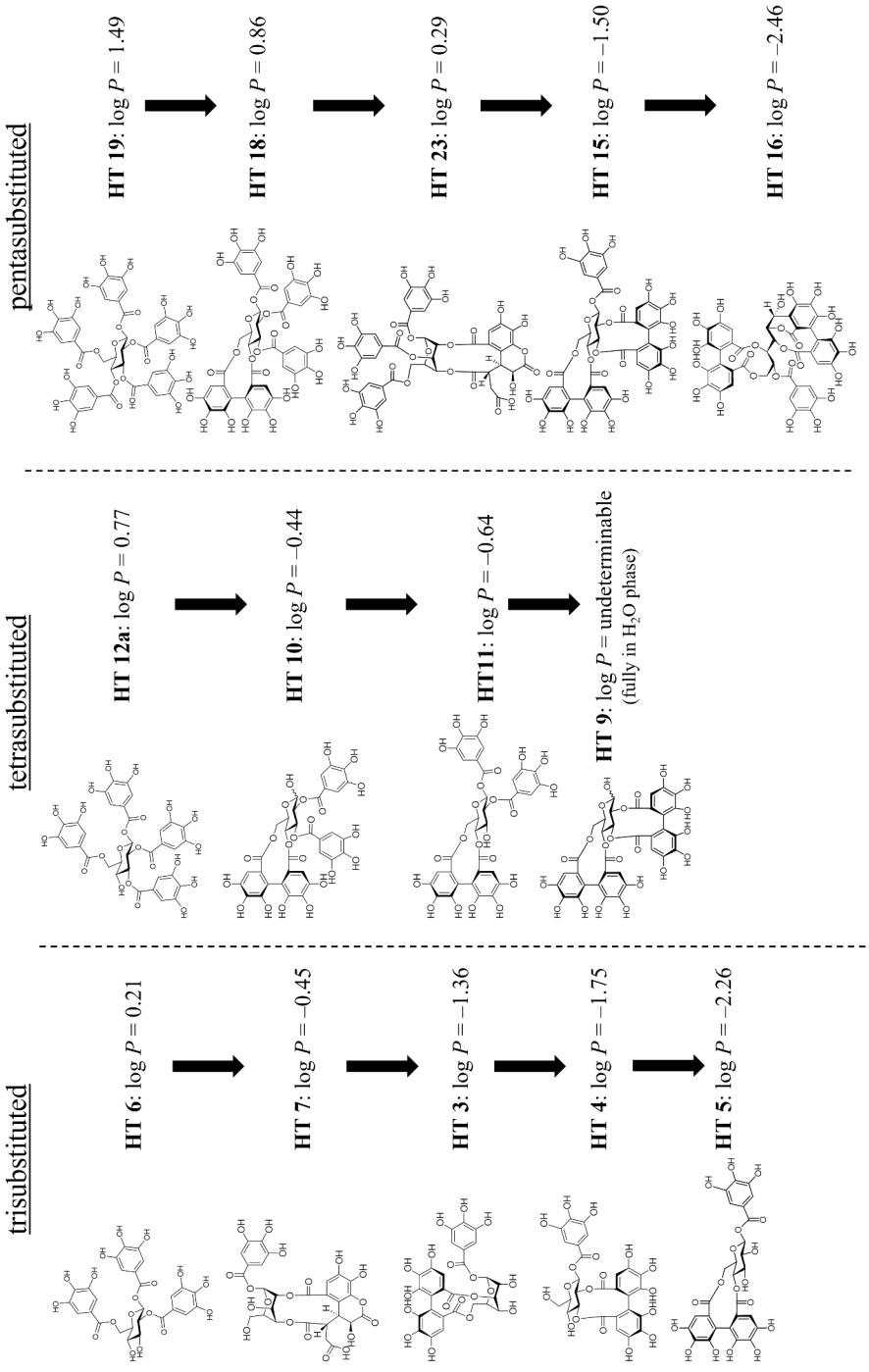

Figure 7. Example structures and determined log *P* values of HTs with tri-, tetra- or pentasubstituted polyol and how the different structures affect the log *P*. Numbering of tannins follows Figures 4 and 5.

HTs **16**, **29**, and **30** were the only monomeric acyclic ETs for which a log *P* could be determined. Despite this high hydrophilicity, the notable observation for the ETs with acyclic sugar moieties was that the α anomer in the anomeric pairs of **16** (α) / **17** (β) and **29** (α) / **30** (β) was the more hydrophobic one. Another interesting comparison can be made between **16** and **15** as both have one galloyl group and two HHDP groups as substituents where the former has an acyclic polyol and the latter a cyclic polyol. The pair effectively demonstrates that the cyclic one is significantly more hydrophobic than the acyclic one reinforcing what was earlier introduced as a general rule.

Larger dimeric and trimeric HTs were observed to be less hydrophobic than their individual monomeric constituents. This trend can be seen from the three oligomeric series that were a part of the studied compounds: i) HTs **10**, **34**, and **44**; ii) HTs **15**, **41**, **45**; iii) HTs **18**, **43**, and **46** (Figure 6). The oligomers also showed similar trends that were observed with the monomeric HTs. Free galloyl groups increased the hydrophobicity whereas structural rigidity, for example in **10** due to its macrocyclic oligomer linkage, decreased the hydrophobicity among other factors. Unfortunately, as larger oligomers than trimers were not included in the study it cannot be unanimously stated whether or not larger oligomers could in fact be more hydrophobic than their monomeric constituents even though the trend in these oligomeric series seems to suggest an upward trajectory moving from the dimers to the trimers.

3.2 Interactions of hydrolysable tannins with bacterial lipid membranes

3.2.1 HR-MAS NMR measurements

To probe the interactions between HTs and phospholipid membranes NMR spectroscopy was utilized to establish whether HTs are able to perturb and penetrate these membrane structures and if there are discernable differences between the different HT structures. The studied HTs were a focused group of compounds selected from the 47 HTs in **Article I** with emphasis on high hydrophobicity but still including some highly hydrophilic compounds to enable more comprehensive structural comparisons. The studied compounds were: **10**, **14**, **15**, **18**, **19**, **20**, **22**, **23**, **25**, **34**, **41**, **44**, and **45** (Figures 4 and 5).

Figure 8 displays an illustration of a phospholipid vesicle with magnification showing the typical phospholipid bilayered membrane structure with the hydrophilic headgroups directed outward and the hydrophobic fatty acid tails inside the bilayer. In this study the phospholipids were primarily present as bilayer sheets instead of a spherical vesicle. Based on research done by Scheidt *et al*., in 2004 and 2008 where

they showed that protons in different parts of some flavonoid aglycone structures displayed different rates of cross relaxation (calculated from NOESY NMR) with different lipid protons, we hypothesized that we would be able to find similar patterns with regards to different tannin substructures.[121,122] The benefit of observing how the cross relaxation rates that different parts (protons) of the studied compound vary in magnitude along the length of the lipid is that one can deduce i) the probable orientation of the studied compound in the perturbed bilayer and ii) how deep within the bilayer structure it is able to penetrate.

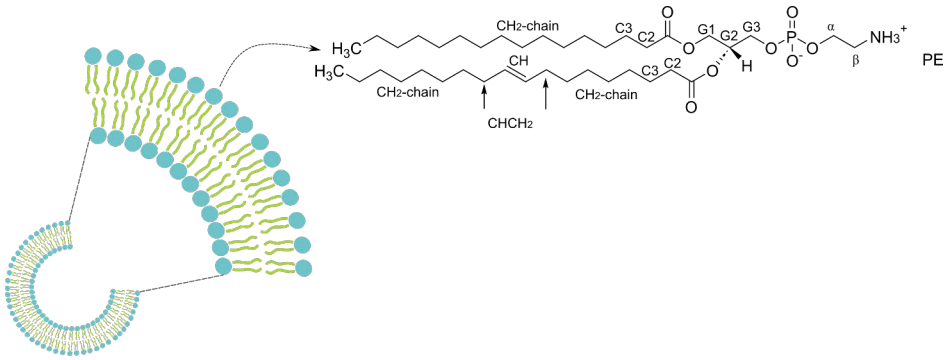

Figure 8. Illustration of a phopspholipid vesicle with the magnification showing the structure of 18:1 L-α-phosphatidylethanolamine (PE), which is the most abundant chain length, degree of unsaturation and lipid class of the commercial *E. coli* lipid extract with notable protons labeled.

In addition to the possible NOE correlations that can be observed between a spatially close HTs aromatic protons and the lipid protons, the vicinity of the HT can also influence the observed ^{1}H chemical shifts of the lipid protons via ring current effects of the HTs aromatic rings. This chemical shift change can also indicate how deep within the bilayer structure the different HTs are able to penetrate but unfortunately without the knowledge on the orientation of the perturbing HT.

Figure 9 displays the chemical shift changes of the phospholipid protons in the presence of the studied HTs. The lipid protons H_{CH} and H_{G2} unfortunately overlapped and showed a very broad signal with the achieved resolution of the utilized 400 MHz instrument, so, the possible change of the H_{G2} signal (residing in the head group) was masked by the non-shifted signals of the saturated chains H_{CH}'s. As a general observation small flexible tannins like **10**, **15**, **18**, and **19** were able to penetrate the membrane structure until the start of the fatty acid tail (H_{C2}, Figure 8) to some degree but larger tannins, like **41** and **45,** induced more relevant change only in the very polar head group (H_{β}). This suggests that larger HTs are not able to penetrate deeply into the bilayer and even smaller HTs do not penetrate all the way along the fatty acid tail.

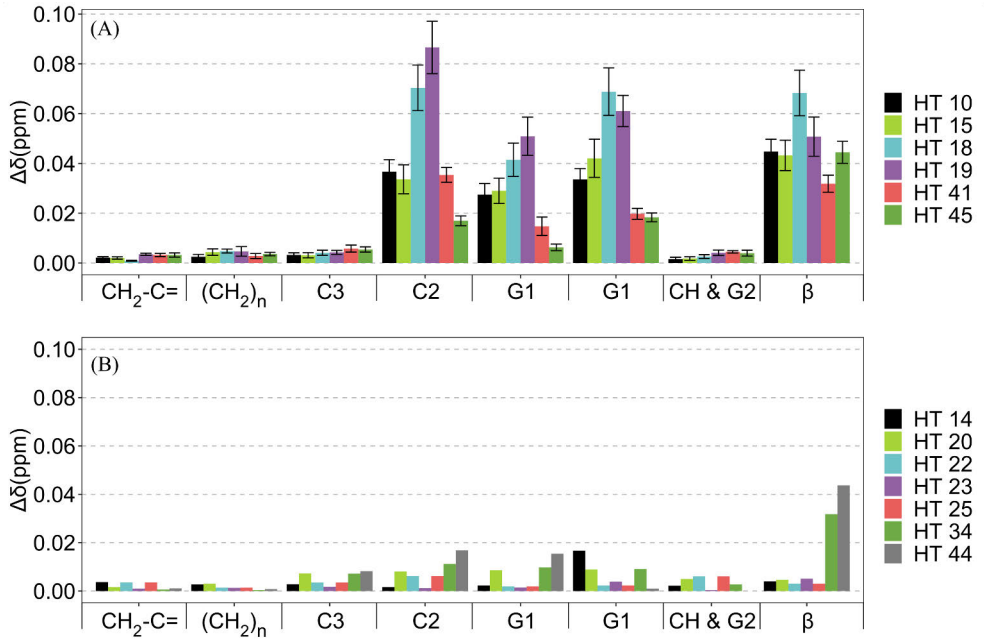

Figure 9. ^{1}H-NMR chemical shift changes (Δδ(ppm), (A): n=4, mean ± standard error, (B): n=1) of the phospholipid protons from the presence of the studied HTs, which influenced A) relevant and B) minor changes. Lipid protons on the x-axis are arranged along the length of the lipid from the fatty acid tail towards the head group. Numbering of tannins follows Figures 4 and 5. Figure adapted from **Article II**.

A surprising result was that the ETs **20**, **22**, and **23**, which are rather hydrophobic, did not influence practically any chemical shift changes suggesting that their structure, hydrophobic as it may be, is otherwise not optimal for bilayer penetration perhaps from the overall structural rigidity or other undefined reasons. Another interesting observation was that oligomers **34** and **44** were able to influence the lipid H_{β}'s to some extent suggesting surface level interaction with the lipid bilayer despite their rather bulky and rigid macrocyclic structures.

NOESY experiments were performed with the six HTs that showed interaction based on the chemical shift changes of the lipid protons. The achieved resolution with the used experimental setup and the 400 MHz instrument did not allow us to measure individual cross relaxation rates for the different aromatic protons of all the HTs as they are located in a very narrow ppm range in the aromatic region due to the similarity of the aromatic groups. However, for **18** the signal separation was sufficient for most of the aromatic protons and the determined cross relaxation rates of different aromatic protons of **18** against lipid protons are shown in Figure 10.

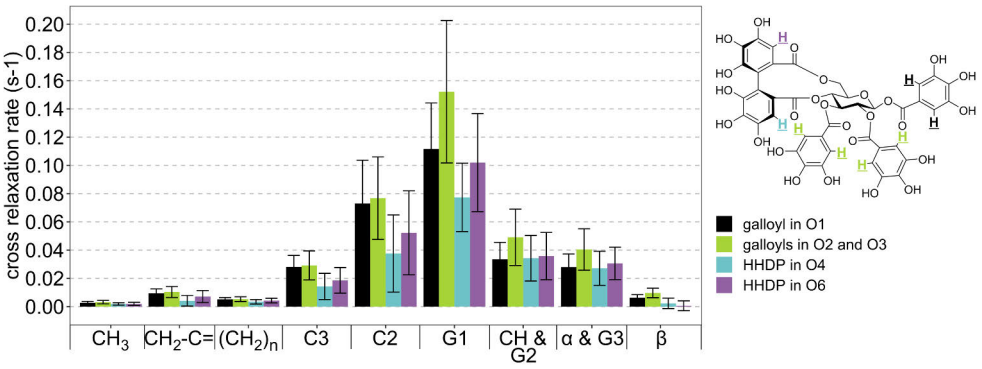

Figure 10. Cross relaxation rates (n=4, mean ± standard error) of the aromatic protons of tellimagrandin II (**18**) against different lipid protons determined from a NOESY experiment with 0.3 s mixing time. Lipid protons (Figure 8) on the x-axis are arranged along the length of the lipid from the fatty acid tail towards the head group. Figure adapted from **Article II**.

The cross relaxation rates verify the same general observation that was made based on the shifted ^{1}H signals, i.e., **18** was able to penetrate the bilayer to the start of the fatty acid chain. The highest cross relaxation rate of **18,** and also the other studied HTs (see **Article II**), was observed against H_{G1}, which resides in the junction between the tail and head groups. The galloyl protons of **18** show higher cross relaxation rates against the "deeper" lipid protons H_{G1}, H_{C2}, and H_{C3} which indicates that the galloyl groups are spatially closer, i.e., **18** is most probably oriented with the galloyl groups facing the membrane and the HHDP group outward (Figure 11).

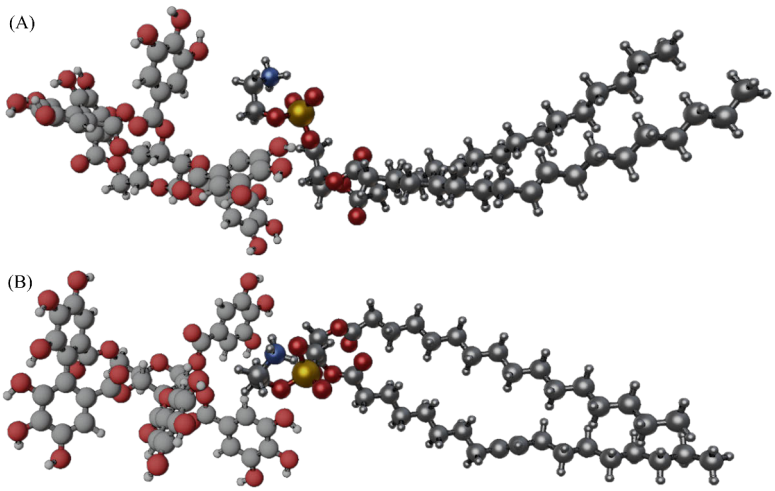

Figure 11. Three-dimensional visualization (from the (A) side and (B) top-down) of the possible vicinity of a tellimagrandin II molecules (left, matte) galloyl groups and 18:1 L-α-phosphatidylethanolamine molecules (right, metallic) head group.

3.2.2 ITC measurements

After studying the HT-lipid interactions with NMR, we attempted to find a method which would enable more structural comparisons, i.e., a method with more sensitivity. Although the NMR method functioned excellently and gave quality results with the effective HTs it did not provide much "range" as even the signals from the effective tannins were relatively modest in magnitude. Additionally, the required measurement time to acquire adequate 2D-NOESY spectra with the used experimental conditions and instrument was quite long (approximately 13 hours each for one mixing time) so the new method would also have to be faster to enable more compounds to be included in the studies while still allowing repetitions. Previously, tannin-protein interactions have been studied with ITC successfully[43,123], and as ITC is a reasonably fast technique and does not require very high concentrations or sample volumes, it was chosen for further HT-lipid interaction screening.

The lipid interaction thermodynamics of a set of 24 HT structures were measured with ITC: **3**–**6**, **9**,**10**, **12**, **14** ,**15**, **18**–**20**, **22**, **23**, **25**, **34**, **36**, **40**–**46**. Figure 12 shows the molar enthalpy changes for a 2 µL injection of HT into the sample cell filled with lipid vesicle solution (for full ITC data see **Article III**). The studied HTs were divided into four groups according to the observed interaction magnitude and their oligomerization degree: A) monomers with weak interaction, B) monomers with strong interaction, C) dimers, and D) trimers. The HTs in group A produced minimal heats of interaction and their thermograms (see **Article III** for full thermograms) closely resembled their control measurements (HT titrated into buffer) indicating that only the heat of dilution from the consecutive injections was measured. A common structural feature with the more effective HTs in groups B–D (B: **18**, **19**; C: **36**, **43**; D: **45**, **46**) is that they contain more free galloyl groups and are thus structurally more flexible than the ones with more oxidized and dehydrogenated substituents. This was the most dominant structural feature but the other substituents do also have an interaction increasing effect e.g. if we compare HTs **6** and **18**, which both have three galloyl groups but in **18** the glucose is also substituted with an HHDP group resulting in a much higher heat of interaction.

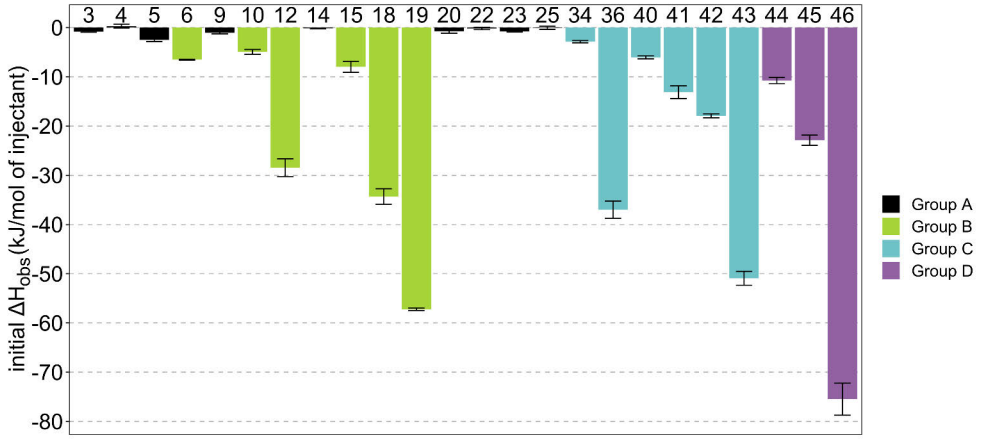

Figure 12. Observed molar enthalpy change (ΔH_{obs}(kJ/mol of injectant), n=3, mean ± standard error) after the first real HT injection into the lipid solution. The HTs are divided into the following groups according to their degree of oligomerization and observed interaction magnitude: A) monomers with weak interaction, B) monomers with strong interaction, C) dimers, and D) trimers. Numbering of tannins follows Figures 4 and 5.

Included in the group A were the relatively hydrophobic ETs **20**, **22**, and **23**, which were observed in the NMR measurements to not penetrate lipid bilayers. Both observations suggest that these rigid structures with $^{1}C_{4}$ glucose polyol do not interact with lipid vesicles in aqueous solution with high affinity.

Another interesting observation was made from one of the control measurements (HT being titrated into buffer), where some of the HTs showed progressively decreasing endothermic (with few exothermic exceptions) heat rates, which is attributed to a deaggregation process (or aggregation with the exothermic exceptions).[123,124] This process occurs when the HTs are titrated from a concentrated solution, where they can aggregate, to a less concentrated solution. The amount of deaggregation will diminish with each injection as the HT concentration starts to increase in the buffer solution.

Figure 13 displays the fitted thermodynamic parameters of the control measurements into an aggregate dissociation model. It is worth noting that this model relies on the assumption that HT aggregates exist predominantly as dimers and larger aggregates are thus not well predicted. Notably the previously mentioned HTs **20**, **22**, and **23** produced significant exothermic heat of deaggregation even though they produced close to no observable heat of interaction with the lipid vesicles. Also, dimer **43** and trimers **45** and **46** were found to heavily deaggregate in these control experiments.

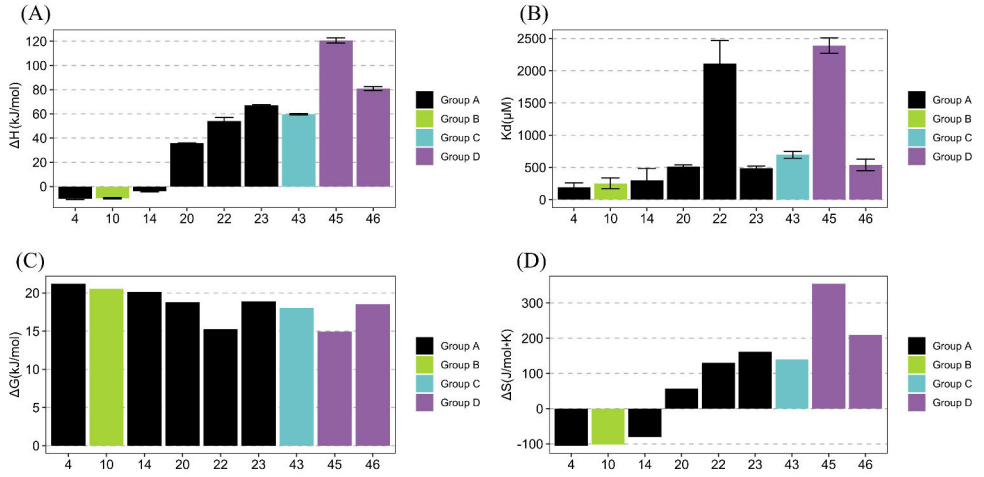

Figure 13. Fitted values of HT to buffer control measurements with an aggregate dissociation model: (A) Δ*H* (kJ/mol), (B) K_d (μM), (C) Δ*G* (kJ/mol), and (D) Δ*S* (J/mol K). Numbering of tannins follows Figures 4 and 5.

3.3 NMR metabolomics of bacterial cultures treated with hydrolysable tannins

As the lipid interaction studies with NMR and ITC demonstrated that certain HTs have a tendency to penetrate and interact with lipid bilayers we next aimed to study these interactions in a more applied setting. HTs have been shown to inhibit several different strains of bacteria[9,14,15,99–103] and as the membrane structures of many of these strains consist of similar phospholipids as we had been thus far experimenting with, we planned to study how different HTs have an effect to the bacterial metabolome and if the detected metabolome changes are linked to the inhibition efficiency of these different HTs. We utilized an untargeted NMR metabolomics approach to study how different HTs cause changes to the metabolome of *E. coli* and *S. aureus* cultures during culture growth. HTs utilized in this study were **5**, **13**, **18**, **19**, **38**, and **43**. In addition to these two purely bacterial sets, the effect of HTs was also tested with a more complex system where donor fecal samples were included in the growth medium of an *S. aureus* culture. The NMR data of the three sets (*E. coli*, *S. aureus*, and fecal batch culture) were processed and then analyzed using principal component analysis (PCA).

Figure 14 shows the PCA score plot of the *E. coli* culture set samples after 24 hours of incubation displaying separation between the different groups, i.e., different HT treatments. For PCA plots of the full set (containing all the incubation timepoint samples), the different incubation times (0 h and 8 h), and the different bacterial sets

see **Article IV**. All of the selected HTs did cause observable changes to the *E. coli* metabolome when compared to the control cultures which were not inhibitied.

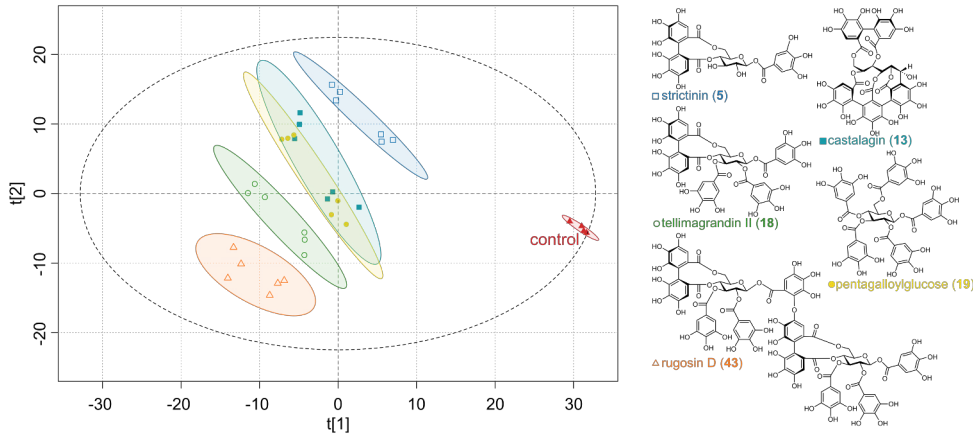

Figure 14. PCA score plot ($R^2X(1) = 0.34$, $R^2Y(2) = 0.16$) from the NMR metabolomics data of *E. coli* culture samples treated with different hydrolysable tannins after 24 hours of incubation. Groups are colored according to hydrolysable tannin treatment and controls. Figure adapted from **Article IV**.

The distance between the control sample cluster and the different HT clusters increases in the following order: **5**, **13**, **18**, **19**, and **43**. This order was also confirmed to correlate with the plated bacterial inhibition experiments (see **Article IV** Figure 11) and literature[14] of these HTs, and thus, the PCA group separation was confirmed to produce valid and comparable "inhibition" data with no colony counting or other laborious procedures. The general observed order made sense considering the determined hydrophobicities of these tannins as well as the extent that they were observed to interact with lipids. Meaning that generally the more hydrophobic HTs induced more changes to the bacterial metabolome. However, it was interesting that pentagalloylglucose (**19**) was found to be less efficient in inhibiting *E. coli* than tellimagrandin II (**18**) and almost as inefficient as castalagin (**13**). This result cannot be explained purely by the determined hydrophobicities and strict aqueous lipid interactions as both **13** and **18** were more hydrophilic and interacted less with lipids than **19**. It seems that the HHDP group (and possibly also the NHTP group in **13**) is beneficial regarding bacterial inhibition either as a part of the intact tannin structure or as a fragmented and lactonized product like ellagic acid or its further metabolized products, urolithins.[125] This observation supports a general theory that has been earlier proposed regarding tannin PPC (now possibly also lipid activity) and AOA activities where it had been noted that the most antimicrobially active tannins are not the most efficient ones in either PPC or AOA but are in the middle with the capability

to interact semi-efficiently with macromolecules but also act as semi-efficient radical scavengers.[75,112,126,127]

The loadings of the PCA models revealed several significant metabolites from the *E. coli* sample set which were behind most of the explained variance in the constructed PCA models. Figure **15** displays the concentration changes of three selected metabolites (lactate, acetate, and succinate; see **Article IV** for the rest) and the growth mediums glucose. The increase of these three overflow metabolites[128] is an indication that microbial growth is still taking place, but their levels stay below that of the control samples demonstrating inhibition. Same can be seen from the decrease of glucose as the microbial growth is using the supplemented glucose where the tannin treated cultures used the glucose slower than control culture.

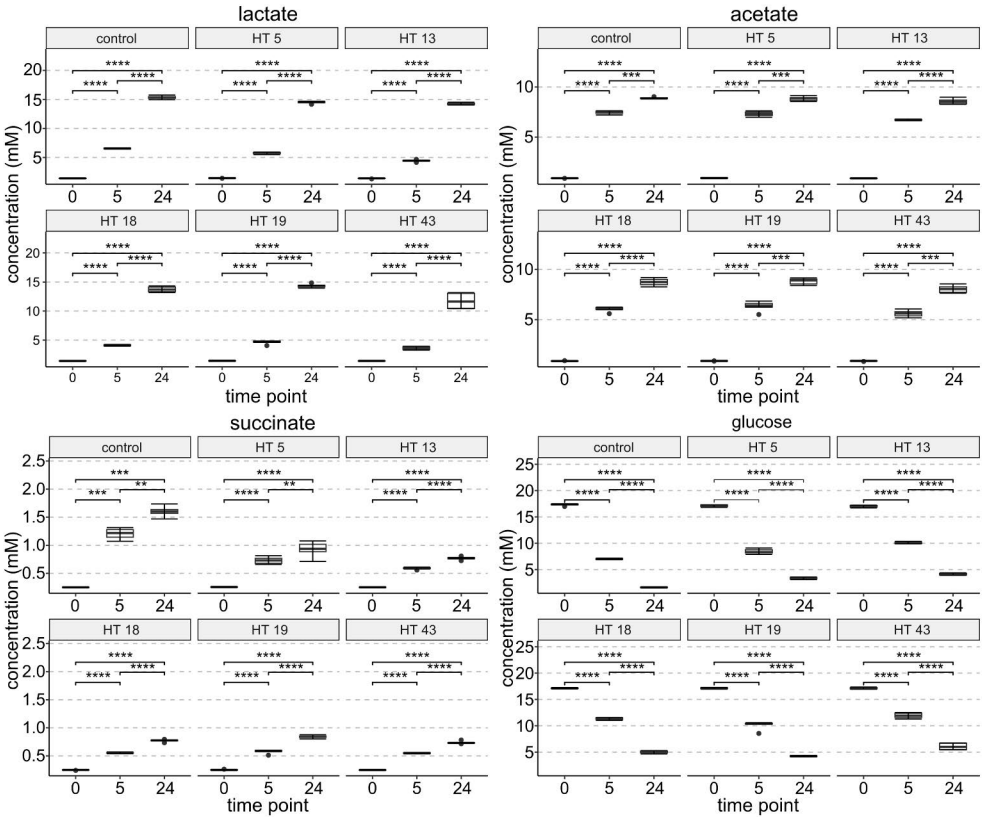

Figure 15. Statistically significant ($P < 0.05$) metabolite concentrations from the *E. coli* set at 0 h, 5 h, and 24 h time points. Numbering of tannins follows Figures 4 and 5. *P* values of difference are from a paired *t*-test (n=6). Levels of significance: **** $P < .0001$; *** $P < .001$; ** $P < .01$; * $P < .05$; ns = non-significant. Figure adapted from **Article IV**.

The metabolome changes of the *S. aureus* cultures induced by the different HT treatments were not as clearly separated in the PCA plot of the 24 hour time point samples (Figure 16) as with the *E. coli* set. All of the HT treatments were however well separated from the control culture cluster indicating that the HT treatments were able to alter the bacterial metabolome. The plated inhibition experiments confirmed that this separation from the control samples correlated with *S. aureus* inhibition (see **Article IV** Figure 12). The inhibition results also clarified why the separation between the different HT treatments in the PCA plot were not clear as all of the HTs were observed to inhibit *S. aureus* very effectively, which led to the HT treated cultures developing similar metabolite compositions. Minor separation can be seen with the bulk of the HT treated samples and the least efficient inhibitors, HTs **5** and **13,** suggesting that they were not quite as efficient *S. aureus* inhibitors as the other tested HTs. It is interesting to note that these cultures treated with **5** and **13** were more inhibited in the earlier 5 h (see **Article IV**) timepoint than in the 24 h timepoint suggesting that the inhibition capacity of these weaker inhibitors diminishes quicker than that of the stronger inhibitors.

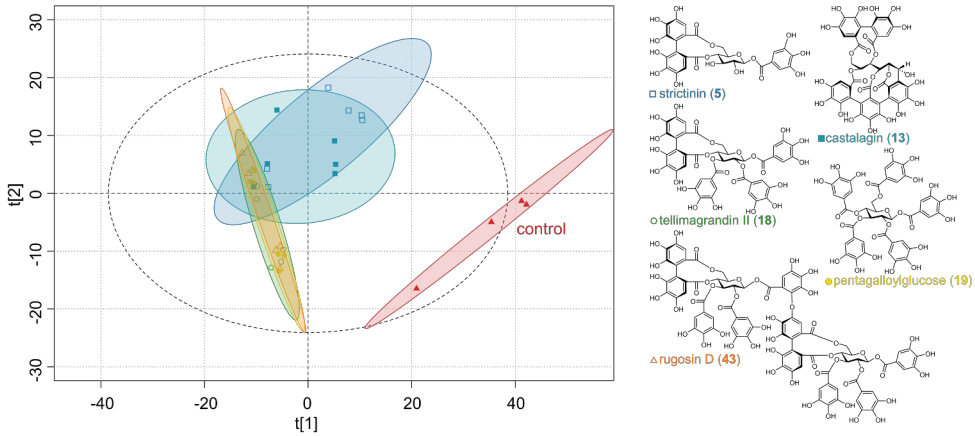

Figure 16. PCA score plot ($R^2X(1)$ = 0.47, $R^2Y(2)$ = 0.19) from the NMR metabolomics data of *S. aureus* culture samples treated with different hydrolysable tannins after 24 hours of incubation. Groups are colored according to hydrolysable tannin treatment and controls. Figure adapted from **Article IV**.

The concentration changes of individual metabolites (Figure 17) in the *S. aureus* cultures verified the observations made from the PCA plot. The cultures treated with HTs **18**, **19**, and **43** produced minor amounts of lactate and acetate corroborating with efficient bacterial inhibition whereas the cultures treated with **5** and **13** started to produce these metabolites in the later 24 h time point indicating that microbial growth was emerging despite the earlier inhibition. The concentration of the growth

medium glucose also corroborates with this as the cultures treated with **5** and **13** started to consume glucose in the 24 h time point.

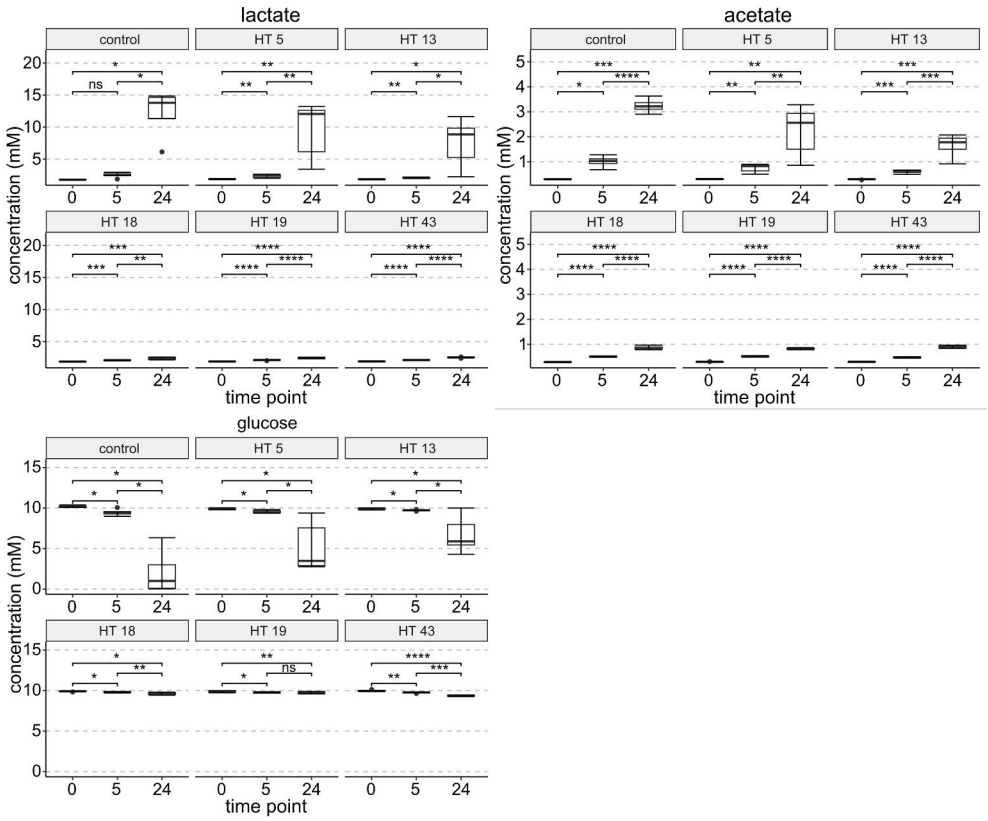

Figure 17. Statistically significant ($p < 0.05$) metabolite concentrations from the *S. aureus* set at 0 h, 5 h, and 24 h time points. Numbering of tannins follows Figures 4 and 5. *P* values of difference are from a paired *t*-test (n=6). Levels of significance: **** $P < .0001$; *** $P < .001$; ** $P < .01$; * $P < .05$; ns = non-significant. Figure adapted from **Article IV**.

The *S. aureus* cultures, which were grown in a medium containing fecal donor samples, were also studied similarly as the previous bacterial sets. Unfortunately, some bacteria of *Enterobacteriaceae* family (see **Article IV** bacterial DNA sequencing section) originating from the donor fecal samples grew so forcibly that it made it difficult to assess the *S. aureus* cultures metabolome changes due to the HT treatments or if they correlated with bacterial inhibition.

4 Conclusions

Studied HT structures ranged from highly hydrophilic to hydrophobic with evident structural reasons behind their determined hydrophobicities. HTs with more flexibility and freely rotating structures were determined to be more hydrophobic than rigid ones and increasing molecular weight was observed to increase the hydrophobicity of the structures.

These more hydrophobic HTs were generally observed to interact with bacterial lipid vesicles and to penetrate to the exterior region of the lipid membranes bilayer structures. There were also some interesting exceptions to this where certain dehydro-ETs, which were determined to be rather hydrophobic, did not penetrate lipid vesicles in aqueous solution or interact with them observably. This observation confirmed that even though hydrophobicity is often considered to effectively predict lipophilicity and membrane permeability of compounds, it cannot be used as a sole definitive factor but should rather be used as a capable guideline. It was also observed that HTs with larger molecular weights, which was generally observed to increase the hydrophobicity, were not able to perturb the lipid bilayer structures deeply and interaction was observed only with the outermost parts of the polar lipid headgroups. This interaction, which was limited only to the surface level, was due to their bulky size.

However, considering the antibacterial activities of HTs it was observed that the most effective HTs in inhibiting different bacterial strains were not the HTs with the most hydrophobic structures but rather compounds that had both hydrophobic (free galloyl groups) and hydrophilic regions (HHDP, NHTP, and other galloyl derivatives). This observation highlighted the importance of these hydrophilic structural moieties that are formed in the biosynthetically more evolved plants and partly reinforced the reason for these plants to produce these structures that have been shown to be less effective in protein interactions, which are generally thought to be one of the main mechanisms of HT antimicrobial activities. Although not proven one hypothesis for this is that the hydrophobic regions enable the HT to reach the area where their activity is required but then the hydrophilic regions are needed for the interactions that promote the bacterial inhibition mechanisms as part of the

intact HT molecule or as metabolism products such as ellagic acid or valoneic acid dilactone.

The results of this thesis work expanded the knowledge of HT hydrophobicities and provided novel information on HT-lipid interactions. The generated chemical knowledge can be utilized multidisciplinarily and is valuable for future applications, for example in agriculture and animal and human nutrition. The obtained antibacterial results were in line with literature and although they offered insights into the structure-activity patterns behind these inhibitory activities they still leave room for future studies to use more structurally different compounds to enable even better comparisons. As a final point, it is remarkable how much the perception of compounds classified as tannins has shifted over the years from just simple leathermaking tools and ink ingredients to genuinely beneficial components of our diets that have the capacity to counter pathogens and reduce inflammation.

Appendix

List of the hydrolysable tannins used in the thesis work with information on plant origin, purity measured by UPLC-DAD at 280 nm, ESI-MS identification (**molecular** and fragment ions) and ^{1}H-NMR assignation with labeled chemical structure (left) and UV spectrum (right). Tannin numbering is presented accoring to **Article I** in the order of ascending molecular weight.

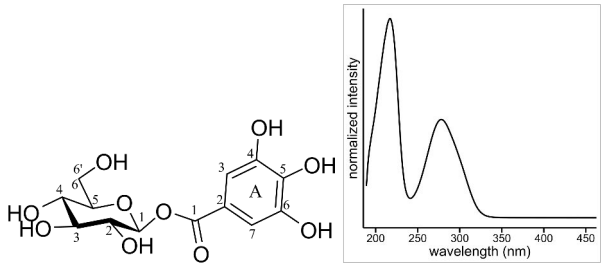

1-*O*-galloyl-β-*D*-glucose (1) was isolated from *Betula pubescens* leaves; purity measured by UPLC-DAD at 280 nm 87.9%; ESI-MS identification: *m/z* at 331.06765 (**[M–H]**$^{-}$, error –1.8 ppm), 169.01502 ([gallic acid–H]$^{-}$, error 4.6 ppm), 125.02571 ([gallic acid–COOH–H]$^{-}$, error 10.3 ppm); ^{1}H-NMR (600 MHz, acetone-d_6, 298 K): δ 3.44–3.55 (m, 4H, H_{glc}-2,3,4,5), 3.69 (br dd, 1H, J=3.0, 12.0 Hz, H_{glc}-6'), 3.82 (br d, 1H, J=11.5 Hz, H_{glc}-6), 5.67 (d, 1H, J=7.8 Hz, H_{glc}-1), 7.17 (s, 2H, H_A-3,7).[129]

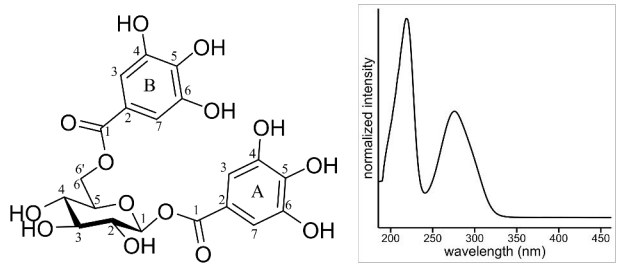

1,6-di-*O*-galloyl-β-*D*-glucose (2) was isolated from *Filipendula ulmaria* flowers; purity measured by UPLC-DAD at 280 nm 99.9%; ESI-MS identification: *m/z* at

483.07850 (**[M–H]**$^-$, error –1.0 ppm), 331.06772 ([M–galloyl–H]$^-$, error 2.0 ppm), 313.05674 ([M–gallic acid–H]$^-$, error 0.8 ppm), 169.01516 ([gallic acid–H]$^-$, error 5.4 ppm), 125.02550 ([gallic acid–COOH–H]$^-$, error 8.7 ppm); ^{1}H-NMR (600 MHz, acetone-d_6, 298 K): δ 3.54–3.64 (m, 3H, H_{glc}-2,3,4), 3.77 (ddd, 1H, J=2.0, 4.9, 9.2 Hz, H_{glc}-5), 4.41 (dd, 1H, J=4.9, 12.1 Hz, H_{glc}-6'), 4.54 (dd, 1H, J=2.0, 12.1 Hz, H_{glc}-6), 5.73 (d, 1H, J=7.7 Hz, H_{glc}-1), 7.13 (s, 2H, H_B-3,7),7.16 (s, 2H, H_A-3,7).[130]

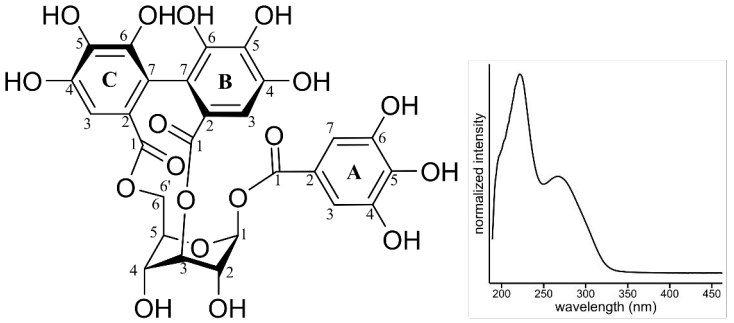

corilagin (3) was isolated from *Terminalia chebula* leaves; purity measured by UPLC-DAD at 280 nm 98.3%; ESI-MS identification: *m/z* at 633.07285 (**[M–H]**$^-$, error –0.8 ppm), 463.05231 ([M–galloyl–H]$^-$, error 1.1 ppm), 300.99889 ([ellagic acid–H]$^-$, error –0.3 ppm); ^{1}H-NMR (600 MHz, acetone-d_6, 298 K): δ 4.06 (br s, 1H, H_{glc}-2), 4.10 (dd, 1H, J=8.1, 11.0 Hz, H_{glc}-6'), 4.46 (br s, 1H, H_{glc}-6'), 4.52 (m, 1H, H_{glc}-5), 4.83 (br s, 1H, H_{glc}-3), 4.97 (t, 1H, J=11.0 Hz, H_{glc}-6), 6.37 (d, 1H, J=2.0 Hz, H_{glc}-1), 6.70 (s, 1H, J=2.0 Hz, H_C-3), 6.84 (s, 1H, J=2.0 Hz, H_B-3), 7.12 (s, 2H, H_A-3,7).[131,132]

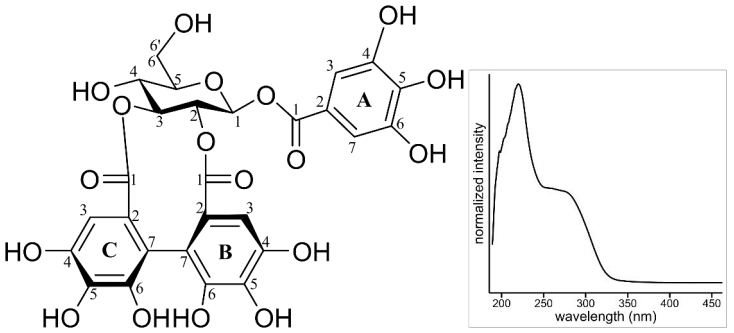

isostrictinin (4) was isolated from *Hippophaë rhamnoides* leaves; purity measured by UPLC-DAD at 280 nm 93.4%; ESI-MS identification: *m/z* at 633.07274 (**[M–H]**$^-$, error –0.9 ppm), 481.06225 ([M–galloyl–H]$^-$, error –0.3 ppm), 463.05150 ([M–gallic acid–H]$^-$, error –0.7 ppm), 300.99875 ([ellagic acid–H]$^-$, error –0.8 ppm); ^{1}H-NMR (500 MHz, acetone-d_6, 298 K): δ 3.74 (ddd, 1H, J=1.9, 4.4, 9.4 Hz, H_{glc}-5),

3.81 (dd, 1H, J=4.6, 12.0 Hz, H_{glc}-6'), 3.91 (dd, 1H, J=1.8, 12.2 Hz, H_{glc}-6'), 3.95 (t, 1H, J=9.5 Hz, H_{glc}-4), 5.00 (t, 1H, J=9.1 Hz, H_{glc}-2), 5.21 (t, 1H, J=9.5 Hz, H_{glc}-3),6.12 (d, 1H, J=8.5 Hz, H_{glc}-1).[133]

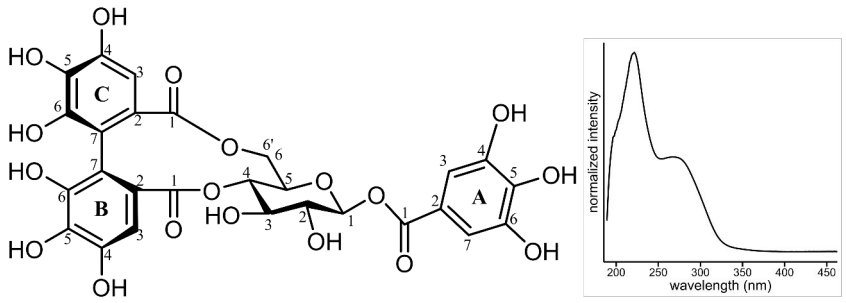

strictinin (5) was isolated from *Hippophaë rhamnoides* leaves; purity measured by UPLC-DAD at 280 nm 98.6%; ESI-MS identification: *m/z* at 633.07297 (**[M–H]**$^-$, error –0.6 ppm), 463.05302 ([M–gallic acid–H]$^-$, error 2.6 ppm), 300.99896 ([ellagic acid–H]$^-$, error –0.1 ppm); ^{1}H-NMR (500 MHz, acetone-d_6, 298 K): δ 3.70 (t, 1H, J=8.5 Hz, H_{glc}-2), 3.78 (d, 1H, J=13.0 Hz, H_{glc}-6'), 3.83 (d, 1H, J=9.3 Hz, H_{glc}-3), 4.11 (dd, 1H, J=5.7, 9.9 Hz, H_{glc}-5), 4.90 (t, 1H, J=9.8 Hz, H_{glc}-4), 5.21 (dd, 1H, J=6.4, 13.3 Hz, H_{glc}-6), 5.74 (d, 1H, J=8.1 Hz, H_{glc}-1), 6.60 (s, 1H, H_C-3), 6.71 (s, 1H, H_B-3), 7.20 (s, 2H, H_A-3,7).[134,135]

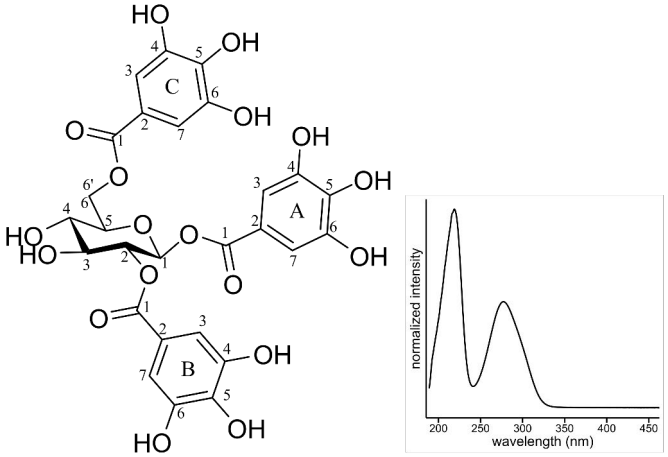

1,2,6-tri-*O*-galloyl-β-*D*-glucose (6) was isolated from *Hippophaë rhamnoides* leaves; purity measured by UPLC-DAD at 280 nm 93.1%; ESI-MS identification: *m/z* at 635.08839 (**[M–H]**$^-$, error –1.0 ppm), 465.06775 ([M–galloyl–H]$^-$, error 0.6 ppm), 313.05681 ([M–galloyl–gallic acid–H]$^-$, error 1.0 ppm), 169.01514 ([M–gallic acid–H]$^-$, error 5.3 ppm), 125.02551 ([gallic acid–COOH–H]$^-$, error 8.7 ppm); ^{1}H-NMR (500 MHz, acetone-d_6, 298 K): δ 3.76 (t, 1H, J=9.3 Hz, H_{glc}-4), 3.92 (ddd,

1H, J=1.9, 4.6, 9.8 Hz, H_{glc}-5), 3.98 (t, 1H, J=9.2 Hz, H_{glc}-3), 4.48 (dd, 1H, J=4.6, 12.1 Hz, H_{glc}-6'), 4.58 (dd, 1H, J=1.8, 12.1 Hz, H_{glc}-6), 5.25 (dd, 1H, J=8.6, 9.4 Hz, H_{glc}-2), 5.99 (d, 1H, J=8.4 Hz, H_{glc}-1), 7.07 (s, 2H, H_A-3,7), 7.10 (s, 2H, H_B-3,7), 7.15 (s, 2H, H_C-3,7).[130,136]

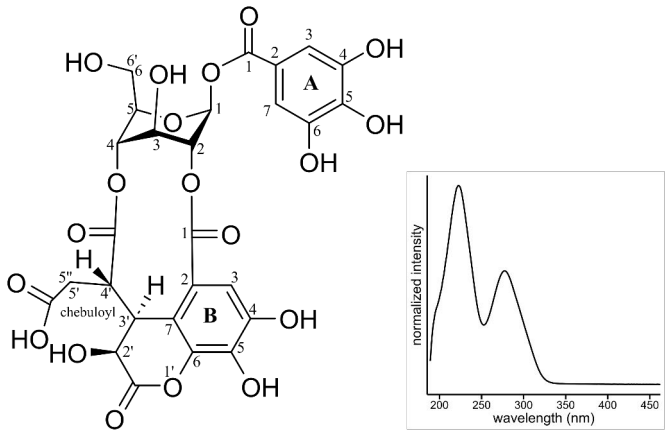

chebulanin (7) was isolated from *Terminalia chebula* leaves; purity measured by UPLC-DAD at 280 nm 97.0%; ESI-MS identification: *m/z* at 651.08319 (**[M–H]**$^-$, error –1.1 ppm), 481.06300 ([M–gallic acid–H]$^-$, error 1.3 ppm), 337.01977 ([chebuloyl–H_2O–H]$^-$, error –1.0 ppm), 169.01320 ([gallic acid–H]$^-$, error –6.2 ppm), 125.02288 ([gallic acid–COOH–H]$^-$, error –12.3 ppm); ^{1}H-NMR (500 MHz, acetone-d_6, 298 K): δ 2.19 (d, 1H, J=4.8 Hz, H_{che}-5''), 2.20 (d, 1H, J=10.3 Hz, H_{che}-5'), 3.90 (ddd, 1H, J=1.4, 4.9, 10.2 Hz, H_{che}-4'), 4.01 (dd, 1H, J=5.4, 11.1 Hz, H_{glc}-6'), 4.15 (br t, 1H, J=8.2 Hz, H_{glc}-6), 4.31 (br t, 1H, J=6.0 Hz, H_{glc}-5), 4.83 (br s, 1H, H_{glc}-3), 4.89 (br d, 1H, J=3.4 Hz, H_{glc}-4), 4.94 (dd, 1H, J=3.9, 7.2 Hz, H_{che}-2'), 5.19 (dd, 1H, J=1.4, 7.2 Hz, H_{che}-3'), 5.24 (br s, 1H, H_{glc}-2), 6.36 (br d, 1H, J=2.9 Hz, H_{glc}-1), 7.20 (s, 2H, H_A-3,7), 7.50 (s, 1H, H_B-3).[137]

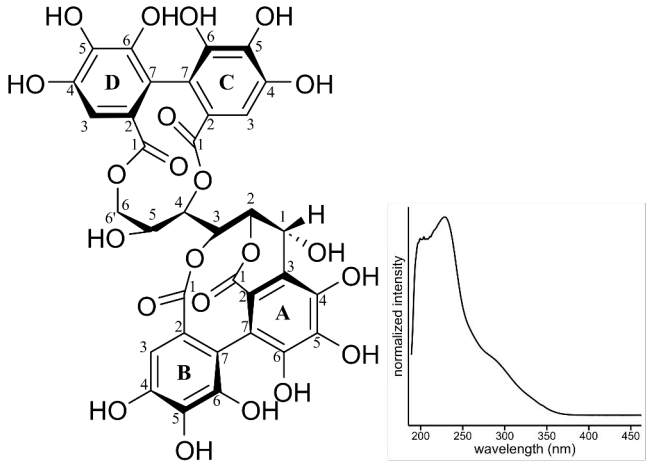

casuariin (8) was isolated from *Hippophaë rhamnoides* leaves; purity measured by UPLC-DAD at 280 nm 92.0%; ESI-MS identification: *m/z* at 783.06786 (**[M–H]**$^-$, error –1.0 ppm), 481.06161 ([M–HHDP–H]$^-$, error –1.6 ppm), 300.99912 ([ellagic acid–H]$^-$, error 0.4 ppm); ^{1}H-NMR (500 MHz, acetone-d_6, 298 K): δ 3.84 (d, 1H, J=12.2 Hz, H_{glc}-6'), 4.13 (dd, 1H, J=2.7, 8.7 Hz, H_{glc}-5), 4.63 (dd, 1H, J=3.2, 12.3 Hz, H_{glc}-6), 4.73 (dd, 1H, J=2.3, 4.7 Hz, H_{glc}-2), 5.00 (dd, 1H, J=2.8, 8.6 Hz, H_{glc}-4), 5.44 (br t, 1H, J=2.5 Hz, H_{glc}-3), 5.65 (d, 1H, J=4.8 Hz, H_{glc}-1), 6.43 (s, 1H, H_B-3), 6.52 (s, 1H, H_C-3), 6.66 (s, 1H, H_D-3).[134,135]

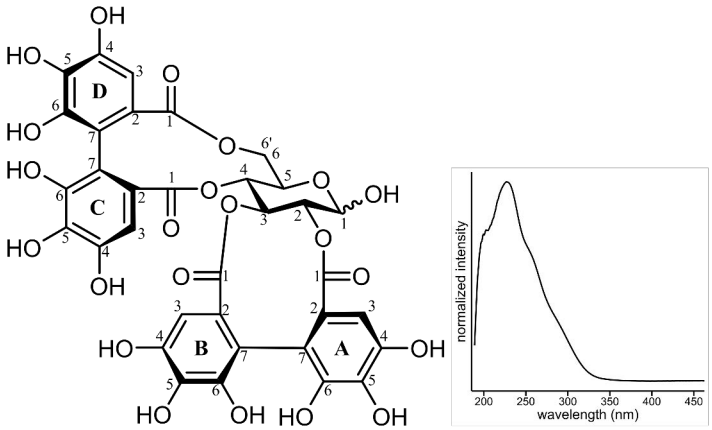

pedunculagin (9) was isolated from *Argentina anserina* leaves; purity measured by UPLC-DAD at 280 nm 98.8%; ESI-MS identification: *m/z* at 783.06806 (**[M–H]**$^-$, error –0.7 ppm), 481.06343 ([M–HHDP–H]$^-$, error 2.2 ppm), 300.99902 ([ellagic acid–H]$^-$, error 0.1 ppm); ^{1}H-NMR (600 MHz, acetone-d_6, 298 K, α-anomer (58%)): δ 3.77 (dd, 1H, J=1.7, 12.8 Hz, H_{glc}-6'), 4.61 (ddd, 1H, J=1.7, 7.1, 10.0 Hz, H_{glc}-5), 5.07 (dd, 1H, J=3.6, 9.5 Hz, H_{glc}-2), 5.089 (t, 1H, J=10.1 Hz, H_{glc}-4), 5.27 (dd, 1H, J=6.9, 12.8 Hz, H_{glc}-6), 5.467 (t, 1H, J=9.8 Hz, H_{glc}-3), 5.474 (br d, 1H, J=3.7 Hz,

H_{glc}-1), 6.329 (s, 1H, H_B-3), 6.56 (s, 1H, H_A-3), 6.60 (s, 1H, H_C-3), 6.67 (s, 1H, H_D-3); ^{1}H-NMR (600 MHz, acetone-d_6, 298 K, β-anomer (42%)): δ 3.84 (dd, 1H, J=1.1, 12.9 Hz, H_{glc}-6'), 4.22 (ddd, 1H, J=1.2, 6.8, 9.8 Hz, H_{glc}-5), 4.84 (dd, 1H, J=8.3, 9.0 Hz, H_{glc}-2), 5.090 (dd, 1H, J=8.5, 10.1 Hz, H_{glc}-4), 5.23 (dd, 1H, J=9.3, 10.1 Hz, H_{glc}-3), 5.30 (dd, 1H, J=6.7, 12.9 Hz, H_{glc}-6), 5.08 (d, 1H, J=8.5 Hz, H_{glc}-1), 6.325 (s, 1H, H_B-3), 6.51 (s, 1H, H_A-3), 6.59 (s, 1H, H_C-3), 6.68 (s, 1H, H_D-3).[135,138,139]

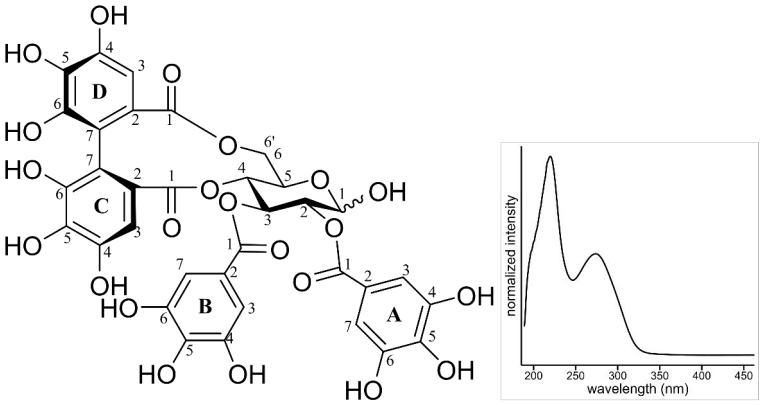

tellimagrandin I (10) was isolated from *Filipendula ulmaria* flowers; purity measured by UPLC-DAD at 280 nm 94.8%; ESI-MS identification: *m/z* at 785.08343 (**[M–H]**$^-$, error –1.1 ppm), 483.07919 ([M–HHDP–H]$^-$, error 2.4 ppm, 300.99864 ([ellagic acid–H]$^-$, error –1.2 ppm); ^{1}H-NMR (600 MHz, acetone-d_6, 298 K, α-anomer (56%)): δ 3.78 (dd, 1H, J=1.4, 13.1 Hz, H_{glc}-6'), 4.68 (ddd, 1H, J=1.0, 6.7, 10.2 Hz, H_{glc}-5), 5.120 (dd, 1H, J=3.9, 10.0 Hz, H_{glc}-2), 5.1205 (t, 1H, J=10.1 Hz, H_{glc}-4), 5.29 (dd, 1H, J=6.8, 13.0 Hz, H_{glc}-6), 5.57 (br s, 1H, H_{glc}-1), 5.89 (t, 1H, J=10.0 Hz, H_{glc}-3), 6.48 (s, 1H, H_C-3), 6.658 (s, 1H, H_D-3), 6.99 (s, 2H, H_B-3,7), 7.07 (s, 2H, H_A-3,7); ^{1}H-NMR (600 MHz, acetone-d_6, 298 K, β-anomer (44%)): δ 3.86 (dd, 1H, J=0.7, 13.1 Hz, H_{glc}-6'), 4.28 (ddd, 1H, J=0.8, 6.6, 9.9 Hz, H_{glc}-5), 5.123 (t, 1H, J=9.9 Hz, H_{glc}-4), 5.25 (dd, 1H, J=7.9, 9.6 Hz, H_{glc}-2), 5.62 (t, 1H, J=9.8, 10.1 Hz, H_{glc}-3), 5.31 (dd, 1H, J=6.2, 13.1 Hz, H_{glc}-6), 5.107 (m, 1H, H_{glc}-1), 6.45 (s, 1H, H_C-3), 6.663 (s, 1H, H_D-3), 6.95 (s, 2H, H_B-3,7), 7.06 (s, 2H, H_A-3,7).[140]

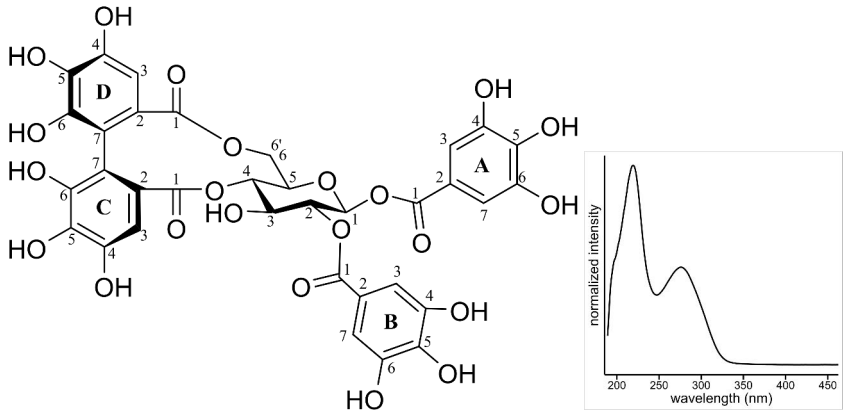

1,2-di-*O*-galloyl-4,6-HHDP-β-*D*-glucose (11) was isolated from *Filipendula ulmaria* flowers; purity measured by UPLC-DAD at 280 nm 95.0%; ESI-MS identification: *m/z* at 785.08413 (**[M–H]**$^-$, error –0.2 ppm), 615.06286 ([M–gallic acid–H]$^-$, error 0.1 ppm), 300.99900 ([ellagic acid–H]$^-$, error 0.03 ppm); ^{1}H-NMR (600 MHz, acetone-d_6, 298 K): δ 3.84 (d, 1H, J=13.2 Hz, H_{glc}-6'), 4.22 (t, 1H, J=9.8 Hz, H_{glc}-3), 4.28 (dd, 1H, J=6.2, 9.8 Hz, H_{glc}-5), 5.06 (t, 1H, J=9.8 Hz, H_{glc}-4), 5.27 (dd, 1H, J=16.5, 13.3Hz, H_{glc}-6), 5.39 (t, 1H, J=8.8 Hz, H_{glc}-2), 5.99 (d, 1H, J=8.3 Hz, H_{glc}-2), 6.62 (s, 1H, H_D-3), 6.72 (s, 1H, H_C-3), 7.09 (s, 2H, H_B-3,7), 7.10 (s, 1H, H_A-3).[141]

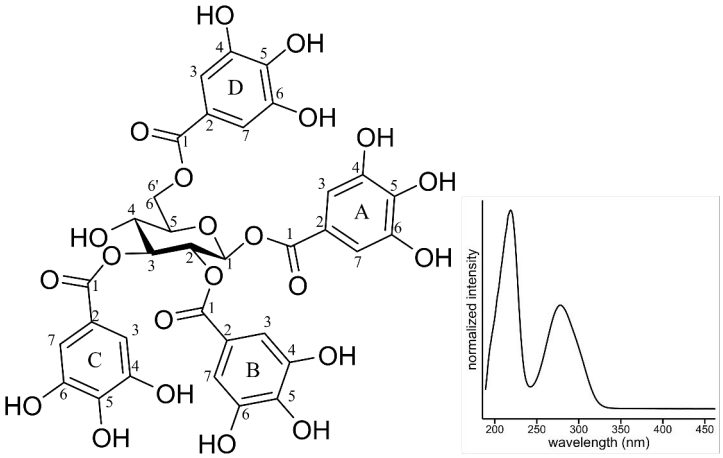

1,2,3,6-tetra-*O*-galloyl-β-*D*-glucose (12a) was isolated from *Acer platanoides* leaves; purity measured by UPLC-DAD at 280 nm 71.4% (largest impurity was a 1,2,4,6-galloylated isomer); ESI-MS identification: *m/z* at 787.09991 (**[M–H]**$^-$, error –0.05 ppm), 635.08896 ([M–galloyl–H]$^-$, error –0.04 ppm), 617.07897 ([M–gallic acid–H]$^-$, error 0.9 ppm), 573.08790 ([M–gallic acid–COOH–H]$^-$, error –1.2 ppm), 465.06807 ([M–gallic acid–galloyl–H]$^-$, error 1.3 ppm), 447.06807 ([M–2gallic

acid–H]⁻, error –1.5 ppm), 313.05666 ([M–gallic acid–2galloyl–H]⁻, error 0.5 ppm), 169.01312 ([gallic acid–H]⁻, error –6.7 ppm), 125.02285 ([gallic acid–COOH–H]⁻, error –12.5 ppm); ^{1}H-NMR (600 MHz, acetone-d_6, 298 K): δ 4.11 (dd, 1H, J=5.6, 9.0 Hz, H_{glc}-4), 4.15 (ddd, 1H, J=2.1, 4.1, 9.8 Hz, H_{glc}-5), 4.57 (dd, 1H, J=4.3, 12.2 Hz, H_{glc}-6'), 4.61 (dd, 1H, J=2.0, 12.1 Hz, H_{glc}-6), 5.47 (dd, 1H, J=8.3, 9.9 Hz, H_{glc}-2), 5.67 (dd, 1H, J=8.9, 9.8 Hz, H_{glc}-3), 6.18 (d, 1H, J=8.3 Hz, H_{glc}-1), 7.00 (s, 2H, H_B-3,7), 7.08 (s, 2H, H_C-3,7), 7.09 (s, 2H, H_A-3,7), 7.18 (s, 2H, H_D-3,7).[130,142]

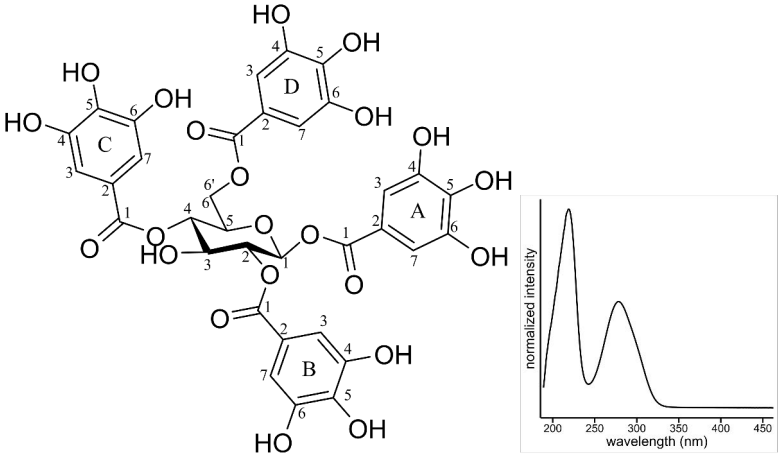

1,2,4,6-tetra-*O*-galloyl-β-*D*-glucose (12b) was isolated from *Acer platanoides* leaves; purity measured by UPLC-DAD at 280 nm 74.7% (largest impurity was a 1,2,3,6-galloylated isomer); ESI-MS identification: *m/z* at 787.09988 (**[M–H]⁻**, error –0.1 ppm), 617.07919 ([M–gallic acid–H]⁻, error 1.2 ppm), 465.066858 ([M–gallic acid–galloyl–H]⁻, error 2.4 ppm), 313.05578 ([M–gallic acid–2galloyl–H]⁻, error –2.3 ppm), 169.01318 ([gallic acid–H]⁻, error –6.3 ppm), 125.02290 ([gallic acid–COOH–H]⁻, error –12.1 ppm); ^{1}H-NMR (600 MHz, acetone-d_6, 298 K): δ 4.27 (dd, 1H, J=4.8, 11.9 Hz, H_{glc}-6'), 4.30 (ddd, 1H, J=1.6, 5.0, 9.7 Hz, H_{glc}-5), 4.39 (t, 1H, 9.4 Hz, H_{glc}-3), 4.50 (dd, 1H, J=1.4, 11.9 Hz, H_{glc}-6), 5.40 (dd, 1H, J=8.4, 9.5 Hz, H_{glc}-2), 5.41 (t, 1H, J=9.5 Hz, H_{glc}-4), 6.11 (d, 1H, J=8.4 Hz, H_{glc}-1), 7.09 (s, 2H, H_A-3,7), 7.11 (s, 2H, H_B-3,7), 7.16 (s, 2H, H_D-3,7), 7.17 (s, 2H, H_C-3,7).[130,131]

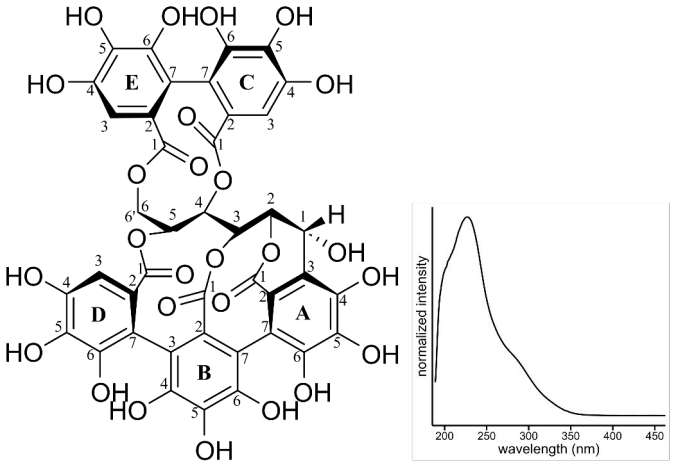

castalagin (13) was isolated from *Quercus robur* acorns; purity measured by UPLC-DAD at 280 nm 99.6%; ESI-MS identification: *m/z* at 933.06192 (**[M–H]**$^-$, error –2.2 ppm), 889.07151 ([M–COOH–H]$^-$, error –2.9 ppm), 631.05763 ([M–HHDP–H]$^-$, error –0.1 ppm), 300.99838 ([ellagic acid–H]$^-$, error –2.0 ppm); ^{1}H-NMR (600 MHz, acetone-d_6, 298 K): δ 4.01 (d, 1H, J=12.5 Hz, H_{glc}-6'), 5.03 (m, 1H, H_{glc}-2), 5.04 (m, 1H, H_{glc}-3), 5.10 (dd, 1H, J=2.6, 13.0 Hz, H_{glc}-6), 5.24 (t, 1H, J=7.3 Hz, H_{glc}-4), 5.61 (ddd, 1H, J=1.0, 2.5, 7.7 Hz, H_{glc}-5), 5.71 (d, 1H, J=4.4 Hz, H_{glc}-1), 6.63 (s, 1H, H_E-3), 6.77 (s, 2H, H_C-3 & H_D-3). [50,143]

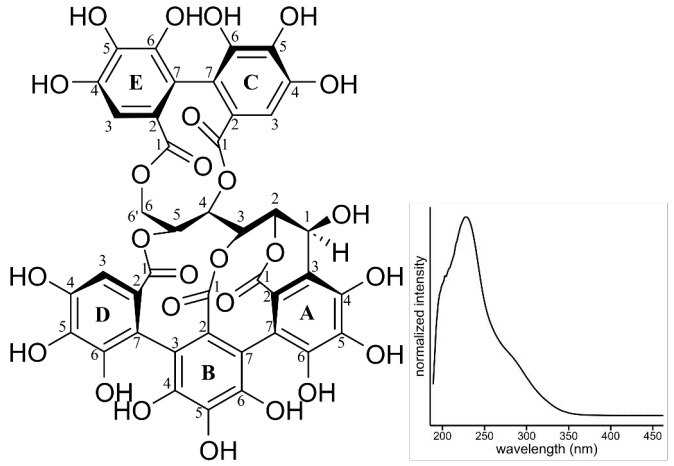

vescalagin (14) was isolated from *Quercus robur* acorns; purity measured by UPLC-DAD at 280 nm 97.0%; ESI-MS identification: *m/z* at 933.06361 (**[M–H]**$^-$, error –0.4 ppm), 915.05479 ([M–H_2O–H]$^-$, error 1.5 ppm), 871.06140 ([M–COOH–H_2O–H]$^-$, error –2.5 ppm), 613.04664 ([M–HHDP–H_2O–H]$^-$, error –0.8 ppm), 300.99902 ([ellagic acid–H]$^-$, error 1.5 ppm); ^{1}H-NMR (600 MHz, acetone-d_6, 298 K): δ 4.01 (d, 1H, J=12.4 Hz, H_{glc}-6'), 4.51 (ddd, 1H, J=0.9, 6.7, 9.9 Hz, H_{glc}-5), 4.57 (dd, 1H,

J=1.4, 6.9 Hz, H_{glc}-3), 4.89 (d, 1H, J=2.1 Hz, H_{glc}-1), 5.09 (dd, 1H, J=2.6, 13.1 Hz, H_{glc}-6), 5.17 (t, 1H, J=9.8 Hz, H_{glc}-4), 5.23 (t, 1H, J=1.6 Hz, H_{glc}-2), 6.61 (s, 1H, H_E-3), 6.76 (s, 1H, H_C-3), 6.77 (s, 1H, H_D-3).[50,143]

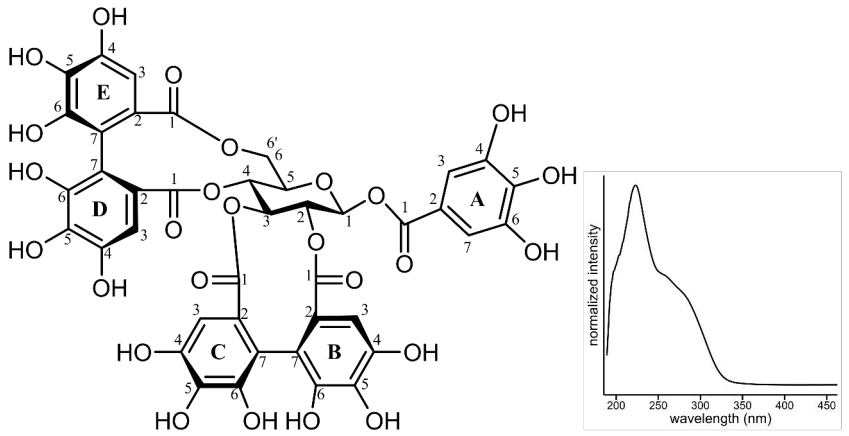

casuarictin (15) was isolated from *Filipendula ulmaria* flowers; purity measured by UPLC-DAD at 280 nm 97.5%; ESI-MS identification: *m/z* at 935.07924 (**[M–H]**$^-$, error –0.4 ppm), 633.07380 ([M–HHDP–H]$^-$, error 0.7 ppm), 300.99913 ([ellagic acid–H]$^-$, error 0.5 ppm); ^{1}H-NMR (600 MHz, acetone-d_6, 298 K): δ 3.88 (dd, 1H, J=0.9, 13.3 Hz, H_{glc}-6'), 4.51 (ddd, 1H, J=0.9, 6.7, 9.9 Hz, H_{glc}-5), 5.17 (t, 1H, J=9.8 Hz, H_{glc}-4), 5.18 (t, 1H, J=8.9 Hz, H_{glc}-2), 5.36 (dd, 1H, J=6.7, 13.3 Hz, H_{glc}-6), 5.45 (dd, 1H, J=9.2, 10.1 Hz, H_{glc}-3), 6.22 (d, 1H, J=8.6 Hz, H_{glc}-1), 6.36 (s, 1H, H_C-3), 6.46 (s, 1H, H_B-3), 6.54 (s, 1H, H_D-3), 6.68 (s, 1H, H_E-3), 7.18 (s, 2H, H_A-3,7).[135]

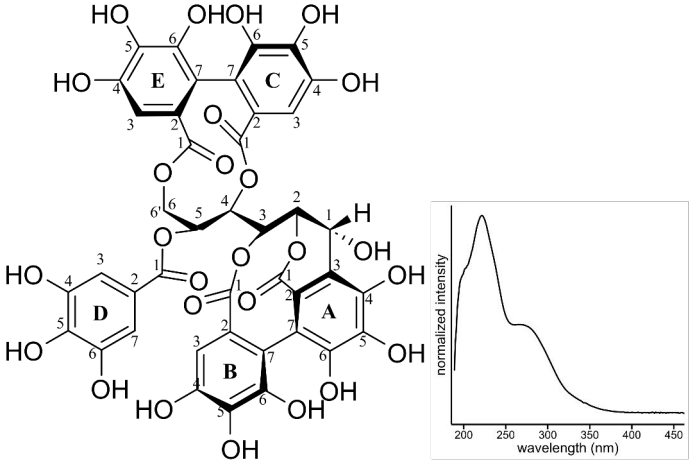

casuarinin (16) was isolated from *Hippophaë rhamnoides* leaves; purity measured by UPLC-DAD at 280 nm 97.5%; ESI-MS identification: *m/z* at 935.07917 (**[M–H]**$^-$

, error –0.5 ppm), 783.06775 ([M–galloyl–H]$^-$, error –1.1 ppm), 633.07343 ([M–HHDP–H]$^-$, error 0.1 ppm), 481.06372 ([M–HHDP–galloyl–H]$^-$, error 2.8 ppm), 300.99942 ([ellagic acid–H]$^-$, error 1.4 ppm); ^{1}H-NMR (600 MHz, acetone-d_6, 298 K): δ 4.07 (d, 1H, J=13.1 Hz, H_{glc}-6'), 4.69 (dd, 1H, J=2.1, 4.9 Hz, H_{glc}-2), 4.78 (dd, 1H, J=3.4, 13.3 Hz, H_{glc}-6), 5.33 (dd, 1H, J=3.2, 9.7, H_{glc}-5), 5.391 (br t, 1H, J=2.0 Hz, H_{glc}-3), 5.394 (dd, 1H, J=2.4, 9.7 Hz, H_{glc}-4), 5.64 (d, 1H, J=4.9 Hz, H_{glc}-1), 6.50 (s, 1H, H_B-3), 6.55 (s, 1H, H_E-3), 6.75 (s, 1H, H_C-3), 7.11 (s, 2H, H_D-3,7).[135]

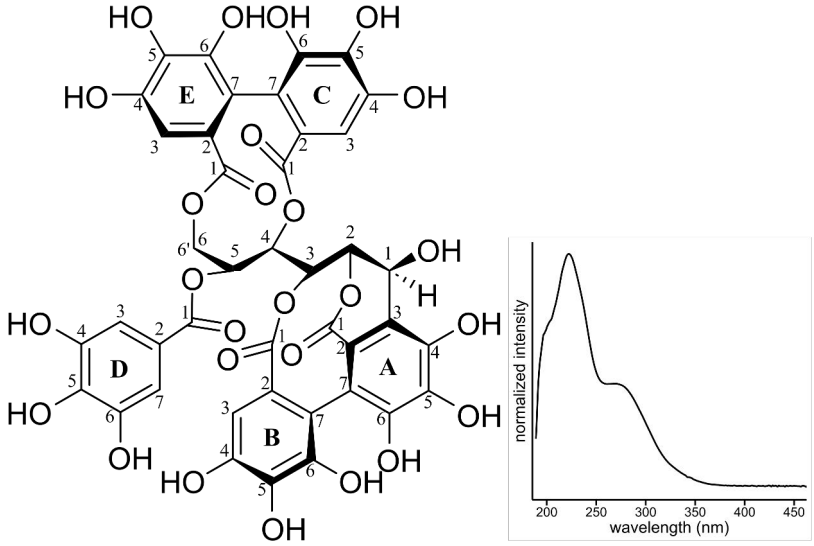

stachyurin (17) was isolated from *Hippophaë rhamnoides* leaves; purity measured by UPLC-DAD at 280 nm 96.8%; ESI-MS identification: *m/z* at 935.07849 (**[M–H]$^-$**, error –1.2 ppm), 917.06580 ([M–H_2O–H]$^-$, error –3.5 ppm), 300.99893 ([ellagic acid–H]$^-$, error –0.2 ppm); ^{1}H-NMR (600 MHz, acetone-d_6, 298 K): δ 4.03 (d, 1H, J=12.9 Hz, H_{glc}-6'), 4.85 (dd, 1H, J=3.5, 13.2 Hz, H_{glc}-6), 4.86 (t, 1H, J=1.8 Hz, H_{glc}-2), 4.93 (d, 1H, J=1.9 Hz, H_{glc}-1), 4.98 (br t, 1H, J=2.3 Hz, H_{glc}-3), 5.36 (dd, 1H, J=2.8, 8.7, H_{glc}-5), 5.67 (dd, 1H, J=2.8, 8.7 Hz, H_{glc}-4), 6.51 (s, 1H, H_B-3), 6.55 (s, 1H, H_E-3), 6.84 (s, 1H, H_C-3), 7.13 (s, 2H, H_D-3,7).[134,135]

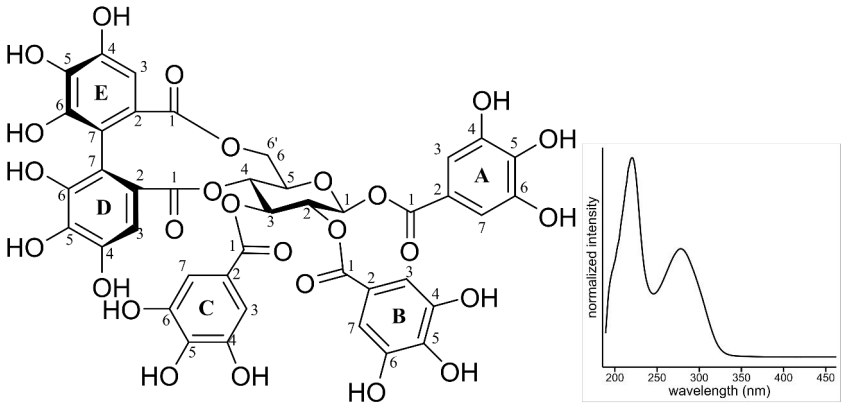

tellimagrandin II (18) was isolated from *Filipdendula ulmaria* flowers; purity measured by UPLC-DAD at 280 nm 90.2%; ESI-MS identification: *m/z* at 937.09507 (**[M–H]**$^-$, error –0.2 ppm), 767.07225 ([M–gallic acid–H]$^-$, error –1.9 ppm), 465.06785 ([M–gallic acid–HHDP–H]$^-$, error 0.8 ppm), 300.99881 ([ellagic acid–H]$^-$, error –0.6 ppm); ^{1}H-NMR (600 MHz, acetone-d_6, 298 K): δ 3.89 (d, 1H, J=13.3 Hz, H_{glc}-6'), 4.55 (dd, 1H, J=6.6, 13.4 Hz, H_{glc}-5), 5.22 (t, 1H, J=10.0 Hz, H_{glc}-4), 5.37 (dd, 1H, J=6.6, 13.4 Hz, H_{glc}-6), 5.60 (dd, 1H, J=8.5, 9.4 Hz, H_{glc}-2), 5.85 (t, 1H, J=9.8 Hz, H_{glc}-3), 6.21 (d, 1H, J=8.3 Hz, H_{glc}-1), 6.47 (s, 1H, H_D-3), 6.66 (s, 1H, H_E-3), 6.98 (s, 2H, H_C-3,7), 7.01 (s, 2H, H_B-3,7), 7.12 (s, 2H, H_A-3,7).[140]

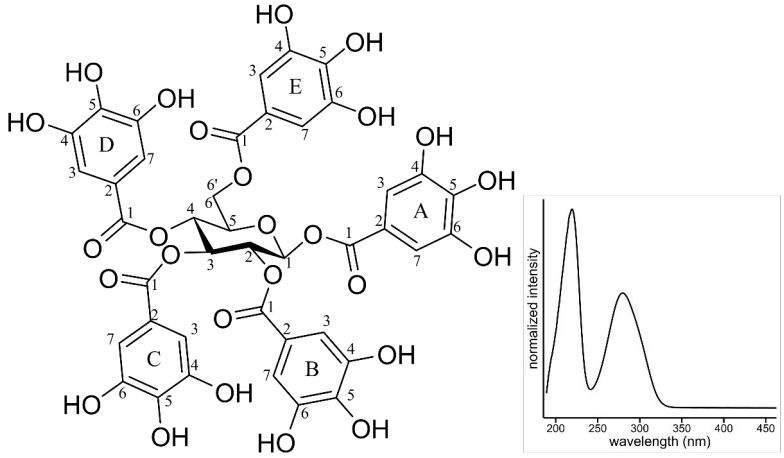

1,2,3,4,6-penta-*O*-galloyl-β-*D*-glucose (19) was prepared from tannic acid via methanolysis; purity measured by UPLC-DAD at 280 nm 98.6%; ESI-MS identification: *m/z* at 939.110111 (**[M–H]**$^-$, error –0.8 ppm), 787.10032 ([M–galloyl–H]$^-$, error 0.5 ppm), 769.08890 ([M–gallic acid–H]$^-$, error –0.6 ppm), 617.07852 ([M–galloyl–gallic acid–H]$^-$, error 0.2 ppm), 599.06766 ([M–2gallic acid–H]$^-$, error –0.3 ppm), 447.05754 ([M–galloyl–2gallic acid–H]$^-$, error 1.4 ppm),

313.05682 ([M–3galloyl–gallic acid–H]$^-$, error 1.0 ppm), 169.01516 ([gallic acid–H]$^-$, error 5.4 ppm), 125.02547 ([gallic acid–COOH–H]$^-$, error 8.4 ppm); ^{1}H-NMR (600 MHz, acetone-d_6, 298 K): δ 4.41 (dd, 1H, J=4.5, 12.5 Hz, H_{glc}-6'), 4.54 (dd, 1H, J=1.5, 13.3 Hz, H_{glc}-6), 4.56 (ddd, 1H, J=1.6, 4.4, 9.9 Hz, H_{glc}-5), 5.61 (dd, 1H, J=8.3, 9.9 Hz, H_{glc}-2), 5.66 (t, 1H, J=9.7 Hz, H_{glc}-4), 6.01 (t, 1H, J=9.8 Hz, H_{glc}-3), 6.34 (d, 1H, J=8.3 Hz, H_{glc}-1), 6.97 (s, 1H, H_C-3,7), 7.01 (s, 1H, H_B-3,7), 7.06 (s, 2H, H_D-3,7), 7.11 (s, 2H, H_A-3,7), 7.18 (s, 2H, H_E-3,7).[130,131]

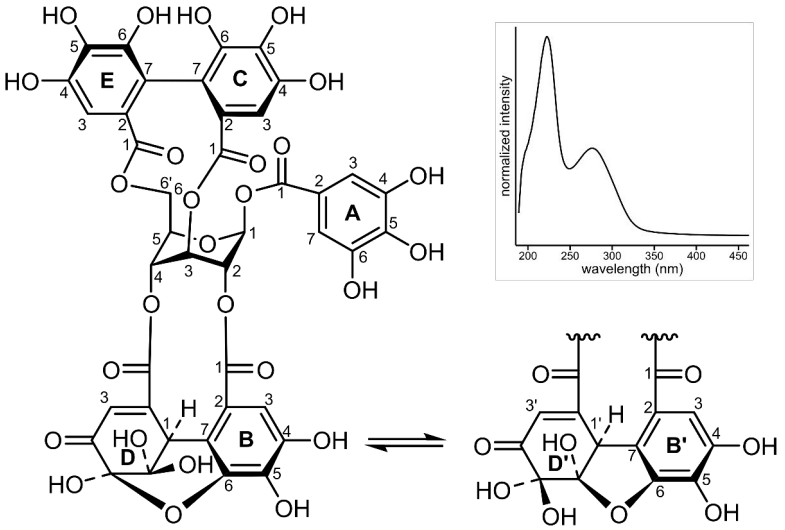

geraniin (20) was isolated from *Geranium sylvaticum* leaves; purity measured by UPLC-DAD at 280 nm 84.8%; ESI-MS identification: *m/z* at 951.07360 (**[M–H]**$^-$, error –1.0 ppm), 933.06500 ([M–H_2O–H]$^-$, error 1.1 ppm), 300.99878 ([ellagic acid–H]$^-$, error –0.7 ppm); ^{1}H-NMR (600 MHz, acetone-d_6, 298 K, (major 6-ring tautomer)): δ 4.31 (dd, 1H, J=8.2, 10.8 Hz, H_{glc}-6'), 4.78 (dd, 1H, J=8.4, 9.9 Hz, H_{glc}-5), 4.93 (t, 1H, J=10.6 Hz, H_{glc}-6), 5.17 (s, 1H, H_D-1), 5.49 (br s, 1H, H_{glc}-3), 5.52 (br s, 1H, H_{glc}-4), 5.56 (br s, 1H, H_{glc}-2), 6.56 (br s, 1H, H_{glc}-1), 6.53 (s, 1H, H_D-3), 6.66 (s, 1H, H_E-3), 7.14 (s, 1H, H_C-3), 7.199 (s, 1H, H_B-3), 7.201 (s, 2H, H_A-3,7).[49,132]

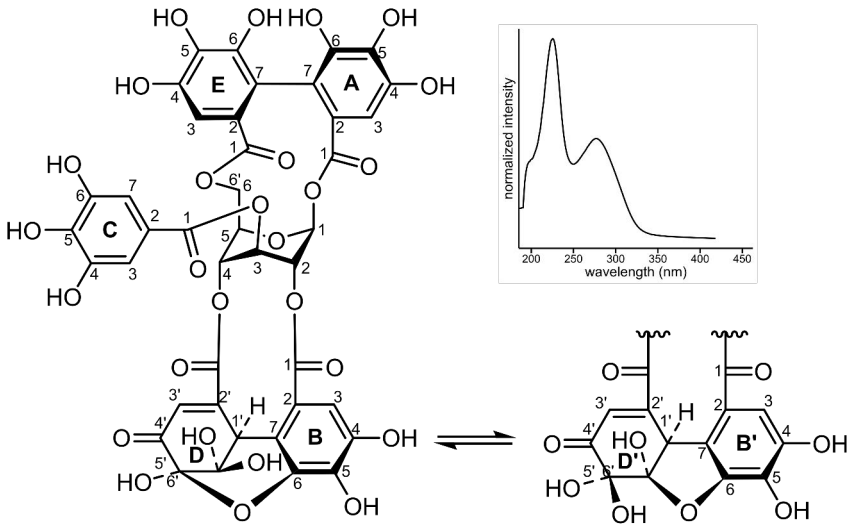

carpinusin (21) was isolated from *Geranium sylvaticum* leaves; purity measured by UPLC-DAD at 280 nm 98.3%; ESI-MS identification: *m/z* at 951.07228 (**[M–H]**$^{-}$, error –2.4 ppm), 933.06206 ([M–H_2O–H]$^{-}$, error –2.0 ppm), 631.05605 ([M–H_2O–HHDP–H]$^{-}$, error –2.6 ppm), 613.04549 ([M–2H_2O–HHDP–H]$^{-}$, error –2.7 ppm), 300.99835 ([ellagic acid–H]$^{-}$, error –2.1 ppm); ^{1}H-NMR (600 MHz, acetone-d_6, 298 K, (6-ring, 73%)): δ 4.24 (dd, 1H, J=5.3, 11.7 Hz, H_{glc}-6'), 4.66 (dd, 1H, J=5.2, 12.9 Hz, H_{glc}-5), 5.13 (br dd, 1H, J=0.8, 3.4 Hz, H_{glc}-2), 5.23 (s, 1H, H_D-1'), 5.39 (br s, 1H, H_{glc}-4), 5.44 (dd, 1H, J=11.9, 12.8 Hz, H_{glc}-6), 5.88 (m, 1H, H_{glc}-3), 6.20 (br s, 1H, H_{glc}-1), 6.57 (s, 1H, H_D-3'), 6.81 (s, 1H, H_A-3), 6.89 (s, 1H, H_E-3), 7.16 (s, 2H, H_C-3,7), 7.27 (s, 1H, H_B-3); ^{1}H-NMR (600 MHz, acetone-d_6, 298 K, (5-ring, 27%)): δ 4.16 (dd, 1H, J=5.2, 11.7 Hz, H_{glc}-6'), 4.70 (dd, 1H, J=5.2, 12.9 Hz, H_{glc}-5), 5.00 (d, 1H, J=1.3 Hz, H_D-1'), 5.05 (br dd, 1H, J=0.6, 3.4 Hz, H_{glc}-2), 5.47 (br s, 1H, H_{glc}-4), 5.48 (dd, 1H, J=11.9, 12.7 Hz, H_{glc}-6), 6.08 (m, 1H, H_{glc}-3), 6.26 (d, 1H, J=1.3 Hz, H_D-3'), 6.27 (br s, 1H, H_{glc}-1), 6.88 (s, 1H, H_A-3), 6.90 (s, 1H, H_E-3), 7.18 (s, 2H, H_C-3,7), 7.29 (s, 1H, H_B-3).[67,144]

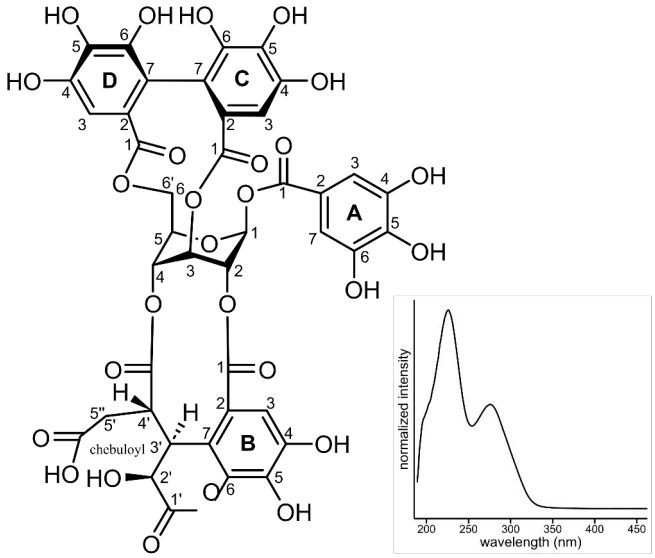

chebulagic acid (22) was isolated from *Terminalia chebula* leaves; purity measured by UPLC-DAD at 280 nm 96.1%; ESI-MS identification: *m/z* at 953.08949 (**[M–H]**$^-$, error –0.7 ppm), 935.07807 ([M–H_2O–H]$^-$, error –1.6 ppm), 801.08036 ([M–galloyl–H]$^-$, error 1.4 ppm), 783.06696 ([M–gallic acid–H]$^-$, error –2.1 ppm), 633.07235 ([M–HHDP–H_2O–H]$^-$, error –1.6 ppm), 481.06275 ([M–HHDP-galloyl–H]$^-$, error 0.8 ppm), 463.05379 ([M–HHDP-gallic acid–H]$^-$, error 4.3 ppm), 337.02138 ([chebuloyl–H_2O–H]$^-$, error 3.7 ppm), 300.99890 ([ellagic acid–H]$^-$, error –0.3 ppm); ^{1}H-NMR (600 MHz, acetone-d_6, 298 K): δ 2.19 (d, 2H, J=7.8 Hz, H_{che}-5), 3.87 (td, 1H, J=1.5, 7.7 Hz, H_{che}-4), 4.40 (dd, 1H, J=6.4, 9.2 Hz, H_{glc}-6'), 4.78 (d, 1H, J=9.5 Hz, H_{glc}-6), 4.80 (d, 1H, J=6.2 Hz, H_{glc}-5), 4.95 (d, 1H, J=7.3 Hz, H_{che}-2), 5.12 (dd, 1H, J= 1.5, 7.2 Hz, H_{che}-3), 5.22 (br d, 1H, J=3.7 Hz, H_{glc}-4), 5.51 (br s, 1H, H_{glc}-2), 5.94 (br s, 1H, H_{glc}-3), 6.51 (br s, 1H, H_{glc}-1), 6.66 (s, 1H, H_D-3), 7.07 (s, 1H, H_C-3), 7.18 (s, 2H, H_A-3,7), 7.52 (s, 1H, H_B-3).[132,145]

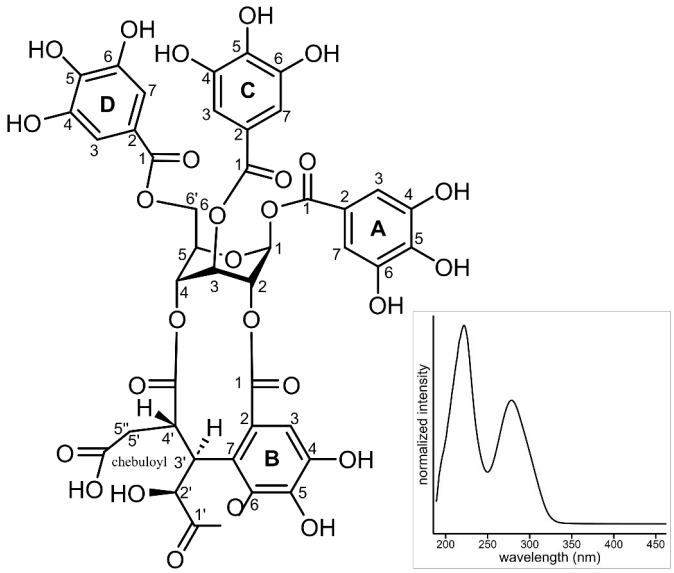

chebulinic acid (23) was isolated from *Terminalia chebula* leaves; purity measured by UPLC-DAD at 280 nm 88.3%; ESI-MS identification: *m/z* at 955.10484 (**[M–H]**$^-$, error –1.0 ppm), 937.09482 ([M–H_2O–H]$^-$, error –0.5 ppm), 911.11312 ([M–COOH–H]$^-$, error –3.1 ppm), 803.09645 ([M–galloyl–H]$^-$, error 2.0 ppm), 785.08389 ([M–gallic acid–H]$^-$, error –0.5 ppm), 767.07387 ([M–gallic acid–H_2O–H]$^-$, error 0.2 ppm), 741.09512 ([M–gallic acid–COOH–H]$^-$, error 0.9 ppm), 633.07239 ([M–galloyl–gallic acid–H]$^-$, error –1.5 ppm), 617.07908 ([M–dehydrated chebuloyl–H]$^-$, error 1.1 ppm), 465.06725 ([M–dehydrated chebuloyl–galloyl–H]$^-$, error –0.5 ppm), 337.02035 ([chebuloyl–H_2O–H]$^-$, error 0.7 ppm), 169.01494 ([chebuloyl–H_2O–H]$^-$, error 4.1 ppm), 125.02551 ([chebuloyl–H_2O–H]$^-$, error 8.7 ppm); ^{1}H-NMR (600 MHz, acetone-d_6, 298 K): δ 2.26 (d, 1H, J=4.1 Hz, H_{che}-5'), 2.28 (d, 1H, J=11.2 Hz, H_{che}-5), 3.96 (ddd, 1H, J=1.5, 4.0, 11.2 Hz, H_{che}-4), 4.72 (m, 1H, H_{glc}-5), 4.75 (m, 1H, H_{glc}-6'), 4.87 (dd, 1H, J=7.7, 11.1 Hz, H_{glc}-6), 4.96 (d, 1H, J=7.1 Hz, H_{che}-2), 5.09 (br d, 1H, J=3.5 Hz, H_{glc}-4), 5.18 (dd, 1H, J= 1.6, 7.1 Hz, H_{che}-3), 5.48 (br s, 1H, H_{glc}-2), 6.35 (br s, 1H, H_{glc}-3), 6.53 (br s, 1H, H_{glc}-1), 7.06 (s, 2H, H_D-3,7), 7.22 (s, 2H, H_A-3,7), 7.29 (s, 2H, H_C-3,7), 7.56 (s, 1H, H_B-3).[145,146]

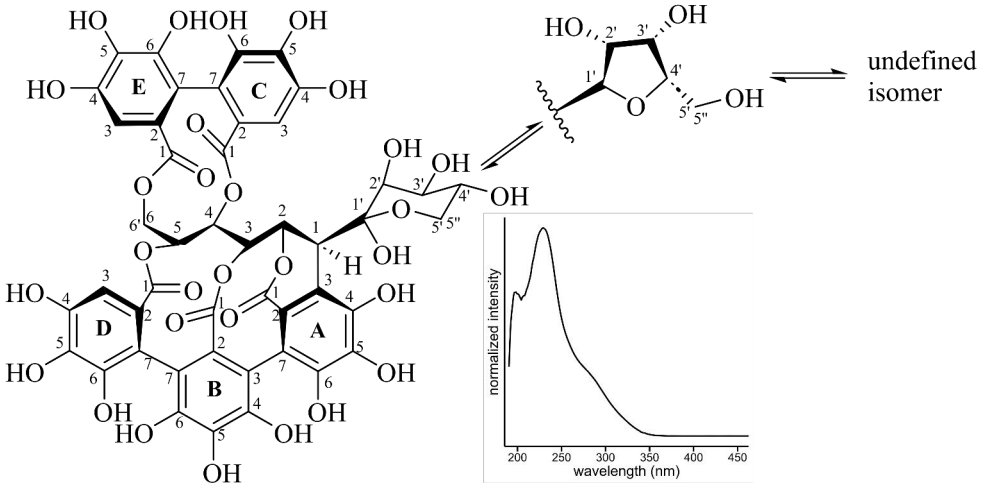

grandinin (24) was received from collaborators (lyxose unit isomerises in acetone solution into pyranose (40.7%), furanose (34.1%), and an undefined isomer (25.2%) of possibly an open chain aldehyde form); purity measured by UPLC-DAD at 280 nm 98.3%; ESI-MS identification: *m/z* at 1065.10279 ([M–H]$^-$, error –2.2 ppm), 931.07593 ([M–lyxose–H]$^-$, error –8.2 ppm), 300.99794 ([ellagic acid–H]$^-$, error 0.2 ppm); ^{1}H-NMR (500 MHz, acetone-d_6, 298 K, (pyranose, 41%)): δ 3.55 (br s, 1H, H_{glc}-1), 3.81 (d, 1H, J=10.1 Hz, H_{lyx}-5''), 3.86 (dd, 1H, J=5.6, 10.9 Hz, H_{lyx}-5'), 3.99 (d, 1H, J=12.2 Hz, H_{glc}-6'), 4.08 (m, 1H, H_{lyx}-4'), 4.12 (td, 1H, J=3.4, 9.3 Hz, H_{lyx}-3'), 4.42 (d, 1H, J=3.0 Hz, H_{lyx}-2'), 4.55 (br d, 1H, J=6.8 Hz, H_{glc}-3), 5.02 (dd, 1H, J=2.3, 12.9 Hz, H_{glc}-6), 5.26 (t, 1H, J=7.0 Hz, H_{glc}-4), 5.52 (br s, 1H, H_{glc}-2), 5.65 (br d, 1H, J=7.1 Hz, H_{glc}-5), 6.58 (s, 1H, H_E-3), 6.75 (s, 1H, H_D-3), 7.47 (s, 1H, H_C-3). ^{1}H-NMR (500 MHz, acetone-d_6, 298 K, (furanose, 34%)): δ 3.33 (br s, 1H, H_{glc}-1), 3.91 (d, 1H, J=5 Hz, H_{lyx}-5''), 3.91 (dd, 1H, J=6.2 Hz, H_{lyx}-5'), 3.98 (d, 1H, J=12.5 Hz, H_{glc}-6'), 4.06 (d, 1H, J=4.5, H_{lyx}-4'), 4.24 (d, 1H, J=4.7 Hz, H_{lyx}-2'), 4.40 (t, 1H, J=4.1 Hz, H_{lyx}-3'), 4.64 (br d, 1H, J=7.1 Hz, H_{glc}-3), 5.08 (dd, 1H, J=2.6, 13.0 Hz, H_{glc}-6), 5.17 (t, 1H, J=7.5 Hz, H_{glc}-4), 5.61 (br d, 1H, J=7.8 Hz, H_{glc}-5), 5.68 (br s, 1H, H_{glc}-2), 6.62 (s, 1H, H_E-3), 6.76 (s, 1H, H_D-3), 7.00 (s, 1H, H_C-3). ^{1}H-NMR (500 MHz, acetone-d_6, 298 K, (undefined isomer, 25%)): δ 3.55 (br s, 1H, H_{glc}-1), 3.81 (d, 1H, J=10.1 Hz, H_{lyx}-5''), 3.86 (dd, 1H, J=5.6, 10.9 Hz, H_{lyx}-5'), 3.99 (d, 1H, J=12.2 Hz, H_{glc}-6'), 4.08 (m, 1H, H_{lyx}-4'), 4.12 (td, 1H, J=3.4, 9.3 Hz, H_{lyx}-3'), 4.42 (d, 1H, J=3.0 Hz, H_{lyx}-2'), 4.55 (br d, 1H, J=6.8 Hz, H_{glc}-3), 5.02 (dd, 1H, J=2.3, 12.9 Hz, H_{glc}-6), 5.26 (t, 1H, J=7.0 Hz, H_{glc}-4), 5.52 (br s, 1H, H_{glc}-2), 5.65 (br d, 1H, J=7.1 Hz, H_{glc}-5), 6.58 (s, 1H, H_E-3), 6.75 (s, 1H, H_D-3), 7.47 (s, 1H, H_C-3).[147,148]

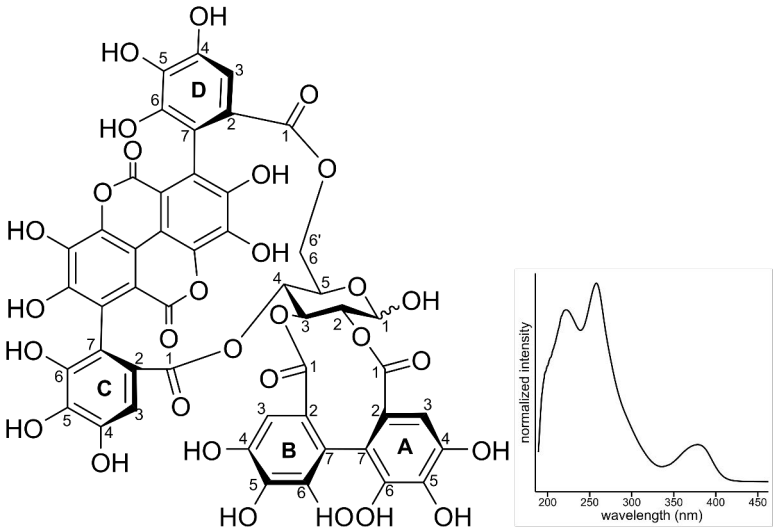

punicalagin (25) was isolated from *Terminalia chebula* leaves; purity measured by UPLC-DAD at 280 nm 98.4%; ESI-MS identification: *m/z* at 1083.05849 (**[M–H]**$^-$, error –0.7 ppm), 781.05230 ([M–HHDP–H]$^-$, error –0.9 ppm), 600.99061 ([gallagyl group–2H_2O–H]$^-$, error 1.7 ppm), 300.99900 ([ellagic acid–H]$^-$, error 0.03 ppm); ^{1}H-NMR (600 MHz, acetone-d_6, 298 K, α-anomer (66%)): δ 2.10 (dd, 1H, J=1.3, 11.0 Hz, H_{glc}-6'), 3.27 (dd, 1H, J=1.5, 10.2 Hz, H_{glc}-5), 4.20 (d, 1H, J=10.7 Hz, H_{glc}-6), 4.76 (dd, 1H, J=9.3, 10.0 Hz, H_{glc}-4), 4.80 (dd, 1H, J=3.6, 9.7 Hz, H_{glc}-2), 5.11 (br d, 1H, J= 3.4 Hz, H_{glc}-1), 5.21 (t, 1H, J=9.5 Hz, H_{glc}-3), 6.52 (s, 1H, H_A-3), 6.583 (s, 1H, H_C-3), 6.588 (s, 1H, H_B-3), 7.02 (s, 1H, H_D-3). ^{1}H-NMR (600 MHz, acetone-d_6, 298 K, β-anomer (34%)): δ 2.17 (dd, 1H, J=1.6, 11.2 Hz, H_{glc}-6'), 2.69 (td, 1H, J=1.6, 14.8 Hz, H_{glc}-5), 4.17 (d, 1H, J=10.6 Hz, H_{glc}-6), 4.64 (dd, 1H, J=8.1, 9.5 Hz, H_{glc}-2), 4.71 (d, 1H, J= 8.0 Hz, H_{glc}-1), 4.79 (t, 1H, J=9.2 Hz, H_{glc}-4), 4.87 (t, 1H, J=9.4 Hz, H_{glc}-3), 6.52 (s, 1H, H_A-3), 6.60 (s, 1H, H_B-3), 6.66 (s, 1H, H_C-3), 7.02 (s, 1H, H_D-3).[70,149]

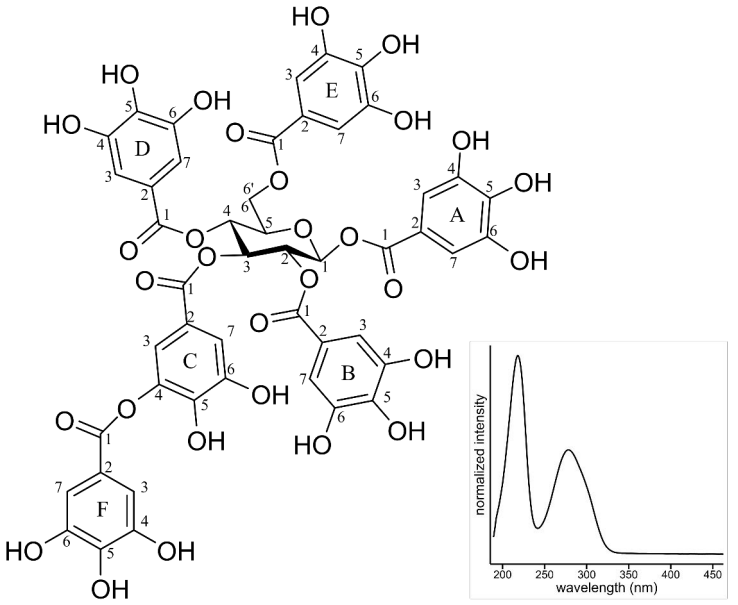

hexagalloylglucose (26) was isolated from *Acer platanoides* leaves; purity measured by UPLC-DAD at 280 nm 94.1%; ESI-MS identification: *m/z* at 1091.12073 (**[M–H]**$^-$, error –1.0 ppm), 939.11323 ([M–galloyl–H]$^-$, error 2.5 ppm), 787.10096 ([M–2galloyl—H]$^-$, error 1.3 ppm), 769.08984 ([M–galloyl–gallic acid–H]$^-$, error 0.6 ppm), 617.07872 ([M–2galloyl–gallic acid–H]$^-$, error 0.5 ppm), 465.06592 ([M–3galloyl–gallic acid–H]$^-$, error –3.3 ppm), 447.05851 ([M–2galloyl–2gallic acid–H]$^-$, error 3.6 ppm), 313.05631 ([M–4galloyl–gallic acid–H]$^-$, error –0.6 ppm), 169.01303 ([gallic acid–H]$^-$, error –7.2 ppm), 125.02297 ([gallic acid–COOH–H]$^-$, error –11.6 ppm); ^{1}H-NMR (600 MHz, acetone-d_6, 298 K (aromatic assignations with an asterisk are not definitive)): δ 4.40 (dd, 1H, J=4.5, 12.5 Hz, H_{glc}-6'), 4.54 (dd, 1H, J=1.8, 12.5 Hz, H_{glc}-6), 4.57 (ddd, 1H, J=2.1, 4.5, 10.2 Hz, H_{glc}-5), 5.64 (dd, 1H, J=8.3, 9.7 Hz, H_{glc}-2), 5.67 (t, 1H, J=9.8 Hz, H_{glc}-4), 6.02 (t, 1H, J=9.7 Hz, H_{glc}-3), 6.35 (d, 1H, J=8.3 Hz, H_{glc}-1), 7.02 (s, 2H, H_B-3,7), 7.07 (s, 2H, H_D-3,7),7.11 (s, 2H, H_A-3,7), 7.17 (s, 2H, H_E-3,7), 7.24 (s, 2H, H_F-3,7), 7.25 (m, 1H, H_C-7*), 7.30 (d, 1H, J=2.0 Hz, H_C-3*).[142,150]

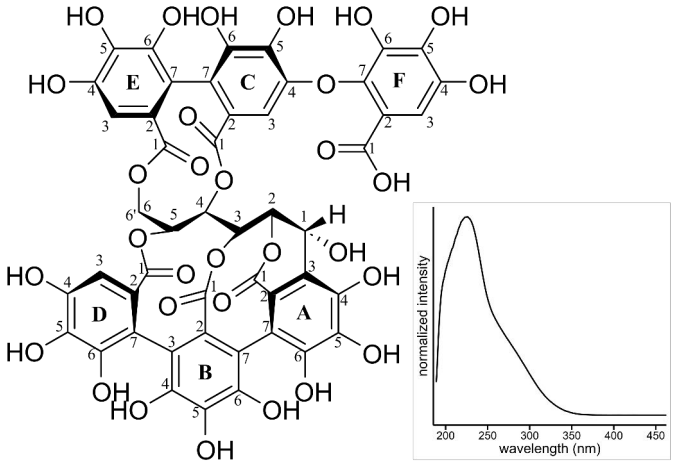

castavaloninic acid (27) was isolated from *Quercus robur* acorns; purity measured by UPLC-DAD at 280 nm 91.7%; ESI-MS identification: *m/z* at 1101.06605 (**[M–H]**$^-$, error –3.4 ppm), 1057.07935 ([M–COOH–H]$^-$, error –0.6 ppm), 1039.06839 ([M–COOH–H_2O–H]$^-$, error –1.0 ppm), 933.05853 ([M–gallic acid–H]$^-$, error –5.1 ppm), 631.06044 ([M–valoneoyl group–H]$^-$, error 4.4 ppm), 425.01432 ([valoneic acid dilactone–H_2O–H]$^-$, error –1.7 ppm), 300.99864 ([ellagic acid–H]$^-$, error –1.2 ppm); ^{1}H-NMR (500 MHz, acetone-d_6, 298 K): δ 3.97 (d, 1H, J=12.8 Hz, H_{glc}-6'), 4.73 (dd, 1H, J=1.4, 4.9 Hz, H_{glc}-2), 4.92 (t, 1H, J=7.2 Hz, H_{glc}-3), 5.11 (dd, 1H, J=2.9, 13.1 Hz, H_{glc}-6), 5.15 (t, 1H, J=7.2 Hz, H_{glc}-4), 5.47 (d, 1H, J=4.8 Hz, H_{glc}-1), 5.53 (ddd, 1H, J=0.8, 2.9, 7.5 Hz, H_{glc}-5), 6.63 (s, 2H, H_C-3 & H_E-3), 6.77 (s, 1H, H_D-3), 7.24 (s, 1H, H_F-3).[151]

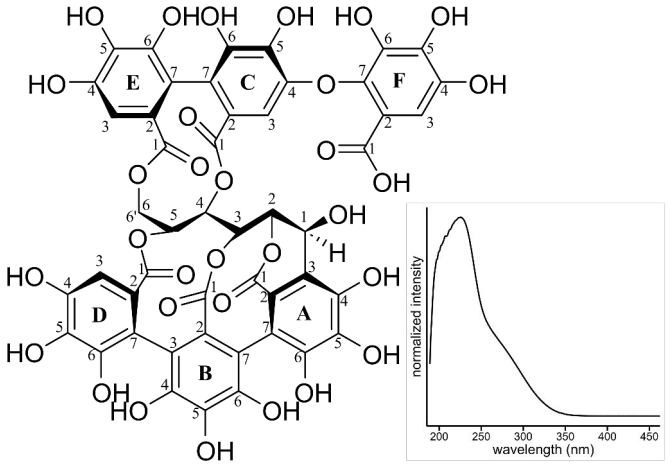

vescavaloninic acid (28) was isolated from *Quercus robur* leaves; purity measured by UPLC-DAD at 280 nm 97.6%; ESI-MS identification: *m/z* at 1101.06694 (**[M–**

H]$^{-}$, error –2.6 ppm), 1083.06042 ([M–H_2O–H]$^{-}$, error 1.1 ppm), 1039.06982 ([M–COOH–H_2O–H]$^{-}$, error 0.4 ppm), 915.05542 ([M–gallic acid–H_2O–H]$^{-}$, error 2.2 ppm), 613.04584 ([M–valoneoyl group–H_2O–H]$^{-}$, error –2.1 ppm), 425.01169 ([valoneic acid dilactone–H_2O–H]$^{-}$, error 6.0 ppm), 300.99875 ([ellagic acid–H]$^{-}$, error –0.8 ppm); ^{1}H-NMR (600 MHz, acetone-d_6, 298 K): δ 4.02 (d, 1H, J=12.4 Hz, H_{glc}-6'), 4.62 (dd, 1H, J=1.3, 6.8 Hz, H_{glc}-3), 4.98 (d, 1H, J=2.1 Hz, H_{glc}-1), 5.05 (dd, 1H, J=2.6, 13.1 Hz, H_{glc}-6), 5.18 (br t, 1H, J=1.7 Hz, H_{glc}-2), 5.22 (t, 1H, J=6.9 Hz, H_{glc}-4), 5.63 (ddd, 1H, J=1.3, 2.3, 7.1 Hz, H_{glc}-5), 6.61 (s, 1H, H_E-3), 6.76 (s, 1H, H_D-3), 7.05 (s, 1H, H_C-3), 7.18 (s, 1H, H_F-3).

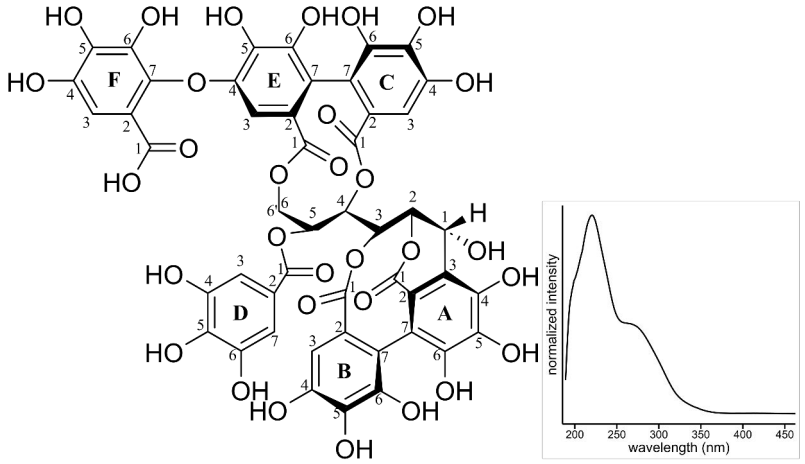

hippophaenin B (29) was isolated from *Hippophaë rhamnoides* leaves; purity measured by UPLC-DAD at 280 nm 99.9%; ESI-MS identification: *m/z* at 1103.08271 ([M–H]$^{-}$, error –2.5 ppm), 1059.09599 ([M–COOH–H]$^{-}$, error 0.3 ppm), 935.07666 ([M–gallic acid–H]$^{-}$, error 3.1 ppm), 633.07186 ([M–valoneic acid dilactone–H]$^{-}$, error –2.3 ppm), 481.06016 ([M–valoneic acid dilactone–galloyl–H]$^{-}$, error –4.6 ppm), 300.99829 ([ellagic acid–H]$^{-}$, error –2.3 ppm), 169.01476 ([gallic acid–H]$^{-}$, error 3.0 ppm), 125.02515 ([gallic acid–COOH–H]$^{-}$, error 5.9 ppm); ^{1}H-NMR (500 MHz, acetone-d_6, 298 K): δ 4.02 (d, 1H, J=13.2 Hz, H_{glc}-6'), 4.66 (dd, 1H, J=2.3, 4.9 Hz, H_{glc}-2), 4.71 (dd, 1H, J=3.6, 13.4 Hz, H_{glc}-6), 5.27 (dd, 1H, J=3.2, 9.3 Hz, H_{glc}-5), 5.35 (dd, 1H, J=2.4, 9.2 Hz, H_{glc}-4), 5.37 (br t, 1H, J=2.3 Hz, H_{glc}-3), 5.64 (d, 1H, J=4.9 Hz, H_{glc}-1), 6.25 (s, 1H, H_E-3), 6.47 (s, 1H, H_B-3), 6.74 (s, 1H, H_C-3), 7.04 (s, 2H, H_D-3,7), 7.13 (s, 1H, H_F-3).[152,153]

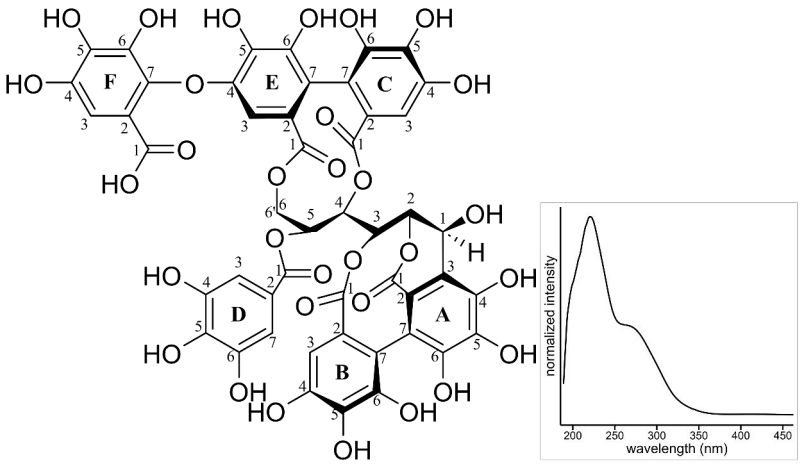

hippophaenin C (30) was isolated from *Hippophaë rhamnoides* leaves; purity measured by UPLC-DAD at 280 nm 96.2%; For the MS and NMR characterization of hippophaenin C see Suvanto *et al*., 2018.[154]

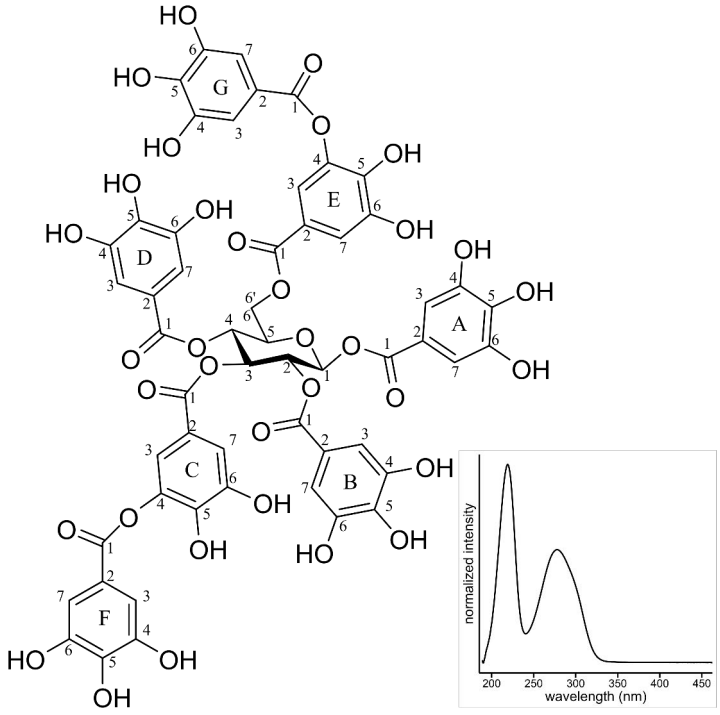

heptagalloylglucose (31) was isolated from *Acer platanoides* leaves; purity measured by UPLC-DAD at 280 nm 97.2%; ESI-MS identification: *m/z* at 1243.13075 (**[M–H]**$^-$, error –1.7 ppm), 1091.11926 ([M–galloyl–H]$^-$, error –2.4 ppm), 939.11058 ([M–2galloyl–H]$^-$, error –0.3 ppm), 787.10165 ([M–3galloyl—H]$^-$

, error –2.2 ppm), 769.09008 ([M–2galloyl–gallic acid–H]$^-$, error 0.9 ppm), 617.07895 ([M–3galloyl–gallic acid–H]$^-$, error 0.6 ppm), 465.06737 ([M–4galloyl–gallic acid–H]$^-$, error –0.2 ppm), 313.05700 ([M–5galloyl–gallic acid–H]$^-$, error 1.6 ppm), 169.01316 ([gallic acid–H]$^-$, error –6.4 ppm), 125.02290 ([gallic acid–COOH–H]$^-$, error –12.1 ppm); ^{1}H-NMR (600 MHz, acetone-d_6, 298 K (aromatic assignations with an asterisk are not definitive)): δ 4.47 (dd, 1H, J=4.8, 12.5 Hz, H_{glc}-6'), 4.54 (dd, 1H, J=2.2, 12.5 Hz, H_{glc}-6), 4.59 (ddd, 1H, J=2.3, 4.8, 10.0 Hz, H_{glc}-5), 5.64 (dd, 1H, J=8.3, 9.8 Hz, H_{glc}-2), 5.67 (t, 1H, J=9.7 Hz, H_{glc}-4), 6.02 (t, 1H, J=9.6 Hz, H_{glc}-3), 6.34 (d, 1H, J=8.3 Hz, H_{glc}-1), 7.01 (s, 2H, H_B-3,7), 7.06 (s, 2H, H_D-3,7), 7.10 (s, 2H, H_A-3,7), 7.24 (s, 3H, H_F-3,7 & H_C-7*), 7.29 (s, 2H, H_G-3,7), 7.30 (d, 1H, J=2.0 Hz, H_C-3*), 7.39 (d, 1H, J=2.0 Hz, H_E-7*), 7.51 (d, 1H, J=2.0 Hz, H_E-3*).[142,150]

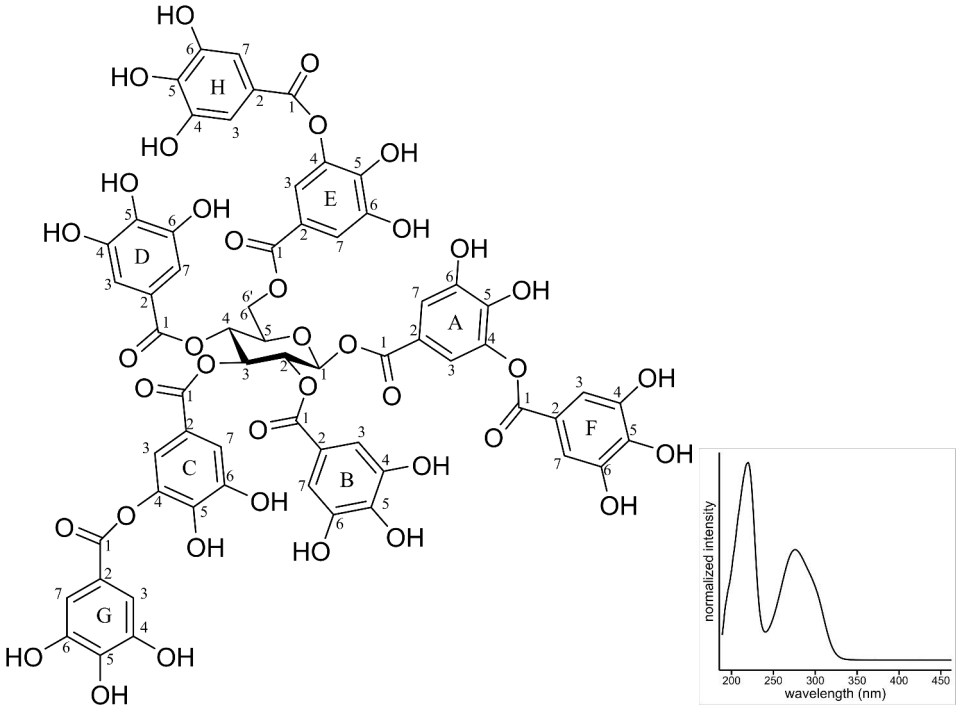

octagalloylglucose (32) was isolated from *Acer platanoides* leaves; purity measured by UPLC-DAD at 280 nm 97.2%; ESI-MS identification: *m/z* at 1395.14564 (**[M–H]**$^-$, error 1.3 ppm), 169.01319 ([gallic acid–H]$^-$, error –6.2 ppm), 125.02290 ([gallic acid–COOH–H]$^-$, error –12.1 ppm); ^{1}H-NMR (600 MHz, acetone-d_6, 298 K (aromatic assignations with an asterisk are not definitive)): δ 4.48 (dd, 1H, J=4.5, 12.3 Hz, H_{glc}-6'), 4.54 (dd, 1H, J=2.0, 12.2 Hz, H_{glc}-6), 4.60 (ddd, 1H, J=2.2, 4.4, 10.0 Hz, H_{glc}-5), 5.65 (dd, 1H, J=8.3, 9.8 Hz, H_{glc}-2), 5.69 (t, 1H, J=9.8 Hz, H_{glc}-4), 6.02 (t, 1H, J=9.6 Hz, H_{glc}-3), 6.36 (d, 1H, J=8.2 Hz, H_{glc}-1), 7.02 (s, 2H, H_B-3,7),

7.06 (s, 2H, H_D-3,7),7.24 (s, 3H, H_F-3,7 & H_C-7*),7.26 (s, 2H, H_H-3,7),7.27 (s, 2H, H_G-3,7),7.28–7.55 (m, 5H, H_C-3*, H_E-3*, H_E-7*, H_A-3* & H_A-7*).[142,150]

gallotannin mixture (33) was isolated from *Acer platanoides* leaves and contains hexa–hexadecagalloylglucoses; purity measured by UPLC-DAD at 280 nm 97.2%; ESI-MS identification: *m/z* at 1305.11113 ([hexadecagalloylglucose–2H]$^{2-}$, error –0.7 ppm), 1229.10762 ([pentadecagalloylglucose–2H]$^{2-}$, error 0.8 ppm), 1153.10186 ([tetradecagalloylglucose–2H]$^{2-}$, error 0.6 ppm), 1077.09562 ([tridecagalloylglucose–2H]$^{2-}$, error –0.03 ppm), 1001.08905 ([dodecagalloylglucose–2H]$^{2-}$, error –1.1 ppm), 925.08349 ([undecagalloylglucose–2H]$^{2-}$, error –1.3 ppm), 849.07826 ([decagalloylglucose–2H]$^{2-}$, error –1.1 ppm), 773.07236 ([nonagalloylglucose–2H]$^{2-}$, error –1.7 ppm), 697.06675 ([octagalloylglucose–2H]$^{2-}$, error –2.2 ppm), 621.06172 ([heptagalloylglucose–2H]$^{2-}$, error –1.7 ppm), 545.05607 ([hexagalloylglucose–2H]$^{2-}$, error –2.2 ppm), 169.01301 ([gallic acid–H]$^-$, error –7.4 ppm), 125.02291 ([gallic acid–COOH–H]$^-$, error –12.1 ppm).

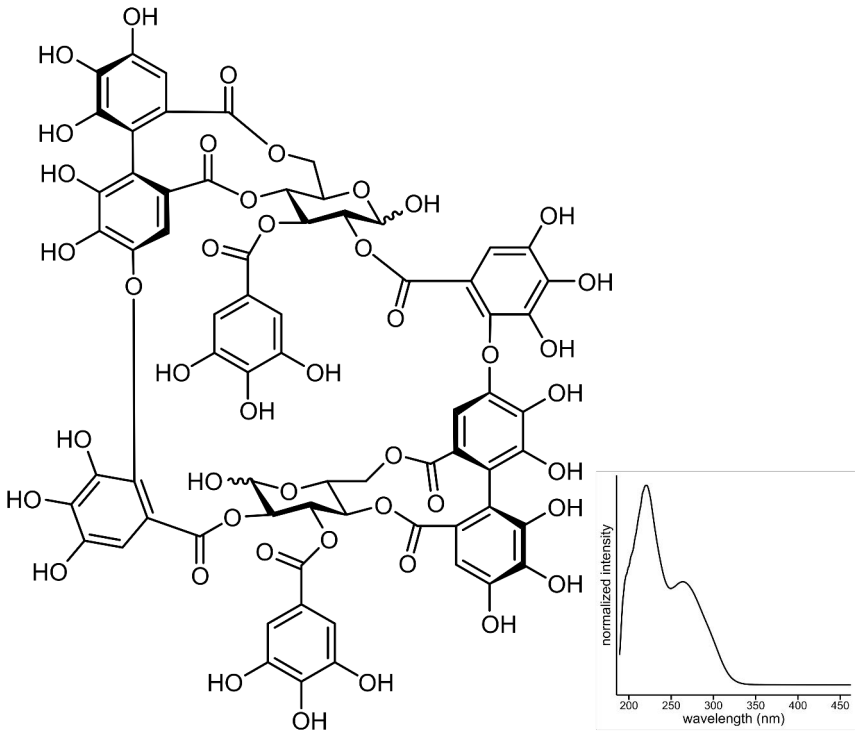

oenothein B (34) was isolated from *Chamaenerion angustifolium* leaves; purity measured by UPLC-DAD at 280 nm 97.6%; ESI-MS identification: *m/z* at 1567.14171 (**[M–H]**$^-$, error –1.8 ppm), 935.07645 ([M–galloyl-HHDP-glucose–H]$^-$, error –3.3 ppm), 785.08270 ([M–digalloyl-HHDP-glucose–H]$^-$, error –2.0 ppm),

783.06794 (**[M–2H]$^{2-}$**, error –0.9 ppm), 765.05828 ([M–digalloyl-HHDP-glucose–H_2O–H]$^-$, error 0.3 ppm), 300.99866 ([ellagic acid–H]$^-$, error –1.1 ppm); ^{1}H-NMR assignations could not be made reliably due to the two anomeric glucoses producing many isomers and furthermore due to the macrocyclic structure slowing down the broad signal producing interconversions.[155]

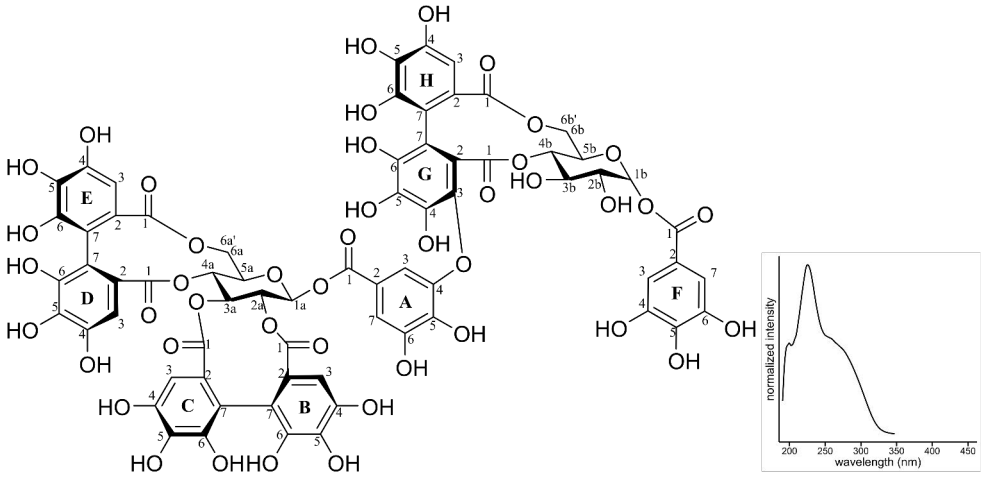

roshenin C (35) was isolated from *Rubus idaeus* leaves; purity measured by UPLC-DAD at 280 nm 94.2%; ESI-MS identification: *m/z* at 1567.14663 (**[M–H]$^-$**, error 2.1 ppm), 1235.07088 ([M–galloylglucose–H]$^-$, error 0.7 ppm), 933.06674 ([M–galloyl-HHDP-glucose–H]$^-$, error 2.8 ppm), 783.06944 (**[M–2H]$^{2-}$**, error 0.8 ppm), 633.07306 ([M–galloyl-diHHDP-glucose–H]$^-$, error –0.3 ppm), 300.99928 ([ellagic acid–H]$^-$, error 0.3 ppm); ^{1}H-NMR (600 MHz, acetone-d_6, 298 K): δ 3.47 (t, 1H, J=9.7 Hz, H_{glc}-5b), 3.69 (dd, 1H, J=4.2, 9.7 Hz, H_{glc}-2b), 3.72 (d, 1H, J=12.9 Hz, H_{glc}-6b'), 3.73 (m, 1H, H_{glc}-3b), 3.75 (d, 1H, J=13.1 Hz, H_{glc}-6a'), 4.21 (ddd, 1H, J=0.9, 6.9, 9.4 Hz, H_{glc}-5a), 4.65 (t, 1H, J=10.0 Hz, H_{glc}-4b), 5.09 (t, 1H, J=10.1 Hz, H_{glc}-4a), 5.21 (d, 1H, J=8.8 Hz, H_{glc}-2a), 5.24 (dd, 1H, J=6.8, 13.3 Hz, H_{glc}-6a), 5.29 (dd, 1H, J=6.7, 13.3 Hz, H_{glc}-6b), 5.35 (dd, 1H, J=9.5, 10.0 Hz, H_{glc}-3a), 6.04 (d, 1H, J=8.4 Hz, H_{glc}-1a), 6.20 (d, 1H, J=4.0 Hz, H_{glc}-6b).[156]

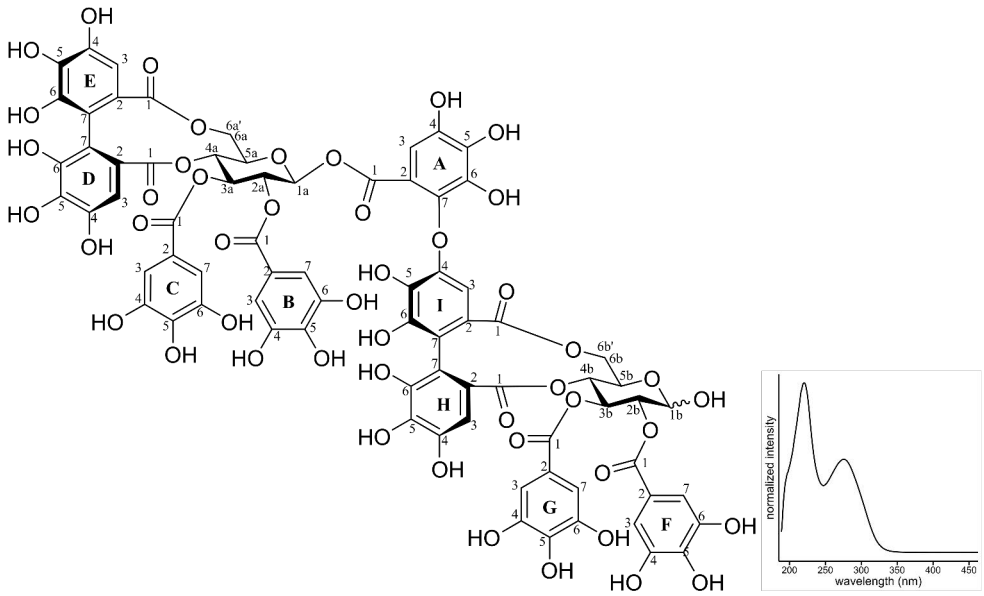

rugosin E (36) was isolated from *Filipdendula ulmaria* flowers; purity measured by UPLC-DAD at 280 nm 91.2%; ESI-MS identification: *m/z* at 1721.17009 (**[M–H]**$^{-}$, error –0.6 ppm), 937.09636 ([M–digalloyl-HHDP-glucose–H]$^{-}$, error 1.2 ppm), 860.08201 (**[M–2H]**$^{2-}$, error 0.1 ppm), 785.08544 ([M–trigalloyl-HHDP-glucose–H]$^{-}$, error 1.5 ppm), 767.07242 ([M– trigalloyl-HHDP-glucose–H_2O–H]$^{-}$, error –1.7 ppm), 300.99898 ([ellagic acid–H]$^{-}$, error –0.03 ppm); ^{1}H-NMR (600 MHz, acetone-d_6, 298 K, α-anomer (70%)): δ 3.67 (d, 1H, J=12.5 Hz, H_{glc}-6b'), 3.82 (d, 1H, J=13.0 Hz, H_{glc}-6a'), 4.50 (dd, 1H, J=6.3, 10.1 Hz, H_{glc}-5a), 4.64 (dd, 1H, J=7.2, 9.6 Hz, H_{glc}-5b), 5.06 (t, 1H, J=10.1 Hz, H_{glc}-4b), 5.14 (dd, 1H, J=3.7, 10.1 Hz, H_{glc}-2b), 5.18 (t, 1H, J=10.0 Hz, H_{glc}-4a), 5.22 (dd, 1H, J=6.6, 12.8 Hz, H_{glc}-6b), 5.32 (dd, 1H, J=6.6, 13.4 Hz, H_{glc}-6a), 5.55 (d, 1H, J=3.7 Hz, H_{glc}-1b), 5.56 (dd, 1H, J=8.8, 9.8 Hz, H_{glc}-2a), 5.80 (t, 1H, J=9.8 Hz, H_{glc}-3a), 5.87 (t, 1H, J=10.0 Hz, H_{glc}-3b), 6.15 (d, 1H, J=8.3 Hz, H_{glc}-1a), 6.24 (s, 1H, H_I-3), 6.47 (s, 1H, H_D-3), 6.49 (s, 1H, H_H-3), 6.66 (s, 1H, H_E-3), 6.98 (s, 2H, H_F-3,7), 7.021 (s, 2H, H_G-3,7), 7.026 (s, 2H, H_B-3,7), 7.16 (s, 1H, H_A-3).^{1}H-NMR (600 MHz, acetone-d_6, 298 K, β-anomer (30%)): δ 3.75 (d, 1H, J=13.0 Hz, H_{glc}-6a'), 3.82 (d, 1H, J=13.2 Hz, H_{glc}-6b'), 4.24 (dd, 1H, J=6.5, 9.9 Hz, H_{glc}-5b), 4.49 (dd, 1H, J=6.1, 10.2 Hz, H_{glc}-5a), 5.07 (t, 1H, J=10.1 Hz, H_{glc}-4b), 5.08 (d, 1H, J=8.1 Hz, H_{glc}-1b), 5.18 (t, 1H, J=10.0 Hz, H_{glc}-4a), 5.24 (dd, 1H, J=6.6, 12.6 Hz, H_{glc}-6b), 5.27 (dd, 1H, J=8.0, 9.5 Hz, H_{glc}-2b), 5.32 (dd, 1H, J=6.5, 12.2 Hz, H_{glc}-6a), 5.55 (dd, 1H, J=7.8, 9.7 Hz, H_{glc}-2a), 5.61 (t, 1H, J=9.8 Hz, H_{glc}-3b), 5.80 (t, 1H, J=9.8 Hz, H_{glc}-3a), 6.14 (d, 1H, J=8.3 Hz, H_{glc}-1a), 6.23 (s, 1H, H_I-3), 6.466 (s, 1H, H_H-3), 6.471 (s, 1H, H_D-3), 6.66 (s, 1H, H_E-3), 6.98 (s, 2H, H_G-3,7), 7.07 (s, 2H, H_F-3,7), 7.02 (s, 2H, H_B-3,7), 7.08 (s, 2H, H_C-3,7), 7.16 (s, 1H, H_A-3).[157,158]

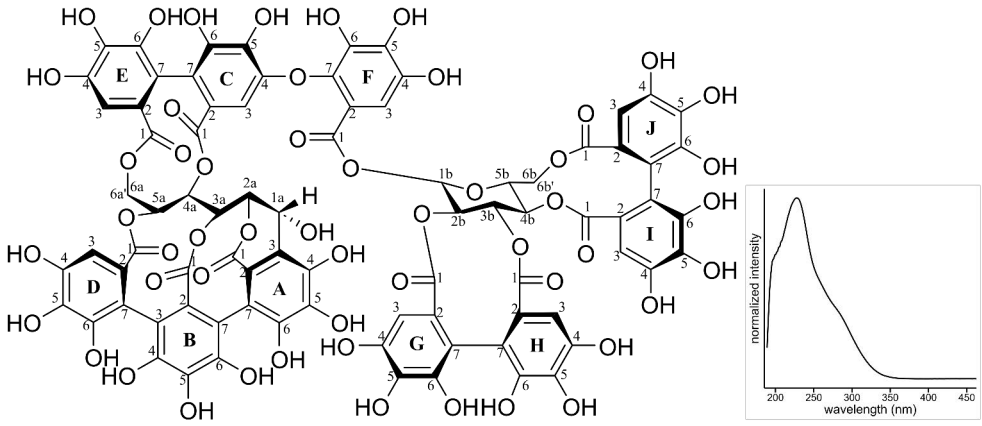

cocciferin D_2 (37) was isolated from *Quercus robur* acorns; purity measured by UPLC-DAD at 280 nm 93.0%; ESI-MS identification: *m/z* at 1867.12800 (**[M–H]**$^-$, error –3.8 ppm), 1567.12757 ([M–HHDP–H]$^-$, error –0.9 ppm), 1101.07569 ([M–diHHDP-glucose–H]$^-$, error 5.3 ppm), 1083.06439 ([M–diHHDP-glucose–H_2O–H]$^-$, error 4.7 ppm), 933.06279 (**[M–2H]**$^{2-}$, error –1.2 ppm), 933.06589 ([M–galloyl-diHHDP-glucose–H]$^-$, error 2.1 ppm), 915.05486 ([M–diHHDP-glucose–H_2O–H]$^-$, error 1.6 ppm), 783.06729 ([M–NHTP-valoneoyl-glucose–H]$^-$, error –1.7 ppm), 631.05688 ([M–diHHDP-valoneoyl-glucose–H]$^-$, error –1.3 ppm), 300.99911 ([ellagic acid–H]$^-$, error 0.4 ppm); ^{1}H-NMR (600 MHz, acetone-d_6, 298 K): δ 3.86 (d, 1H, J=12.8 Hz, H_{glc}-6b'), 3.98 (d, 1H, J=12.9 Hz, H_{glc}-6a'), 4.43 (ddd, 1H, J=0.9, 6.9, 9.8 Hz, H_{glc}-5b), 4.77 (dd, 1H, J=1.2, 4.9 Hz, H_{glc}-2a), 4.91 (dd, 1H, J=1.1, 6.9 Hz, H_{glc}-5), 5.12 (t, 1H, J=7.3 Hz, H_{glc}-4a), 5.13 (t, 1H, J=8.8 Hz, H_{glc}-2b), 5.14 (dd, 1H, J=1.8, 12.8 Hz, H_{glc}-6a), 5.14 (t, 1H, J=10.1 Hz, H_{glc}-4b), 5.31 (dd, 1H, J=6.8, 13.3 Hz, H_{glc}-6b), 5.38 (dd, 1H, J=9.4, 10.0 Hz, H_{glc}-3a), 5.41 (d, 1H, J=4.9 Hz, H_{glc}-1a), 5.55 (dd, 1H, J=2.2, 7.4 Hz, H_{glc}-3b), 6.15 (d, 1H, J=8.6 Hz, H_{glc}-1b), 6.35 (s, 1H, H_H-3), 6.41 (s, 1H, H_C-3), 6.49 (s, 1H, H_G-3), 6.51 (s, 1H, H_I-3), 6.59 (s, 1H, H_E-3), 6.68 (s, 1H, H_J-3), 6.78 (s, 1H, H_D-3), 7.27 (s, 1H, H_F-3).[71]

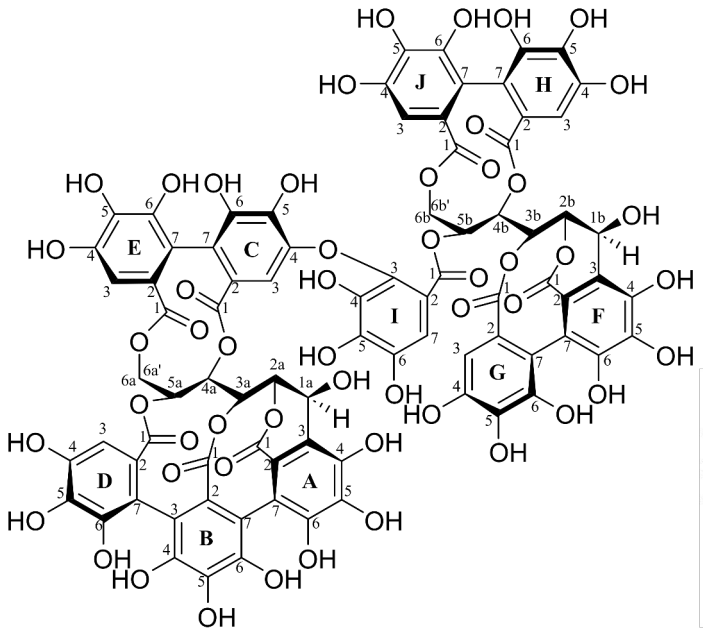

salicarinin A (38) was isolated from *Lythrum salicaria* leaves; purity measured by UPLC-DAD at 280 nm 96.0%; ESI-MS identification: *m/z* at 1867.13022 (**[M–H]**$^{-}$, error –2.7 ppm), 1083.05526 ([M–diHHDP-glucose–H]$^{-}$, error –3.7 ppm), 933.06297 (**[M–2H]**$^{2-}$, error –1.1 ppm), 933.06588 ([M–galloyl-diHHDP-glucose–H]$^{-}$, error 2.1 ppm), 924.05736 ([M–H_2O–2H]$^{2-}$, error –1.4 ppm), 915.05204 ([M–$2H_2O$–2H]$^{2-}$, error –1.5 ppm), 915.05429 ([M–galloyl-diHHDP-glucose–H_2O–H]$^{-}$, error –2.7 ppm), 300.99885 ([ellagic acid–H]$^{-}$, error -0.5 ppm); ^{1}H-NMR (500 MHz, acetone-d_6, 298 K): δ 3.89 (d, 1H, J=12.9 Hz, H_{glc}-6b'), 3.95 (d, 1H, J=12.5 Hz, H_{glc}-6a'), 4.64 (dd, 1H, J=1.1, 6.7 Hz, H_{glc}-3a), 4.83 (m, 2H, H_{glc}-1b & H_{glc}-2b), 4.85 (dd, 1H, J=3.5, 13.4 Hz, H_{glc}-6b), 4.927 (t, 1H, J=2.0 Hz, H_{glc}-3b), 4.929 (d, 1H, J=2.0 Hz, H_{glc}-1a), 5.08 (dd, 1H, J=2.4, 13.1 Hz, H_{glc}-6a), 5.14 (br s, 1H, H_{glc}-2a), 5.19 (t, 1H, J=6.8 Hz, H_{glc}-4a), 5.40 (dd, 1H, J=3.5, 13.4 Hz, H_{glc}-5b), 5.55 (dd, 1H, J=2.5, 8.6 Hz, H_{glc}-4b), 5.63 (br d, 1H, J=6.8 Hz, H_{glc}-5a), 6.54 (s, 1H, H_G-3), 6.59 (s, 1H, H_E-3), 6.62 (s, 1H, H_J-3), 6.78 (s, 1H, H_D-3), 6.83 (s, 1H, H_C-3), 6.86 (s, 1H, H_H-3), 7.07 (s, 1H, H_I-3).[159]

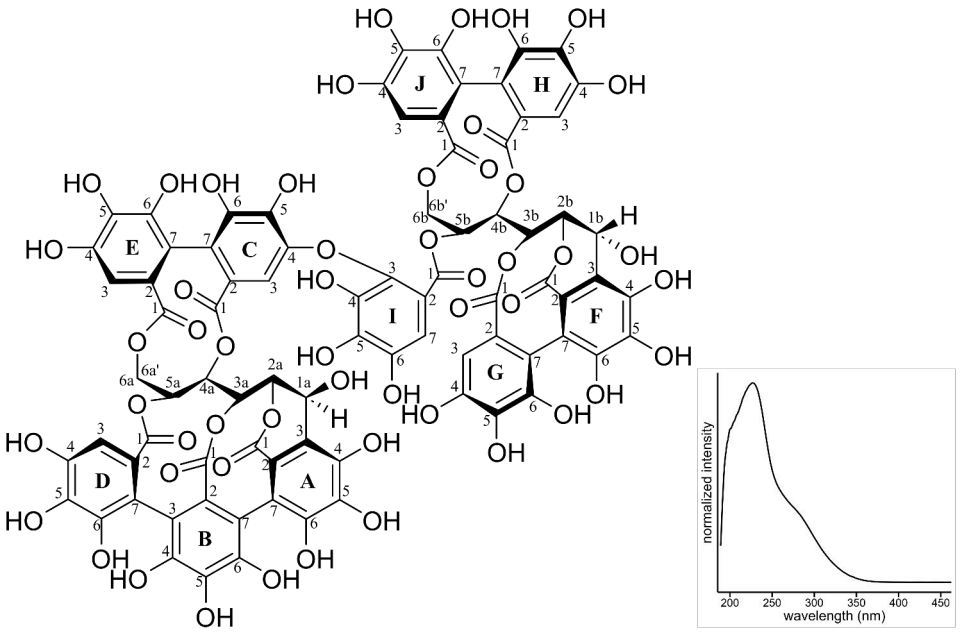

salicarinin B (39) was isolated from *Lythrum salicaria* leaves; purity measured by UPLC-DAD at 280 nm 75.2%; ESI-MS identification: *m/z* at 1867.12697 (**[M–H]**$^{-}$, error –4.4 ppm), 935.08098 ([M–NHTP-HHDP-glucose–H]$^{-}$, error 1.5 ppm), 933.06568 (**[M–2H]**$^{2-}$, error –1.5 ppm), 933.06588 ([M–galloyl-diHHDP-glucose–H]$^{-}$, error 1.9 ppm), 924.05744 ([M–H_2O–2H]$^{2-}$, error –1.3 ppm), 915.05408 ([M–galloyl-diHHDP-glucose–H_2O–H]$^{-}$, error 0.8 ppm), 300.99897 ([ellagic acid–H]$^{-}$, error –0.1 ppm); ^{1}H-NMR (500 MHz, acetone-d_6, 298 K): δ 4.04 (d, 1H, J=12.1 Hz, H_{glc}-6a'), 4.21 (d, 1H, J=13.3 Hz, H_{glc}-6b'), 4.51 (dd, 1H, J=2.1, 5.0 Hz, H_{glc}-2b), 4.74 (dd, 1H, J=3.9, 13.4 Hz, H_{glc}-6b), 4.89 (dd, 1H, J=0.9, 6.7 Hz, H_{glc}-3a), 4.94 (br t, 1H, J=2.0 Hz, H_{glc}-3b), 5.11 (dd, 1H, J=2.3, 9.2 Hz, H_{glc}-4b), 5.15 (d, 1H, J=2.0 Hz, H_{glc}-1a), 5.17 (dd, 1H, J=2.5, 13.4 Hz, H_{glc}-6a), 5.21 (m, 1H, H_{glc}-2a), 5.22 (t, 1H, J=6.4 Hz, H_{glc}-4a), 5.32 (dd, 1H, J=3.6, 9.3 Hz, H_{glc}-5b), 5.47 (d, 1H, J=5.0 Hz, H_{glc}-1b), 5.69 (br d, 1H, J=5.8 Hz, H_{glc}-5a), 6.52 (s, 1H, H_G-3), 6.72 (s, 1H, H_J-3), 6.77 (s, 1H, H_E-3), 6.78 (s, 1H, H_H-3), 6.82 (s, 1H, H_D-3), 6.94 (s, 1H, H_I-3), 7.01 (s, 1H, H_C-3).[159]

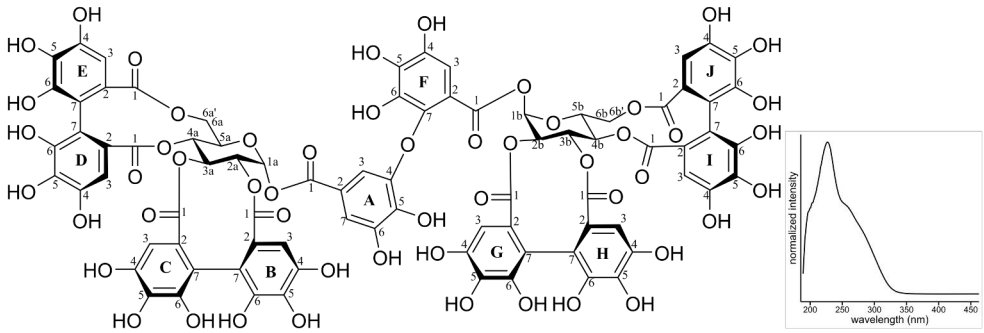

agrimoniin (40) was isolated from *Argentina anserina* leaves; purity measured by UPLC-DAD at 280 nm 97.6%; ESI-MS identification: *m/z* at 1869.14605 (**[M–H]**$^{-}$, error –2.6 ppm), 1085.07578 ([M–diHHDP-glucose–H]$^{-}$, error 0.8 ppm), 935.07890 ([M–galloyl-diHHDP-glucose–H]$^{-}$, error –0.8 ppm), 934.07168 (**[M–2H]**$^{2-}$, error –0.1 ppm), 915.05659 ([M–galloyl-diHHDP-glucose–H_2O–H]$^{-}$, error –0.8 ppm), 783.006953 ([M–digalloyl-diHHDP-glucose–H_2O–H]$^{-}$, error 1.1 ppm), 631.07502 ([M–galloyl-diHHDP-glucose–HHDP–H]$^{-}$, error 2.7 ppm), 300.99857 ([ellagic acid–H]$^{-}$, error –1.4 ppm); ^{1}H-NMR (600 MHz, acetone-d_6, 298 K): δ 3.69 (d, 1H, J=13.0 Hz, H_{glc}-6b'), 3.79 (d, 1H, J=12.8 Hz, H_{glc}-6a'), 4.49 (dd, 1H, J=6.5, 10.2 Hz, H_{glc}-5b), 4.65 (dd, 1H, J=6.5, 10.2 Hz, H_{glc}-5a), 5.16 (t, 1H, J=10.4 Hz, H_{glc}-4b), 5.20 (t, 1H, J=10.3 Hz, H_{glc}-4a), 5.23 (dd, 1H, J=6.5, 13.2 Hz, H_{glc}-6a), 5.32 (dd, 1H, J=6.6, 13.4 Hz, H_{glc}-6b), 5.36 (dd, 1H, J=3.9, 9.5 Hz, H_{glc}-2b), 5.37 (dd, 1H, J=3.8, 9.6 Hz, H_{glc}-2a), 5.49 (t, 1H, J=9.8 Hz, H_{glc}-3b), 5.55 (t, 1H, J=9.8 Hz, H_{glc}-3a), 6.34 (s, 1H, H_H-3), 6.35 (s, 1H, H_C-3), 6.44 (s, 1H, H_G-3), 6.54 (dd, 1H, J=4.0 Hz, H_{glc}-1a), 6.55 (s, 1H, H_B-3), 6.56 (dd, 1H, J=4.0 Hz, H_{glc}-1b), 6.60 (s, 1H, H_D-3), 6.61 (s, 1H, H_I-3), 6.65 (s, 1H, H_E-3), 6.66 (s, 1H, H_J-3), 6.94 (d, 1H, J=1.9 Hz, H_A-7), 7.30 (s, 1H, H_F-3), 7.39 (d, 1H, J=1.9 Hz, H_A-3).[160]

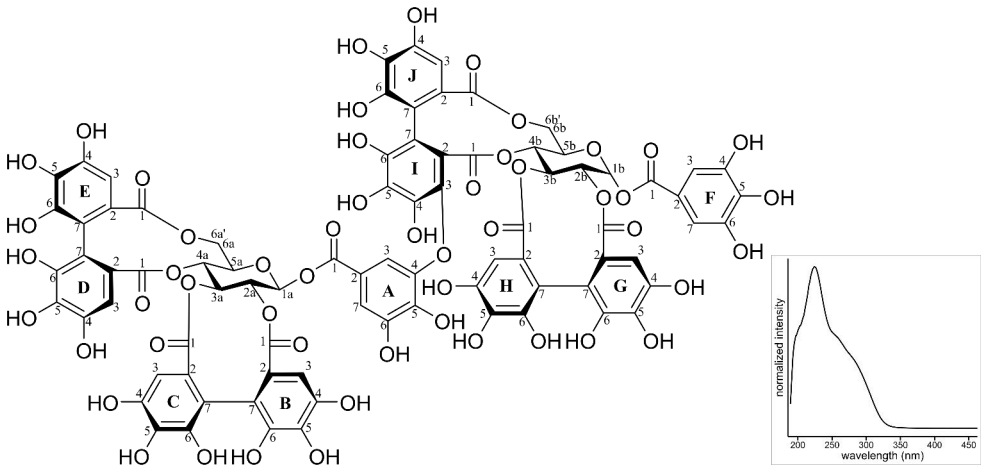

sanguiin H-6 (41) was isolated from *Rubus idaeus* leaves; purity measured by UPLC-DAD at 280 nm 97.1%; ESI-MS identification: *m/z* at 1869.14662 (**[M–H]**$^{-}$, error –2.3 ppm), 1235.06944 ([M–diHHDP-glucose–H]$^{-}$, error –0.6 ppm), 935.07820 ([M–galloyl-diHHDP-glucose–H]$^{-}$, error –1.5 ppm), 934.07153 (**[M–2H]**$^{2-}$, error –0.3 ppm), 633.07401 ([M–galloyl-diHHDP-glucose–HHDP–H]$^{-}$, error 1.1 ppm), 300.99875 ([ellagic acid–H]$^{-}$, error –0.8 ppm); ^{1}H-NMR (600 MHz, acetone-d_6, 298 K): δ 3.79 (d, 1H, J=13.1 Hz, H_{glc}-6a'), 3.90 (d, 1H, J=12.9 Hz, H_{glc}-6b'), 4.22 (br t, 1H, J=7.6 Hz, H_{glc}-5b), 4.36 (dd, 1H, J=7.0, 9.4 Hz, H_{glc}-5a), 5.02 (br t, 1H, J=9.5 Hz, H_{glc}-4b), 5.07 (br t, 1H, J=7.6 Hz, H_{glc}-3b), 5.11 (t, 1H, J=10.1 Hz, H_{glc}-4a), 5.20 (t, 1H, J=8.8 Hz, H_{glc}-2a), 5.24 (dd, 1H, J=6.6, 13.4 Hz, H_{glc}-6a), 5.28 (dd, 1H, J=4.0, 9.4 Hz, H_{glc}-2b), 5.37 (dd, 1H, J=9.2, 10.2 Hz, H_{glc}-3a), 5.58 (dd, 1H, J=6.5, 13.2 Hz, H_{glc}-6b), 6.17 (d, 1H, J=8.5 Hz, H_{glc}-1a), 6.300 (s, 1H, H_H-3), 6.303 (s, 1H, H_C-3), 6.38 (s, 1H, H_G-3), 6.47 (s, 1H, H_B-3), 6.50 (s, 1H, H_D-3), 6.53 (d, 1H, J=4.0 Hz, H_{glc}-1b), 6.76 (s, 1H, H_E-3), 6.78 (s, 1H, H_J-3), 7.10 (s, 2H, H_F-3,7), 7.14 (d, 1H, J=1.9 Hz, H_A-7), 7.28 (d, 1H, J=1.9 Hz, H_A-3).[138]

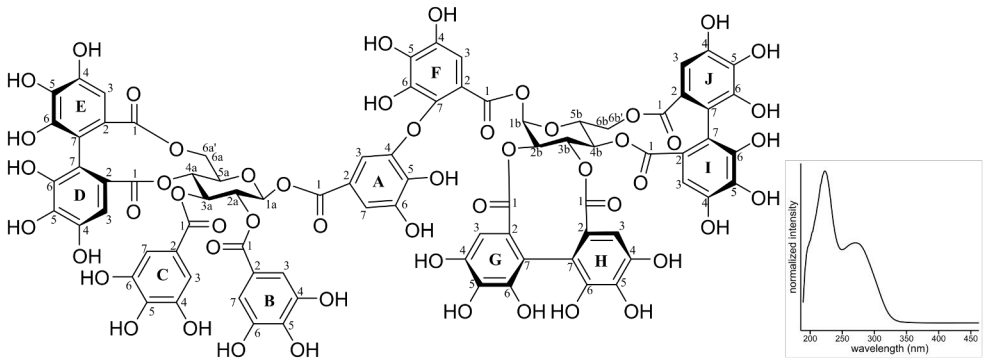

gemin A (42) was isolated from *Geum urbanum* leaves; purity measured by UPLC-DAD at 280 nm 96.9%; ESI-MS identification: *m/z* at 1871.16171 (**[M–H]**$^{-}$, error –2.6 ppm), 1087.08928 ([M–digalloyl-HHDP-glucose–H]$^{-}$, error –1.2 ppm), 937.09322 ([M–galloyl-diHHDP-glucose–H]$^{-}$, error –2.1 ppm), 935.07873 ([M–trigalloyl-HHDP-glucose–H]$^{-}$, error –0.9 ppm), 935.07866 (**[M–2H]**$^{2-}$, error –1.0 ppm), 785.08147([M–digalloyl-diHHDP-glucose–H]$^{-}$, error –3.6 ppm), 783.06924 ([M–tetragalloyl-HHDP-glucose–H]$^{-}$, error 0.8 ppm), 633.07541 ([M–digalloyl-diHHDP-glucose–galloyl–H]$^{-}$, error 3.3 ppm), 300.99871 ([ellagic acid–H]$^{-}$, error –0.9 ppm); ^{1}H-NMR (600 MHz, acetone-d_6, 298 K): δ 3.64 (d, 1H, J=13.3 Hz, H_{glc}-6b'), 3.75 (d, 1H, J=13.4 Hz, H_{glc}-6a'), 4.47 (dd, 1H, J=6.5, 10.2 Hz, H_{glc}-5b), 4.49 (dd, 1H, J=6.7, 9.4 Hz, H_{glc}-5a), 5.15 (t, 1H, J=10.3 Hz, H_{glc}-4b), 5.18 (t, 1H, J=10.0 Hz, H_{glc}-4a), 5.20 (dd, 1H, J=6.3, 12.9 Hz, H_{glc}-6a), 5.27 (dd, 1H, J=6.6, 13.4 Hz, H_{glc}-6b), 5.34 (dd, 1H, J=4.1, 9.3 Hz, H_{glc}-2b), 5.49 (t, 1H, J=9.8 Hz, H_{glc}-3b), 5.56 (dd, 1H, J=8.4, 9.5 Hz, H_{glc}-2a), 5.81 (t, 1H, J=9.8 Hz, H_{glc}-3a), 6.13 (d, 1H, J=8.3 Hz, H_{glc}-1a), 6.35 (s, 1H, H_H-3), 6.44 (s, 1H, H_G-3), 6.47 (s, 1H, H_I-3), 6.51 (d, 1H, J=4.0 Hz, H_{glc}-1b), 6.61 (s, 1H, H_D-3), 6.63 (s, 1H, H_J-3), 6.67 (s, 1H, H_E-3), 6.84 (d, 1H, J=1.9 Hz, H_A-7), 6.96 (s, 2H, H_C-3,7), 7.01 (s, 2H, H_B-3,7), 7.27 (d, 1H, J=1.9 Hz, H_A-3), 7.31 (s, 1H, H_F-3).[161]

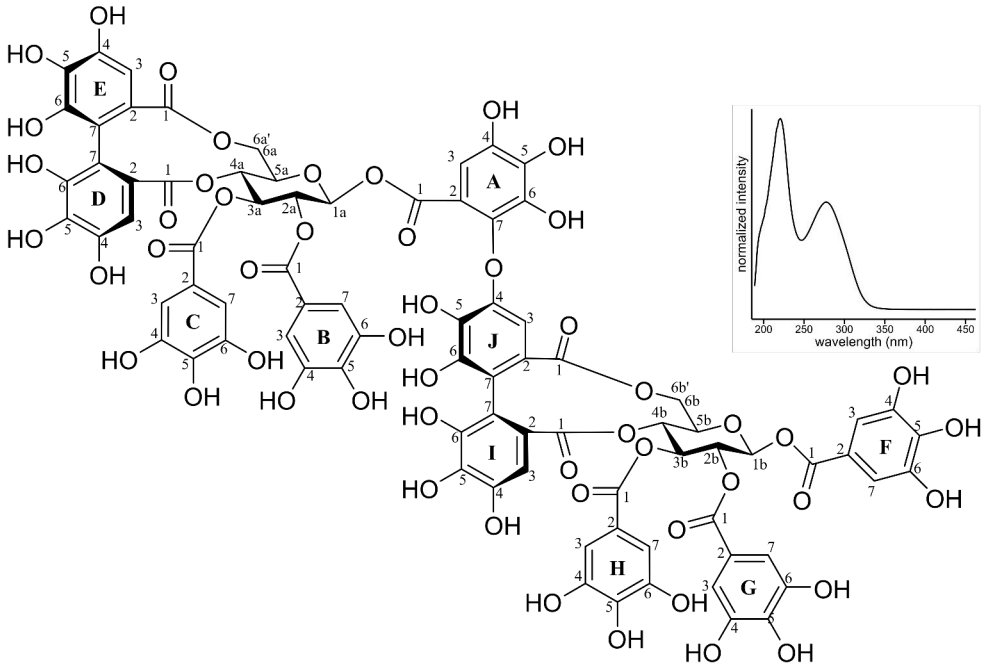

rugosin D (43) was isolated from *Filipendula ulmaria* flowers; purity measured by UPLC-DAD at 280 nm 90.7%; ESI-MS identification: *m/z* at 1873.17804 (**[M–H]**$^{-}$, error –2.2 ppm), 1087.08719 ([M–digalloyl-HHDP-glucose–H]$^{-}$, error –3.1 ppm), 937.09667 ([M–trigalloyl-HHDP-glucose–H]$^{-}$, error 1.5 ppm), 936.08715 (**[M–2H]**$^{2-}$, error –0.3 ppm), 785.08567 ([M–trigalloyl-valoneoyl-glucose–H]$^{-}$, error 1.8 ppm), 300.99901 ([ellagic acid–H]$^{-}$, error 0.1 ppm); ^{1}H-NMR (600 MHz, acetone-d_6, 298 K): δ 3.82 (d, 1H, J=13.4 Hz, H_{glc}-6a'), 3.79 (d, 1H, J=13.4 Hz, H_{glc}-6b'), 4.48 (dd, 1H, J=7.2, 10.0 Hz, H_{glc}-5a), 4.52 (dd, 1H, J=6.3, 10.0 Hz, H_{glc}-5b), 5.166 (t, 1H, J=10.0 Hz, H_{glc}-4b), 5.167 (t, 1H, J=10.0 Hz, H_{glc}-4a), 5.31 (dd, 1H, J=6.5, 13.4 Hz, H_{glc}-6b), 5.32 (dd, 1H, J=6.6, 13.5 Hz, H_{glc}-6a), 5.54 (dd, 1H, J=8.4, 9.5 Hz, H_{glc}-2a), 5.61 (dd, 1H, J=8.3, 9.5 Hz, H_{glc}-2b), 5.79 (t, 1H, J=9.8 Hz, H_{glc}-3a), 5.84 (t, 1H, J=9.7 Hz, H_{glc}-3b), 6.13 (d, 1H, J=8.3 Hz, H_{glc}-1a), 6.19 (d, 1H, J=8.3 Hz, H_{glc}-1b), 6.24 (s, 1H, H_J-3), 6.47 (s, 1H, H_I-3), 6.49 (s, 1H, H_D-3), 6.66 (s, 1H, H_E-3), 6.98 (s, 2H, H_B-3,7), 7.008 (s, 2H, H_G-3,7), 7.012 (s, 2H, H_C-3,7), 7.02 (s, 2H, H_H-3,7), 7.13 (s, 1H, H_F-3), 7.14 (s, 1H, H_A-3).[157,158]

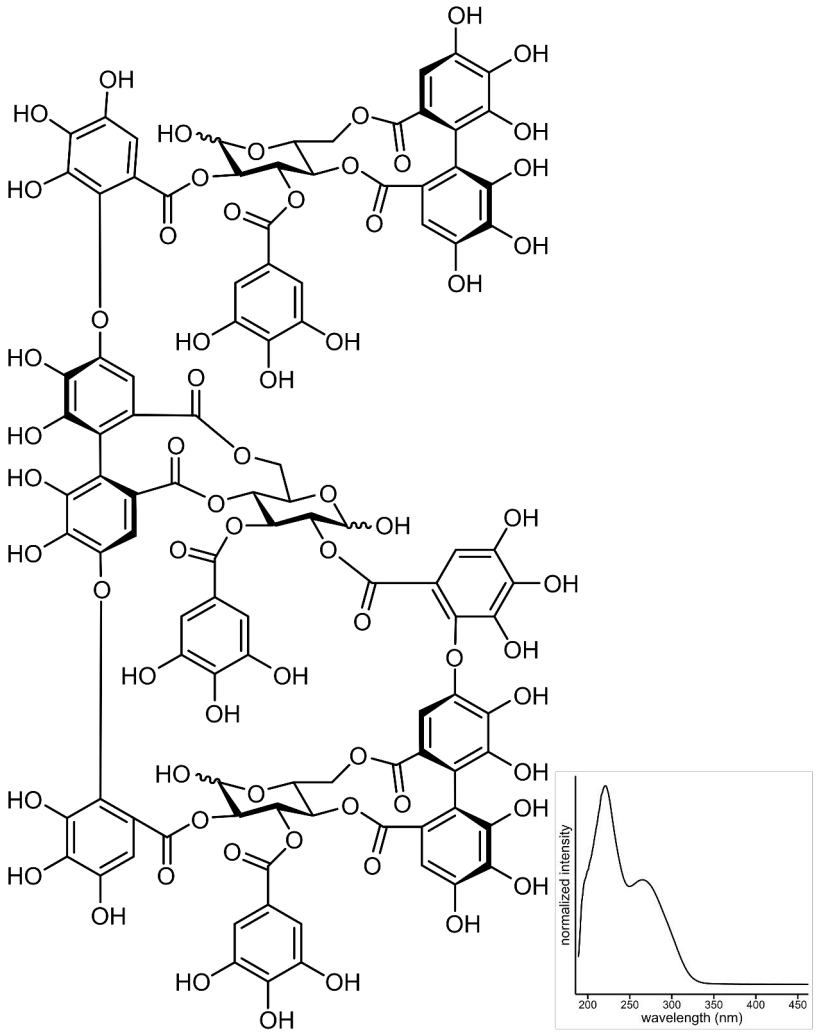

oenothein A (44) was isolated from *Chamaenerion angustifolium* leaves; purity measured by UPLC-DAD at 280 nm 84.5%; ESI-MS identification: *m/z* at 1719.15215 ([M–galloyl-HHDP-glucose–H]$^-$, error –2.0 ppm), 1567.14396 ([M–digalloyl-HHDP-glucose–H]$^-$, error –0.4 ppm), 1175.10645 (**[M–2H]$^{2-}$**, error –0.1 ppm), 935.07823 ([digalloyl-valonoeoyl-glucose–H]$^-$, error –1.5 ppm), 785.08300 ([digalloyl-HHDP-glucose–H]$^-$, error –1.7 ppm), 783.06889 (**[M–3H]$^{3-}$**, error 0.3 ppm), 633.07476 ([galloyl-HHDP-glucose–H]$^-$, error 2.2 ppm), 300.99868 ([ellagic acid–H]$^-$, error –1.0 ppm); ^{1}H-NMR assignations could not be made reliably due to the three anomeric glucoses producing many isomers and furthermore due to the macrocyclic structure slowing down the broad signal producing interconversions.[20]

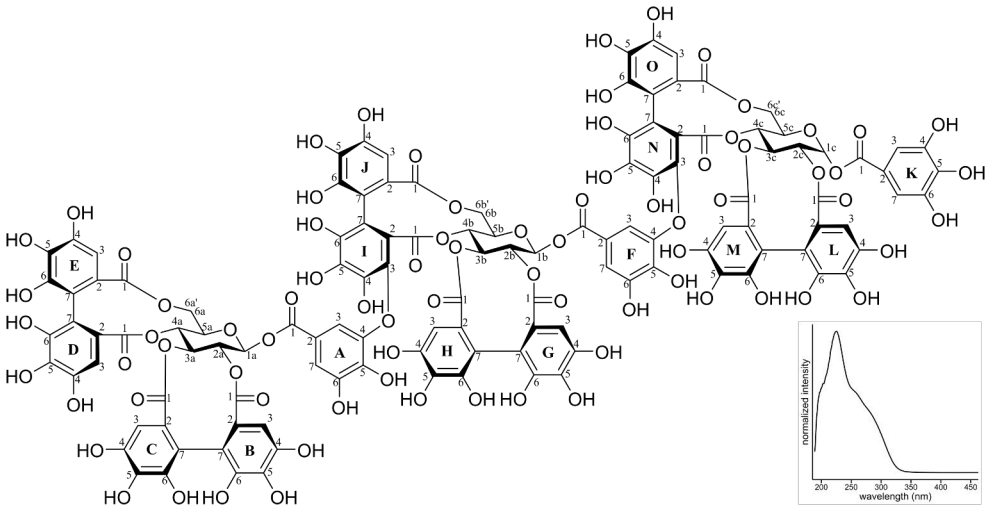

lambertianin C (45) was isolated from *Rubus idaeus* leaves; purity measured by UPLC-DAD at 280 nm 98.2%; ESI-MS identification: *m/z* at 1567.14103 ([M–diHHDP-valoneoyl-glucose–H]$^-$, error –2.3 ppm), 1401.10537 (**[M–2H]$^{2-}$**, error –1.4 ppm), 933.73523 (**[M–3H]$^{3-}$**, error –0.7 ppm), 935.08023 ([galloyl-diHHDP-glucose–H]$^-$, error 0.7 ppm), 633.07526 ([galloyl-HHDP-glucose–H]$^-$, error 3.0 ppm), 300.99878 ([ellagic acid–H]$^-$, error 0.7 ppm); ^{1}H-NMR (600 MHz, acetone-d_6, 298 K): δ 3.83 (d, 1H, J=13.2 Hz, H_{glc}-6b'), 3.88 (d, 1H, J=13.3 Hz, H_{glc}-6c'), 3.90 (d, 1H, J=13.3 Hz, H_{glc}-6a'), 4.03 (dd, 1H, J=6.1, 8.6 Hz, H_{glc}-5b), 4.17 (br t, 1H, J=7.2 Hz, H_{glc}-5c), 4.46 (ddd, 1H, J=1.0, 6.8, 9.8 Hz, H_{glc}-5a), 4.94 (m, 2H, H_{glc}-3b & H_{glc}-4b), 5.00 (t, 1H, J=10.2 Hz, H_{glc}-4c), 5.09 (t, 1H, J=8.8Hz, H_{glc}-3c), 5.11 (t, 1H, J=8.9 Hz, H_{glc}-2b), 5.13 (t, 1H, J=10.1 Hz, H_{glc}-4a), 5.17 (t, 1H, J=8.9 Hz, H_{glc}-2a), 5.27 (dd, 1H, J=4.0, 9.4 Hz, H_{glc}-2c), 5.35 (dd, 1H, J=6.7, 13.3 Hz, H_{glc}-6a), 5.44 (dd, 1H, J=9.3, 10.1 Hz, H_{glc}-3a), 5.49 (dd, 1H, J=6.5, 13.2 Hz, H_{glc}-6c), 5.62 (dd, 1H, J=6.4, 13.4 Hz, H_{glc}-6b), 5.98 (d, 1H, J=8.5 Hz, H_{glc}-1b), 6.17 (d, 1H, J=8.5 Hz, H_{glc}-1a), 6.26 (s, 1H, H_M-3), 6.28 (s, 1H, H_H-3), 6.34 (s, 2H, H_C-3 & H_D-3), 6.38 (s, 1H, H_L-3), 6.52 (d, 1H, J=3.9 Hz, H_{glc}-1c), 6.53 (s, 1H, H_B-3 & H_G-3), 6.68 (s, 1H, H_E-3), 6.78 (s, 1H, H_J-3), 6.85 (s, 1H, H_O-3), 7.06 (d, 1H, J=1.8 Hz, H_F-7), 7.11 (s, 2H, H_K-3,7), 7.12 (d, 1H, J=2.0 Hz, H_A-7), 7.16 (d, 1H, J=1.7 Hz, H_A-3), 7.25 (d, 1H, J=1.5 Hz, H_F-3).[138]

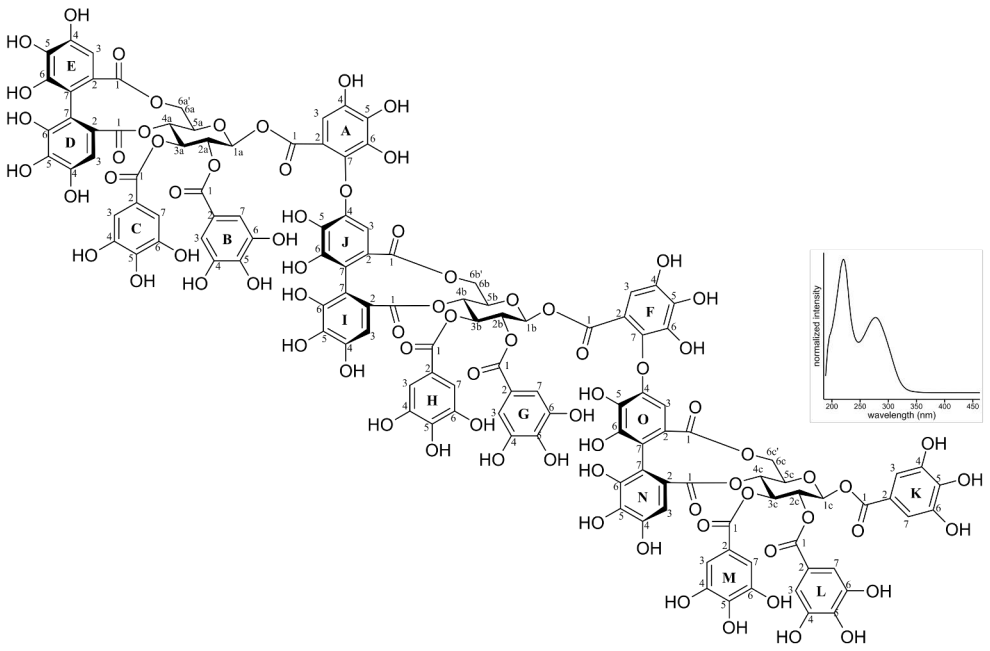

rugosin G (46) was isolated from *Filipendula ulmaria* flowers; purity measured by UPLC-DAD at 280 nm 90.3%; ESI-MS identification: *m/z* at 1873.17850 ([M–trigalloyl-HHDP-glucose–H]$^-$, error –1.9 ppm), 1721.17145 ([M–trigalloyl-HHDP-glucose–galloyl–H]$^-$, error 0.2 ppm), 1404.12780 (**[M–2H]$^{2-}$**, error –2.2 ppm), 1087.09079 ([M–trigalloyl-HHDP-glucose–digalloyl-glucose–H]$^-$, error 0.2 ppm), 937.09732 ([M–2trigalloyl-HHDP-glucose–H]$^-$, error 2.2 ppm), 935.75089 (**[M–3H]$^{3-}$**, error –0.6 ppm), 785.08538 ([M–2trigalloyl-HHDP-glucose–galloyl–H]$^-$, error 1.4 ppm), 300.99869 ([ellagic acid–H]$^-$, error –1.0 ppm); ^{1}H-NMR (600 MHz, acetone-d_6, 298 K): δ 3.71 (d, 1H, J=13.3 Hz, H_{glc}-6b'), 3.78 (d, 1H, J=13.3 Hz, H_{glc}-6c'), 3.81 (d, 1H, J=13.3 Hz, H_{glc}-6a'), 4.43 (dd, 1H, J=6.8, 10.0 Hz, H_{glc}-5b), 4.47 (dd, 1H, J=7.0, 9.7 Hz, H_{glc}-5a), 4.53 (dd, 1H, J=6.6, 10.1 Hz, H_{glc}-5c), 5.09 (t, 1H, J=10.0 Hz, H_{glc}-4b), 5.15 (t, 1H, J=9.9 Hz, H_{glc}-4a), 5.16 (t, 1H, J=10.0 Hz, H_{glc}-4c), 5.233 (dd, 1H, J=6.6, 13.5 Hz, H_{glc}-6b), 5.281 (dd, 1H, J=6.6, 13.7 Hz, H_{glc}-6c), 5.31 (dd, 1H, J=6.5, 13.4 Hz, H_{glc}-6a), 5.53 (dd, 2H, J=8.5, 9.5 Hz, H_{glc}-2a & H_{glc}-2b), 5.62 (dd, 1H, J=8.4, 9.5 Hz, H_{glc}-2c), 5.77 (t, 1H, J=9.8 Hz, H_{glc}-3b), 5.78 (t, 1H, J=9.8 Hz, H_{glc}-3a), 5.84 (t, 1H, J=9.8 Hz, H_{glc}-3c), 6.09 (d, 1H, J=8.3 Hz, H_{glc}-1b), 6.118 (d, 1H, J=8.3 Hz, H_{glc}-1a), 6.193 (d, 1H, J=8.3 Hz, H_{glc}-1c), 6.22/6.23 (s, 1H each, H_J-3 & H_O-3), 6.458 (s, 1H, H_N-3), 6.462 (s, 1H, H_I-3), 6.47 (s, 1H, H_D-3), 6.67 (s, 1H, H_E-3), 6.97/6.99/7.00 (s, 2H each, H_C-3,7 & H_H-3,7 & H_M-3,7), 7.01/7.02/7.03 (s, 2H each, H_B-3,7 & H_G-3,7 & H_L-3,7), 7.13 (s, 1H, H_A-3), 7.150 (s, 1H, H_K-3), 7.154 (s, 1H, H_F-3).[157,158]

Acknowledgements

This PhD work was conducted in the Natural Chemistry Research Group at the Department of Chemistry, University of Turku, during 2019–2023. The funding from Academy of Finland project LipidET (grant number 310549 to Maarit Karonen) and the University of Turku Graduate School: Doctoral program in Exact Sciences (previously Physical and Chemical Sciences) are greatly acknowledged for enabling me to work full time on my research.

First, I want to thank Prof. Perttu Permi and Prof. Hideyuki Ito for taking the time and reviewing my thesis and providing valuable comments. I also want to thank Dr. Ana Reis for agreeing to act as the opponent in my dissertation.

I am indebted to my supervisor Docent Maarit Karonen for offering me a place in her Academy of Finland project to pursue a doctorate. You have always been a very warm and caring person that I found very easy to approach with anything I had in mind. My work would not have been possible without the guidance and knowledge you have offered me, but you have also given me a healthy dose of scientific freedom to independently work and grow as a scientist. You have offered irreplaceable help and direction with everything related to mass spectrometry and even though my original publications do not include much in the way of mass spectrometry it has been priceless in other activities and hopefully also in the future.

Looking further back and trying to remember what exactly it was that gave the spark and pushed me to start working on a PhD project I have to also offer an immense thanks to Prof. Juha-Pekka Salminen. You have given me and so many other undergraduate students priceless opportunities with summer jobs, hourly jobs, sharing the wealth of polyphenol and analytical knowledge and many other things. These opportunities integrated me to our research group and made me all the more curious even beyond what our masters level courses could offer. I greatly appreciate your enthusiasm to inspire young students of many levels to be more interested in chemistry which is something that I'm sure will bring fruit in the years to come.

My other supervisor, Docent Petri Tähtinen, I am deeply grateful for all the NMR knowledge and help you have offered me as well as all the other fruitful discussions. Beginning from your "Spektroskopian perusteet" course and my bachelors' lab work (which you also supervised!) all the way to the NMR containing NCRG masters'

courses were what gave me a solid appreciation and understanding for NMR. My PhD work ended up containing a surprising amount of NMR spectroscopy compared to what I had envisioned at the beginning, so your teachings were all the more appreciated. Even though it was work I was doing with others, you were never too busy and always had the time to thoroughly explain anything I had to ask.

Dr. Marica Engström you have been immensely helpful starting from my masters' lab work report for which you took great care to correct and help me grow as an academic writer. You have been the academic goalpost for many of us younger NCRG scientist that we have been striving to match in many regards and I have great appreciation for your colossal work ethic.

I want to extend my thanks also to the backbone of our department, Kirsi Laaksonen, Mauri Nauma and Kari Loikas. You have all made my PhD journey much easier than it would have been without your support. Especially "Sir Loikas" I want to thank for all the IT related difficulties you have helped me with, and I wish you all the best in your recent retirement.

For my whole PhD journey and the prior undergraduate years, I have been a part of the best research group, NCRG. I have always found it easy to come to work, knowing I will have the supporting environment from our great group. The awesome people and sometimes even a little raucous sense of humor in our group is what made it so joyful and enjoyable time for me. For the current group members, thank you for every coffee break, after work activity and conference trip: Dr. Marianna Manninen, Suvi Vanhakylä, Jussi Suvanto, Juuso Laitila, Niko Luntamo, Ilari Kuukkanen, Mimosa Sillanpää and Ville Fock. Just as huge thanks to the former group members Dr. Elina Puljula, Dr. Milla Leppä, Dr. Jorma Kim, Dr Iqbal Bin Imran, and Anne Koivuniemi. Special thanks to Anne for her help in multiple aspects of my PhD work and in the time before that as well. Immense thanks to Elina for her input and expertise in the articles we are co-authoring.

When I started my university studies, I ended up performing my military service after the first semester. Luckily, when I came back, I was able to find great friends from the new student class; thank you Joona Arvola, Eerik Piirtola, Jenna Hannonen, Lassi Raivonen, Petteri Lepistö and Heidi Lepistö for the undergraduate years and everything in them.

I also want to thank all my friends outside the University for all the countless great moments in the free time whether it be skiing trips, festivals, cottage weekends or LAN parties. You have all helped me stay motivated and sane so thank you Riku Poutanen, Antti Parkkonen, Matias Liljavirta, Lauri Virtanen, Matias Lajunen, Jami Spännäri, Harto Saarinen, Sami Virta, Pietari Huuskonen, Aku Kuusisto and Santeri Salminen.

I wish to sincerely thank my parents Juha and Maria, and my sister Emma for their support and all the encouragement they have offered in everything I have done.

Finally, I wish to thank my partner Paula for everything. During all the years, I have forced you to listen to countless unfinished presentations and read through as many bungled writings. There is no telling how long my bachelor's/master's degree would have taken without the support you offered me. You have made my days so much brighter, and I am unimaginably lucky to have you by my side.

September 2023

Valtteri Virtanen

"The good thing about science is that it is true whether or not you believe in it."

-Neil deGrasse Tyson

"Until man duplicates a blade of grass, nature can laugh at his so-called scientific knowledge."

-Thomas Edison

List of References

(1) Okuda, T.; Kimura, Y.; Yoshida, T.; Hatano, T.; Okuda, H.; Arichi, S. Studies on the Activities of Tannins and Related Compounds from Medicinal Plants and Drugs. I. Inhibitory Effects on Lipid Peroxidation in Mitochondria and Microsomes of Liver. *Chem Pharm Bull (Tokyo)* **1983**, *31* (5), 1625–1631. https://doi.org/10.1248/cpb.31.1625.

(2) Hatano, T.; Edamatsu, R.; Hiramatsu, M.; Mori, A.; Fujita, Y.; Yasuhara, T.; Yoshida, T.; Okuda, T. Effects of the Interaction of Tannins with Co-Existing Substances. VI. Effects of Tannins and Related Polyphenols on Superoxide Anion Radical, and on 1,1-Diphenyl-2-Picrylhydrazyl Radical. *Chem Pharm Bull (Tokyo)* **1989**, *37* (8), 2016–2021. https://doi.org/10.1248/cpb.37.2016.

(3) Okuda, T.; Yoshida, T.; Hatano, T. Antioxidant Effects of Tannins and Related Polyphenols; 1992; pp 87–97. https://doi.org/10.1021/bk-1992-0507.ch007.

(4) Okuda, T. Structure-Activity Relationship of Antioxidant and Antitumor Polyphenols. In *Food Factors for Cancer Prevention*; Springer Japan: Tokyo, 1997; pp 280–285. https://doi.org/10.1007/978-4-431-67017-9_56.

(5) Moilanen, J.; Salminen, J.-P. Ecologically Neglected Tannins and Their Biologically Relevant Activity: Chemical Structures of Plant Ellagitannins Reveal Their in Vitro Oxidative Activity at High PH. *Chemoecology* **2008**, *18* (2), 73–83. https://doi.org/10.1007/s00049-007-0395-7.

(6) Nonaka, G.; Nishioka, I.; Nishizawa, M.; Yamagishi, T.; Kashiwada, Y.; Dutschman, G. E.; Bodner, A. J.; Kilkuskie, R. E.; Cheng, Y.-C.; Lee, K.-H. Anti-Aids Agents, 2: Inhibitory Effect of Tannins on HIV Reverse Transcriptase and HIV Replication in H9 Lymphocyte Cells. *J Nat Prod* **1990**, *53* (3), 587–595. https://doi.org/10.1021/np50069a008.

(7) Corthout, J.; Pieters, L. A.; Claeys, M.; Vanden Berghe, D. A.; Vlietinck, A. J. Antiviral Ellagitannins from Spondias Mombin. *Phytochemistry* **1991**, *30* (4), 1129–1130. https://doi.org/10.1016/S0031-9422(00)95187-2.

(8) Quideau, S.; Varadinova, T.; Karagiozova, D.; Jourdes, M.; Pardon, P.; Baudry, C.; Genova, P.; Diakov, T.; Petrova, R. Main Structural and Stereochemical Aspects of the Antiherpetic Activity of Nonahydroxyterphenoyl-Containing C-Glycosidic Ellagitannins. *Chem Biodivers* **2004**, *1* (2), 247–258. https://doi.org/10.1002/cbdv.200490021.

(9) Funatogawa, K.; Hayashi, S.; Shimomura, H.; Yoshida, T.; Hatano, T.; Ito, H.; Hirai, Y. Antibacterial Activity of Hydrolyzable Tannins Derived from Medicinal Plants against *Helicobacter Pylori*. *Microbiol Immunol* **2004**, *48* (4), 251–261. https://doi.org/10.1111/j.1348-0421.2004.tb03521.x.

(10) Saha, R. K.; Takahashi, T.; Kurebayashi, Y.; Fukushima, K.; Minami, A.; Kinbara, N.; Ichitani, M.; Sagesaka, Y. M.; Suzuki, T. Antiviral Effect of Strictinin on Influenza Virus Replication. *Antiviral Res* **2010**, *88* (1), 10–18. https://doi.org/10.1016/j.antiviral.2010.06.008.

(11) Liu, G.; Xiong, S.; Xiang, Y. F.; Guo, C. W.; Ge, F.; Yang, C. R.; Zhang, Y. J.; Wang, Y. F.; Kitazato, K. Antiviral Activity and Possible Mechanisms of Action of Pentagalloylglucose (PGG) against Influenza A Virus. *Arch Virol* **2011**, *156* (8), 1359–1369. https://doi.org/10.1007/s00705-011-0989-9.

(12) Nitta, Y.; Kikuzaki, H.; Azuma, T.; Ye, Y.; Sakaue, M.; Higuchi, Y.; Komori, H.; Ueno, H. Inhibitory Activity of *Filipendula Ulmaria* Constituents on Recombinant Human Histidine Decarboxylase. *Food Chem* **2013**, *138* (2–3), 1551–1556. https://doi.org/10.1016/j.foodchem.2012.10.074.

(13) Karonen, M.; Ahern, J. R.; Legroux, L.; Suvanto, J.; Engström, M. T.; Sinkkonen, J.; Salminen, J.-P.; Hoste, H. Ellagitannins Inhibit the Exsheathment of *Haemonchus Contortus* and *Trichostrongylus Colubriformis* Larvae: The Efficiency Increases Together with the Molecular Size. *J Agric Food Chem* **2020**, *68* (14), 4176–4186. https://doi.org/10.1021/acs.jafc.9b06774.

(14) Puljula, E.; Walton, G.; Woodward, M. J.; Karonen, M. Antimicrobial Activities of Ellagitannins against *Clostridiales Perfringens*, *Escherichia Coli*, *Lactobacillus Plantarum* and *Staphylococcus Aureus*. *Molecules* **2020**, *25* (16), 3714. https://doi.org/10.3390/molecules25163714.

(15) Aguilera-Correa, J. J.; Fernández-López, S.; Cuñas-Figueroa, I. D.; Pérez-Rial, S.; Alakomi, H.-L.; Nohynek, L.; Oksman-Caldentey, K.-M.; Salminen, J.-P.; Esteban, J.; Cuadros, J.; Puupponen-Pimiä, R.; Perez-Tanoira, R.; Kinnari, T. J. Sanguiin H-6 Fractionated from Cloudberry (*Rubus Chamaemorus*) Seeds Can Prevent the Methicillin-Resistant *Staphylococcus Aureus* Biofilm Development during Wound Infection. *Antibiotics* **2021**, *10* (12), 1481. https://doi.org/10.3390/antibiotics10121481.

(16) Nakashima, H.; Murakami, T.; Yamamoto, N.; Sakagami, H.; Tanuma, S.; Hatano, T.; Yoshida, T.; Okuda, T. Inhibition of Human Immunodeficiency Viral Replication by Tannins and Related Compounds. *Antiviral Res* **1992**, *18* (1), 91–103. https://doi.org/10.1016/0166-3542(92)90008-S.

(17) Okuda, T.; Yoshida, T.; Hatano, T. Polyphenols from Asian Plants: Structural Diversity and Antitumor and Antiviral Activities; 1992; pp 160–183. https://doi.org/10.1021/bk-1992-0507.ch013.

(18) Miyamoto, K. I.; Murayama, T.; Yoshida, T.; Hatano, T.; Okuda, T. Anticarcinogenic Activities of Polyphenols in Foods and Herbs. *ACS Symposium Series* **1997**, *662*, 245–259. https://doi.org/10.1021/bk-1997-0662.ch014.

(19) Miyamoto, K.; Nomura, M.; Sasakura, M.; Matsui, E.; Koshiura, R.; Murayama, T.; Furukawa, T.; Hatano, T.; Yoshida, T.; Okuda, T. Antitumor Activity of Oenothein B, a Unique Macrocyclic Ellagitannin. *Japanese Journal of Cancer Research* **1993**, *84* (1), 99–103. https://doi.org/10.1111/j.1349-7006.1993.tb02790.x.

(20) Yoshida, T.; Chou, T.; Matsuda, M.; Yasuhara, T.; Yazaki, K.; Hatano, T.; Nitta, A.; Okuda, T. Tannins and Related Polyphenols of *Lythraceous* Plants. Part2. Woodfordin D and Oenothein A, Trimeric Hydrolyzable Tannins of Macro-Ring Structure with Antitumor Activity. *Chem Pharm Bull (Tokyo)* **1991**, *39* (5), 1157–1162. https://doi.org/10.1248/cpb.39.1157.

(21) Thomas, M. L. R. M. G.; Filho, J. M. B. Anti-Inflammatory Actions of Tannins Isolated from the Bark of *Anacardwm Occidentale* L. *J Ethnopharmacol* **1985**, *13* (3), 289–300. https://doi.org/10.1016/0378-8741(85)90074-1.

(22) Liu, J. B.; Ding, Y. S.; Zhang, Y.; Chen, J. B.; Cui, B. S.; Bai, J. Y.; Lin, M. B.; Hou, Q.; Zhang, P. C.; Li, S. Anti-Inflammatory Hydrolyzable Tannins from *Myricaria Bracteata*. *J Nat Prod* **2015**, *78* (5), 1015–1025. https://doi.org/10.1021/np500953e.

(23) Scalbert, A. Antimicrobial Properties of Tannins. *Phytochemistry* **1991**, *30* (12), 3875–3883. https://doi.org/10.1016/0031-9422(91)83426-L.

(24) Buzzini, P.; Arapitsas, P.; Goretti, M.; Branda, E.; Turchetti, B.; Pinelli, P.; Ieri, F.; Romani, A. Antimicrobial and Antiviral Activity of Hydrolysable Tannins. *Mini-Reviews in Medicinal Chemistry* **2008**, *8* (12), 1179–1187. https://doi.org/10.2174/138955708786140990.

(25) Okuda, T.; Yoshida, T.; Hatano, T. Classification of Oligomeric Hydrolysable Tannins and Specificity of Their Occurrence in Plants. *Phytochemistry* **1993**, *32* (3), 507–521. https://doi.org/10.1016/S0031-9422(00)95129-X.

(26) Okuda, T.; Yoshida, T.; Hatano, T. Correlation of Oxidative Transformations of Hydrolyzable Tannins and Plant Evolution. *Phytochemistry* **2000**, *55* (6), 513–529. https://doi.org/10.1016/S0031-9422(00)00232-6.
(27) Moilanen, J.; Koskinen, P.; Salminen, J. P. Distribution and Content of Ellagitannins in Finnish Plant Species. *Phytochemistry* **2015**, *116* (1), 188–197. https://doi.org/10.1016/j.phytochem.2015.03.002.
(28) Quideau, S. *Chemistry and Biology of Ellagitannins: An Underestimated Class of Bioactive Plant Polyphenols*; 2009. https://doi.org/10.1142/6795.
(29) Okuda, T.; Ito, H. Tannins of Constant Structure in Medicinal and Food Plants—Hydrolyzable Tannins and Polyphenols Related to Tannins. *Molecules* **2011**, *16* (3), 2191–2217. https://doi.org/10.3390/molecules16032191.
(30) Cardona, F.; Andrés-Lacueva, C.; Tulipani, S.; Tinahones, F. J.; Queipo-Ortuño, M. I. Benefits of Polyphenols on Gut Microbiota and Implications in Human Health. *J Nutr Biochem* **2013**, *24* (8), 1415–1422. https://doi.org/10.1016/j.jnutbio.2013.05.001.
(31) Santhakumar, A. B.; Battino, M.; Alvarez-Suarez, J. M. Dietary Polyphenols: Structures, Bioavailability and Protective Effects against Atherosclerosis. *Food and Chemical Toxicology* **2018**, *113*, 49–65. https://doi.org/10.1016/j.fct.2018.01.022.
(32) Visioli, F.; Borsani, L.; Galli, C. *Diet and Prevention of Coronary Heart Disease: The Potential Role of Phytochemicals*; 2000; Vol. 47. www.elsevier.com/locate/cardioreswww.elsevier.nl/locate/cardiores.
(33) Okuda, T. Systematics and Health Effects of Chemically Distinct Tannins in Medicinal Plants. *Phytochemistry* **2005**, *66* (17), 2012–2031. https://doi.org/10.1016/j.phytochem.2005.04.023.
(34) Okuda, T.; Yoshida, T.; Hatano, T. Ellagitannins as Active Constituents of Medicinal Plants. *Planta Med* **1989**, *55* (02), 117–122. https://doi.org/10.1055/s-2006-961902.
(35) Ferguson, L. R. Role of Plant Polyphenols in Genomic Stability. *Mutation Research/Fundamental and Molecular Mechanisms of Mutagenesis* **2001**, *475* (1–2), 89–111. https://doi.org/10.1016/S0027-5107(01)00073-2.
(36) Andjelković, M.; van Camp, J.; de Meulenaer, B.; Depaemelaere, G.; Socaciu, C.; Verloo, M.; Verhe, R. Iron-Chelation Properties of Phenolic Acids Bearing Catechol and Galloyl Groups. *Food Chem* **2006**, *98* (1), 23–31. https://doi.org/10.1016/j.foodchem.2005.05.044.
(37) Wright, J. S.; Johnson, E. R.; DiLabio, G. A. Predicting the Activity of Phenolic Antioxidants: Theoretical Method, Analysis of Substituent Effects, and Application to Major Families of Antioxidants. *J Am Chem Soc* **2001**, *123* (6), 1173–1183. https://doi.org/10.1021/ja002455u.
(38) Brieger, K.; Schiavone, S.; Miller, F. J.; Krause, K. H. Reactive Oxygen Species: From Health to Disease. *Swiss Medical Weekly*. August 2012. https://doi.org/10.4414/smw.2012.13659.
(39) Panche, A. N.; Diwan, A. D.; Chandra, S. R. Flavonoids: An Overview. *J Nutr Sci* **2016**, *5*, e47. https://doi.org/10.1017/jns.2016.41.
(40) Haslam, E. Polyphenol-Protein Interactions. *Biochemical Journal* **1974**, *139* (1), 285–288. https://doi.org/10.1042/bj1390285.
(41) Okuda, T.; Mori, K.; Hatano, T. Relationship of the Structures of Tannins to the Binding Activities with Hemoglobin and Methylene Blue. *Chem Pharm Bull (Tokyo)* **1985**, *33* (4), 1424–1433. https://doi.org/10.1248/cpb.33.1424.
(42) Kawamoto, H.; Nakatsubo, F.; Murakami, K. Stoichiometric Studies of Tannin-Protein Co-Precipitation. *Phytochemistry* **1996**, *41* (5), 1427–1431. https://doi.org/10.1016/0031-9422(95)00728-8.
(43) Karonen, M.; Oraviita, M.; Mueller-Harvey, I.; Salminen, J.-P.; Green, R. J. Ellagitannins with Glucopyranose Cores Have Higher Affinities to Proteins than Acyclic Ellagitannins by Isothermal Titration Calorimetry. *J Agric Food Chem* **2019**, *67* (46), 12730–12740. https://doi.org/10.1021/acs.jafc.9b04353.
(44) Engström, M. T.; Arvola, J.; Nenonen, S.; Virtanen, V. T. J.; Leppä, M. M.; Tähtinen, P.; Salminen, J.-P. Structural Features of Hydrolyzable Tannins Determine Their Ability to Form

Insoluble Complexes with Bovine Serum Albumin. *J Agric Food Chem* **2019**, *67* (24). https://doi.org/10.1021/acs.jafc.9b02188.

(45) Le Bourvellec, C.; Renard, C. M. G. C. Interactions between Polyphenols and Macromolecules: Quantification Methods and Mechanisms. *Crit Rev Food Sci Nutr* **2012**, *52* (3), 213–248. https://doi.org/10.1080/10408398.2010.499808.

(46) Le Bourvellec, C.; Renard, C. M. G. C. Interactions between Polyphenols and Macromolecules: Effect of Tannin Structure. In *Encyclopedia of Food Chemistry*; Elsevier, 2018; pp 515–521. https://doi.org/10.1016/B978-0-08-100596-5.21486-8.

(47) Karonen, M. Insights into Polyphenol–Lipid Interactions: Chemical Methods, Molecular Aspects and Their Effects on Membrane Structures. *Plants*. MDPI July 1, 2022. https://doi.org/10.3390/plants11141809.

(48) Schmidt, O. Th.; Mayer, W. Natürliche Gerbstoffe. *Angewandte Chemie* **1956**, *68* (3), 103–115. https://doi.org/10.1002/ange.19560680305.

(49) Okuda, T.; Yoshida, T.; Nayeshiro, H. Constituents of *Geranium Thunbergii* Sieb. et Zucc. IV. Ellagitannins. 2. Structure of Geraniin. *Chem Pharm Bull (Tokyo)* **1977**, *25* (8), 1862–1869. https://doi.org/10.1248/cpb.25.1862.

(50) Matsuo, Y.; Wakamatsu, H.; Omar, M.; Tanaka, T. Reinvestigation of the Stereochemistry of the C-Glycosidic Ellagitannins, Vescalagin and Castalagin. *Org Lett* **2015**, *17* (1), 46–49. https://doi.org/10.1021/ol503212v.

(51) Yamada, H.; Wakamori, S.; Hirokane, T.; Ikeuchi, K.; Matsumoto, S. Structural Revisions in Natural Ellagitannins. *Molecules*. MDPI AG 2018. https://doi.org/10.3390/molecules23081901.

(52) Baert, N.; Karonen, M.; Salminen, J. P. Isolation, Characterisation and Quantification of the Main Oligomeric Macrocyclic Ellagitannins in *Epilobium Angustifolium* by Ultra-High Performance Chromatography with Diode Array Detection and Electrospray Tandem Mass Spectrometry. *J Chromatogr A* **2015**, *1419*, 26–36. https://doi.org/10.1016/j.chroma.2015.09.050.

(53) Salminen, J. P.; Karonen, M.; Sinkkonen, J. Chemical Ecology of Tannins: Recent Developments in Tannin Chemistry Reveal New Structures and Structure-Activity Patterns. *Chemistry - A European Journal* **2011**, *17* (10), 2806–2816. https://doi.org/10.1002/chem.201002662.

(54) Okuda, T.; Yoshida, T.; Hatano, T.; Koga, T.; Toh, N.; Kuriyama, K. Circular Dichroism of Hydrolysable Tannins-I Ellagitannins and Gallotannins. *Tetrahedron Lett* **1982**, *23* (38), 3937–3940. https://doi.org/10.1016/S0040-4039(00)87748-5.

(55) Okuda, T.; Yoshida, T.; Hatano, T.; Koga, T.; Toh, N.; Kuriyama, K. Circular Dichroism of Hydrolysable Tannins-II Dehydroellagitannins. *Tetrahedron Lett* **1982**, *23* (38), 3941–3944. https://doi.org/10.1016/S0040-4039(00)87749-7.

(56) Haslam, E. Plant Polyphenols (Syn. Vegetable Tannins) and Chemical Defense-A Reappraisal. *J Chem Ecol* **1988**, *14* (10), 1789–1805. https://doi.org/10.1007/BF01013477.

(57) Haslam, E.; Cai, Y. Plant Polyphenols (Vegetable Tannins): Gallic Acid Metabolism. *Nat Prod Rep* **1994**, *11*, 41–66. https://doi.org/10.1039/NP9941100041.

(58) Tan, H. P.; Ling, S. K.; Chuah, C. H. Characterisation of Galloylated Cyanogenic Glucosides and Hydrolysable Tannins from Leaves of *Phyllagathis Rotundifolia* by LC-ESI-MS/MS. *Phytochemical Analysis* **2011**, *22* (6), 516–525. https://doi.org/10.1002/pca.1312.

(59) Arapitsas, P. Hydrolyzable Tannin Analysis in Food. *Food Chemistry*. December 1, 2012, pp 1708–1717. https://doi.org/10.1016/j.foodchem.2012.05.096.

(60) Engström, M. T.; Pälijärvi, M.; Salminen, J. P. Rapid Fingerprint Analysis of Plant Extracts for Ellagitannins, Gallic Acid, and Quinic Acid Derivatives and Quercetin-, Kaempferol- and Myricetin-Based Flavonol Glycosides by UPLC-QqQ-MS/MS. *J Agric Food Chem* **2015**, *63* (16), 4068–4079. https://doi.org/10.1021/acs.jafc.5b00595.

(61) Niemetz, R.; Gross, G. G.; Schilling, G. Ellagitannin Biosynthesis: Oxidation of Pentagalloylglucose to Tellimagrandin II by an Enzyme from *Tellima Grandiflora* Leaves. *Chemical Communications* **2001**, No. 1, 35–36. https://doi.org/10.1039/b006270g.

(62) Niemetz, R.; Gross, G. G. Oxidation of Pentagalloylglucose to the Ellagitannin, Tellimagrandin II, by a Phenol Oxidase from *Tellima Grandiflora* Leaves. *Phytochemistry* **2003**, *62* (3), 301–306. https://doi.org/10.1016/S0031-9422(02)00557-5.

(63) Gross, G. G. Synthesis of Mono-, Di-and Trigalloyl-β-D-Glucose by β-Glucogallin-Dependent Galloyltransferases from Oak Leaves. *Zeitschrift für Naturforschung C* **1983**, *38* (7–8), 519–523. https://doi.org/10.1515/znc-1983-7-804.

(64) Quideau, S.; Feldman, K. S. Ellagitannin Chemistry. The First Synthesis of Dehydrohexahydroxydiphenoate Esters from Oxidative Coupling of Unetherified Methyl Gallate. *J Org Chem* **1997**, *62* (25), 8809–8813. https://doi.org/10.1021/jo971354k.

(65) Malik, G.; Natangelo, A.; Charris, J.; Pouységu, L.; Manfredini, S.; Cavagnat, D.; Buffeteau, T.; Deffieux, D.; Quideau, S. Synthetic Studies toward C-Glucosidic Ellagitannins: A Biomimetic Total Synthesis of 5-O-Desgalloylepipunicacortein A. *Chemistry - A European Journal* **2012**, *18* (29), 9063–9074. https://doi.org/10.1002/chem.201200517.

(66) Yamashita, T.; Matsuo, Y.; Saito, Y.; Tanaka, T. Formation of Dehydrohexahydroxydiphenoyl Esters by Oxidative Coupling of Galloyl Esters in an Aqueous Medium Involved in Ellagitannin Biosynthesis. *Chem Asian J* **2021**, *16* (13), 1735–1740. https://doi.org/10.1002/asia.202100380.

(67) Nonaka, G.; Nonaka, G.; Akazawa, M.; Nishioka, I. Two New Ellagitannin Metabolites, Carpinusin and Carpinusin from *Carpinus Laxiflora*. *Heterocycles* **1992**, *33* (2), 597. https://doi.org/10.3987/COM-91-S49.

(68) Cai, Y.; Luo, Q.; Sun, M.; Corke, H. Antioxidant Activity and Phenolic Compounds of 112 Traditional Chinese Medicinal Plants Associated with Anticancer. *Life Sci* **2004**, *74* (17), 2157–2184. https://doi.org/10.1016/j.lfs.2003.09.047.

(69) Mayer, W.; Görner, A.; Andrä, K. Punicalagin Und Punicalin, Zwei Gerbstoffe Aus Den Schalen Der Granatäpfel. *Justus Liebigs Ann Chem* **1977**, *1977* (11–12), 1976–1986. https://doi.org/10.1002/jlac.197719771119.

(70) Tanaka, T.; Nonaka, G.-I.; Nishioka, I. Tannins and Related Compounds. XL. Revision of the Structures of Punicalin and Punicalagin, and Isolation and Characterization of 2-O-Galloylpunicalin from the Bark of *Punica Granatum* L. *Chem Pharm Bull (Tokyo)* **1986**, *34* (2), 650–655. https://doi.org/10.1248/cpb.34.650.

(71) Ito, H.; Yamaguchi, K.; Kim, T. H.; Khennouf, S.; Gharzouli, K.; Yoshida, T. Dimeric and Trimeric Hydrolyzable Tannins from *Quercus Coccifera* and *Quercus Suber*. *J Nat Prod* **2002**, *65* (3), 339–345. https://doi.org/10.1021/np010465i.

(72) Karonen, M.; Oraviita, M.; Mueller-Harvey, I.; Salminen, J. P.; Green, R. J. Binding of an Oligomeric Ellagitannin Series to Bovine Serum Albumin (BSA): Analysis by Isothermal Titration Calorimetry (ITC). *J Agric Food Chem* **2015**, *63* (49), 10647–10654. https://doi.org/10.1021/acs.jafc.5b04843.

(73) Engström, M. T.; Virtanen, V.; Salminen, J. P. Influence of the Hydrolyzable Tannin Structure on the Characteristics of Insoluble Hydrolyzable Tannin-Protein Complexes. *J Agric Food Chem* **2022**. https://doi.org/10.1021/acs.jafc.2c01765.

(74) Hagerman, A. E. Tannin—Protein Interactions. **2009**, No. 4, 236–247. https://doi.org/10.1021/bk-1992-0506.ch019.

(75) Hagerman, A. E.; Riedl, K. M.; Jones, G. A.; Sovik, K. N.; Ritchard, N. T.; Hartzfeld, P. W.; Riechel, T. L. *High Molecular Weight Plant Polyphenolics (Tannins) as Biological Antioxidants*; 1998. https://pubs.acs.org/sharingguidelines.

(76) Haslam, E. Natural Polyphenols (Vegetable Tannins) as Drugs: Possible Modes of Action. *J Nat Prod* **1996**, *59* (2), 205–215. https://doi.org/10.1021/np960040+.

(77) Tanaka, T.; Zhang, H.; Jiang, Z. H.; Kouno, I. Relationship between Hydrophobicity and Structure of Hydrolyzable Tannins, and Association of Tannins with Crude Drug Constituents in Aqueous Solution. *Chem Pharm Bull (Tokyo)* **1997**, *45* (12), 1891–1897. https://doi.org/10.1248/cpb.45.1891.

(78) Verma, J.; Khedkar, V.; Coutinho, E. 3D-QSAR in Drug Design - A Review. *Curr Top Med Chem* **2010**, *10* (1), 95–115. https://doi.org/10.2174/156802610790232260.
(79) Hansch, C.; Maloney, P. P.; Fujita, T.; Muir, R. M. Correlation of Biological Activity of Phenoxyacetic Acids with Hammett Substituent Constants and Partition Coefficients. *Nature* **1962**, *194* (4824), 178–180. https://doi.org/10.1038/194178b0.
(80) Leo, A.; Hansch, C.; Elkins, D. Partition Coefficients and Their Uses. *Chem Rev* **1971**, *71* (6), 525–616. https://doi.org/10.1021/cr60274a001.
(81) *Test No. 107: Partition Coefficient (n-Octanol/Water): Shake Flask Method*; OECD, 1995. https://doi.org/10.1787/9789264069626-en.
(82) EPA. *Product Properties Test Guidelines OPPTS 830.7550 Partition Coefficient (n-Octanol/Water), Shake Flask Method*; 1996. https://www.oecd-ilibrary.org/docserver/9789264069626-en.pdf?expires=1678781481&id=id&accname=ocid195730&checksum=567358563B0BD2EE63EFD01364532474 (accessed 2023-03-14).
(83) Wang, R.; Fu, Y.; Lai, L. A New Atom-Additive Method for Calculating Partition Coefficients. *J Chem Inf Comput Sci* **1997**, *37* (3), 615–621. https://doi.org/10.1021/ci960169p.
(84) Wang, R.; Gao, Y.; Lai, L. Calculating Partition Coefficient by Atom-Additive Method. *Perspectives in Drug Discovery and Design* **2000**, *19*, 47–66. https://doi.org/DOI:10.1023/A:1008763405023.
(85) Cheng, T.; Zhao, Y.; Li, X.; Lin, F.; Xu, Y.; Zhang, X.; Li, Y.; Wang, R.; Lai, L. Computation of Octanol-Water Partition Coefficients by Guiding an Additive Model with Knowledge. *J Chem Inf Model* **2007**, *47* (6), 2140–2148. https://doi.org/10.1021/ci700257y.
(86) Ghose, A. K.; Crippen, G. M. Atomic Physicochemical Parameters for Three-Dimensional Structure-Directed Quantitative Structure-Activity Relationships I. Partition Coefficients as a Measure of Hydrophobicity. *J Comput Chem* **1986**, *7* (4), 565–577. https://doi.org/10.1002/jcc.540070419.
(87) Chou, J. T.; Jurs, P. C. Computer-Assisted Computation of Partition Coefficients from Molecular Structures Using Fragment Constants. *J Chem Inf Comput Sci* **1979**, *19* (3), 172–178. https://doi.org/10.1021/ci60019a013.
(88) Meylan, W. M.; Howard, P. H. Atom/Fragment Contribution Method for Estimating Octanol–Water Partition Coefficients. *J Pharm Sci* **1995**, *84* (1), 83–92. https://doi.org/10.1002/jps.2600840120.
(89) Meylan, W. M.; Howard, P. H. Estimating Log P with Atom/Fragments and Water Solubility with Log P. *Perspectives in Drug Discovery and Design* **2000**, *19*, 67–84. https://doi.org/10.1023/A:1008715521862.
(90) Cumming, H.; Rücker, C. Octanol–Water Partition Coefficient Measurement by a Simple ^{1}H NMR Method. *ACS Omega* **2017**, *2* (9), 6244–6249. https://doi.org/10.1021/acsomega.7b01102.
(91) Nakayama, T.; Kajiya, K.; Kumazawa, S. Chapter 4: Interaction of Plant Polyphenols with Liposomes. *Advances in Planar Lipid Bilayers and Liposomes*. 2006, pp 107–133. https://doi.org/10.1016/S1554-4516(06)04004-X.
(92) Conradi, R. A.; Burton, P. S.; Borchardt, R. T. Physico-Chemical and Biological Factors That Influence a Drug's Cellular Permeability by Passive Diffusion. *Lipophilicity in Drug Action and Toxicology* **1996**, *4*, 233–252. https://doi.org/10.1002/9783527614998.ch14.
(93) Artursson, P.; Magnusson, C. Epithelial Transport of Drugs in Cell Culture. II: Effect of Extracellular Calcium Concentration on the Paracellular Transport of Drugs of Different Lipophilicities across Monolayers of Intestinal Epithelial (Caco-2) Cells. *J Pharm Sci* **1990**, *79* (7), 595–600. https://doi.org/10.1002/jps.2600790710.
(94) Caturla, N.; Vera-Samper, E.; Villalaín, J.; Mateo, C. R.; Micol, V. The Relationship between the Antioxidant and the Antibacterial Properties of Galloylated Catechins and the Structure of Phospholipid Model Membranes. *Free Radic Biol Med* **2003**, *34* (6), 648–662. https://doi.org/10.1016/S0891-5849(02)01366-7.

(95) Okuda, T.; Yoshida, T.; Hatano, T. Pharmacologically Active Tannins Isolated from Medicinal Plants. In *Plant Polyphenols*; Springer US: Boston, MA, 1992; pp 539–569. https://doi.org/10.1007/978-1-4615-3476-1_31.

(96) Takechi, M.; Tanaka, Y.; Takehara, M.; Nonaka, G.-I.; Nishioka, I. Structure and Antiherpetic Activity among the Tannins. *Phytochemistry* **1985**, *24* (10), 2245–2250. https://doi.org/10.1016/S0031-9422(00)83018-6.

(97) Fukuchi, K.; Sakagami, H.; Okuda, T.; Hatano, T.; Tanuma, S.; Kitajima, K.; Inoue, Y.; Inoue, S.; Ichikawa, S.; Nonoyama, M.; Konno, K. Inhibition of Herpes Simplex Virus Infection by Tannins and Related Compounds. *Antiviral Res* **1989**, *11* (5–6), 285–297. https://doi.org/10.1016/0166-3542(89)90038-7.

(98) Xie, L.; Xie, J.-X.; Kashiwada, Y.; Cosentino, L. M.; Liu, S.-H.; Pai, R. B.; Cheng, Y.-C.; Lee, K.-H. Anti-AIDS (Acquired Immune Deficiency Syndrome) Agents. 17. New Brominated Hexahydroxybiphenyl Derivatives as Potent Anti-HIV Agents. *J Med Chem* **1995**, *38* (16), 3003–3008. https://doi.org/10.1021/jm00016a002.

(99) Hatano, T.; Kusuda, M.; Inada, K.; Ogawa, T. O.; Shiota, S.; Tsuchiya, T.; Yoshida, T. Effects of Tannins and Related Polyphenols on Methicillin-Resistant *Staphylococcus Aureus*. In *Phytochemistry*; Elsevier Ltd, 2005; Vol. 66, pp 2047–2055. https://doi.org/10.1016/j.phytochem.2005.01.013.

(100) Machado, T. B.; Pinto, A. V.; Pinto, M. C. F. R.; Leal, I. C. R.; Silva, M. G.; Amaral, A. C. F.; Kuster, R. M.; Netto-dosSantos, K. R. In Vitro Activity of Brazilian Medicinal Plants, Naturally Occurring Naphthoquinones and Their Analogues, against Methicillin-Resistant *Staphylococcus Aureus*. *Int J Antimicrob Agents* **2003**, *21* (3), 279–284. https://doi.org/10.1016/S0924-8579(02)00349-7.

(101) Ranilla, L. G.; Apostolidis, E.; Shetty, K. Antimicrobial Activity of an Amazon Medicinal Plant (Chancapiedra) (*Phyllanthus Niruri* L.) against *Helicobacter Pylori* and Lactic Acid Bacteria. *Phytotherapy Research* **2012**, *26* (6), 791–799. https://doi.org/10.1002/ptr.3646.

(102) Liu, X. L.; Hao, Y. Q.; Jin, L.; Xu, Z. J.; McAllister, T. A.; Wang, Y. Anti-*Escherichia Coli* O157:H7 Properties of Purple Prairie Clover and Sainfoin Condensed Tannins. *Molecules* **2013**, *18* (2), 2183–2199. https://doi.org/10.3390/molecules18022183.

(103) Masota, N. E.; Ohlsen, K.; Schollmayer, C.; Meinel, L.; Holzgrabe, U. Isolation and Characterization of Galloylglucoses Effective against Multidrug-Resistant Strains of Escherichia Coli and Klebsiella Pneumoniae. *Molecules* **2022**, *27* (15). https://doi.org/10.3390/molecules27155045.

(104) Shiota, S.; Shimizu, M.; Mizushima, T.; Ito, H.; Hatano, T.; Yoshida, T.; Tsuchiya, T. Marked Reduction in the Minimum Inhibitory Concentration (MIC) of β-Lactams in Methicillin-Resistant *Staphylococcus Aureus* Produced by Epicatechin Gallate, an Ingredient of Green Tea (*Camellia Sinensis*). *Biol Pharm Bull* **1999**, *22* (12), 1388–1390. https://doi.org/10.1248/bpb.22.1388.

(105) Shimizu, M.; Shiota, S.; Mizushima, T.; Ito, H.; Hatano, T.; Yoshida, T.; Tsuchiya, T. Marked Potentiation of Activity of β-Lactams against Methicillin-Resistant *Staphylococcus Aureus* by Corilagin. *Antimicrob Agents Chemother* **2001**, *45* (11), 3198–3201. https://doi.org/10.1128/AAC.45.11.3198-3201.2001.

(106) Olchowik-Grabarek, E.; Sekowski, S.; Bitiucki, M.; Dobrzynska, I.; Shlyonsky, V.; Ionov, M.; Burzynski, P.; Roszkowska, A.; Swiecicka, I.; Abdulladjanova, N.; Zamaraeva, M. Inhibition of Interaction between *Staphylococcus Aureus* α-Hemolysin and Erythrocytes Membrane by Hydrolysable Tannins: Structure-Related Activity Study. *Sci Rep* **2020**, *10* (1). https://doi.org/10.1038/s41598-020-68030-1.

(107) Olchowik-Grabarek, E.; Sękowski, S.; Kwiatek, A.; Płaczkiewicz, J.; Abdulladjanova, N.; Shlyonsky, V.; Swiecicka, I.; Zamaraeva, M. The Structural Changes in the Membranes of *Staphylococcus Aureus* Caused by Hydrolysable Tannins Witness Their Antibacterial Activity. *Membranes (Basel)* **2022**, *12* (11). https://doi.org/10.3390/membranes12111124.

(108) Engström, M. T.; Pälijärvi, M.; Fryganas, C.; Grabber, J. H.; Mueller-Harvey, I.; Salminen, J. P. Rapid Qualitative and Quantitative Analyses of Proanthocyanidin Oligomers and Polymers by UPLC-MS/MS. *J Agric Food Chem* **2014**, *62* (15), 3390–3399. https://doi.org/10.1021/jf500745y.
(109) Grélard, A.; Loudet, C.; Diller, A.; Dufourc, E. J. NMR Spectroscopy of Lipid Bilayers. *Methods Mol Biol* **2010**, *654* (1), 341–359. https://doi.org/10.1007/978-1-60761-762-4_18.
(110) Salminen, J. P.; Ossipov, V.; Loponen, J.; Haukioja, E.; Pihlaja, K. Characterisation of Hydrolysable Tannins from Leaves of *Betula Pubescens* by High-Performance Liquid Chromatography-Mass Spectrometry. *J Chromatogr A* **1999**, *864* (2), 283–291. https://doi.org/10.1016/S0021-9673(99)01036-5.
(111) Salminen, J.-P.; Ossipov, V.; Haukioja, E.; Pihlaja, K. Seasonal Variation in the Content of Hydrolysable Tannins in Leaves of *Betula Pubescens*. *Phytochemistry* **2001**, *57* (1), 15–22. https://doi.org/10.1016/S0031-9422(00)00502-1.
(112) Salminen, J. P.; Karonen, M. Chemical Ecology of Tannins and Other Phenolics: We Need a Change in Approach. *Funct Ecol* **2011**, *25* (2), 325–338. https://doi.org/10.1111/j.1365-2435.2010.01826.x.
(113) R Core Team (2022). *R: A language and environment for statistical computing.* R Foundation for Statistical Computing, Vienna, Austria. https://www.R-project.org/.
(114) Allaire, J. J. *RStudio: Integrated Development Environment for R*. https://www.rstudio.org/.
(115) Wickham, H. *Ggplot2: Elegant Graphics for Data Analysis*; Springer-Verlag: New York, 2009.
(116) Kassambara A (2022). *ggpubr: "ggplot2" Based Publication Ready Plots. R package version 0.5.0*. https://CRAN.R-project.org/package=ggpubr.
(117) Kucheryavskiy, S. Mdatools – R Package for Chemometrics. *Chemometrics and Intelligent Laboratory Systems* **2020**, *198*, 103937. https://doi.org/10.1016/j.chemolab.2020.103937.
(118) Community, B. O. Blender - a 3D Modelling and Rendering Package. Stichting Blender Foundation, Amsterdam 2018. http://www.blender.org.
(119) Jacob, D.; Deborde, C.; Lefebvre, M.; Maucourt, M.; Moing, A. NMRProcFlow: A Graphical and Interactive Tool Dedicated to 1D Spectra Processing for NMR-Based Metabolomics. *Metabolomics* **2017**, *13* (4), 36. https://doi.org/10.1007/s11306-017-1178-y.
(120) Spencer, C. M.; Cai, Y.; Martin, R.; Lilley, T. H.; Haslam, E. The Metabolism of Gallic Acid and Hexahydroxydiophenic Acid in Higher Plants Part 4; Polyphenol Interactions Part 3. Spectroscopic and Physical Properties of Esters of Gallic Acid and (S)-Hexahydroxydiphenic Acid with D-Glucopyranose (4 C 1). *Journal of the Chemical Society, Perkin Transactions 2* **1990**, No. 4, 651. https://doi.org/10.1039/p29900000651.
(121) Scheidt, H. A.; Pampel, A.; Nissler, L.; Gebhardt, R.; Huster, D. Investigation of the Membrane Localization and Distribution of Flavonoids by High-Resolution Magic Angle Spinning NMR Spectroscopy. *Biochimica et Biophysica Acta (BBA) - Biomembranes* **2004**, *1663* (1–2), 97–107. https://doi.org/10.1016/j.bbamem.2004.02.004.
(122) Scheidt, H. A.; Huster, D. The Interaction of Small Molecules with Phospholipid Membranes Studied by ^{1}H NOESY NMR under Magic-Angle Spinning. *Acta Pharmacol Sin* **2008**, *29* (1), 35–49. https://doi.org/10.1111/j.1745-7254.2008.00726.x.
(123) Frazier, R. A.; Papadopoulou, A.; Mueller-Harvey, I.; Kissoon, D.; Green, R. J. Probing Protein-Tannin Interactions by Isothermal Titration Microcalorimetry. *J Agric Food Chem* **2003**, *51* (18), 5189–5195. https://doi.org/10.1021/jf021179v.
(124) Charlton, A. J.; Baxter, N. J.; Khan, M. L.; Moir, A. J. G.; Haslam, E.; Davies, A. P.; Williamson, M. P. Polyphenol/Peptide Binding and Precipitation. *J Agric Food Chem* **2002**, *50* (6), 1593–1601. https://doi.org/10.1021/jf010897z.
(125) Espín, J. C.; González-Barrio, R.; Cerdá, B.; López-Bote, C.; Rey, A. I.; Tomás-Barberán, F. A. Iberian Pig as a Model to Clarify Obscure Points in the Bioavailability and Metabolism of Ellagitannins in Humans. *J Agric Food Chem* **2007**, *55* (25), 10476–10485. https://doi.org/10.1021/jf0723864.

(126) Barbehenn, R. V.; Jones, C. P.; Hagerman, A. E.; Karonen, M.; Salminen, J. P. Ellagitannins Have Greater Oxidative Activities than Condensed Tannins and Galloyl Glucoses at High PH: Potential Impact on Caterpillars. *J Chem Ecol* **2006**, *32* (10), 2253–2267. https://doi.org/10.1007/s10886-006-9143-7.
(127) Okuda, T.; Yoshida, T.; Hatano, T.; Ito, H. Ellagitannins Renewed the Concept of Tannins. In *Chemistry and Biology of Ellagitannins*; WORLD SCIENTIFIC, 2009; pp 1–54. https://doi.org/10.1142/9789812797414_0001.
(128) Yasid, N. A.; Rolfe, M. D.; Green, J.; Williamson, M. P. Homeostasis of Metabolites in *Escherichia Coli* on Transition from Anaerobic to Aerobic Conditions and the Transient Secretion of Pyruvate. *R Soc Open Sci* **2016**, *3* (8). https://doi.org/10.1098/rsos.160187.
(129) Kim, H. G.; Kim, K. S.; Kim, M.; Shin, S. H.; Lee, Y. G.; Bang, M. H.; Lee, D. G.; Baek, N. I. β-Glucogallin Isolated from *Fusidium Coccineum* and Its Enhancement of Skin Barrier Effects. *Appl Biol Chem* **2020**, *63* (1). https://doi.org/10.1186/s13765-020-00563-5.
(130) Haddock, E. A.; Gupta, R. K.; Al-Shafi, S. M. K.; Haslam, E.; Magnolato, D. The Metabolism of Gallic Acid and Hexahydroxydiphenic Acid in Plants. Part 1. Introduction. Naturally Occurring Galloyl Esters. *J Chem Soc Perkin 1* **1982**, 2515–2524. https://doi.org/10.1039/P19820002515.
(131) Tanaka, T.; Nonaka, G.-I.; Nishioka, I. Punicafolin, an Ellagitannin from the Leaves of *Punica Granatum*. *Phytochemistry* **1985**, *24* (9), 2075–2078. https://doi.org/10.1016/S0031-9422(00)83125-8.
(132) Hatano, T.; Yoshida, T.; Shingu, T.; Okuda, T. ^{13}C Nuclear Magnetic Resonance Spectra of Hydrolyzable Tannins. III. Tannins Having $^{1}C_4$ Glucose and C-Glucosidic Linkage. *Chem Pharm Bull (Tokyo)* **1988**, *36* (10), 3849–3856. https://doi.org/10.1248/cpb.36.3849.
(133) Okuda, T.; Yoshida, T.; Hatano, T.; Yazaki, K.; Ashida, M. Ellagitannins of the *Casuarinaceae*, *Stachyuraceae* and *Myrtaceae*. *Phytochemistry* **1980**, *21* (12), 2871–2874. https://doi.org/10.1016/0031-9422(80)85058-8.
(134) Okuda, T.; Yoshida, T.; Ashida, M.; Yazaki, K. Casuariin, Stachyurin and Strictinin, New Ellagitannins from *Casuarina Stricta* and *Stachyurus Praecox*. *Chemical Pharmaceutical Bulletin* **1982**, *30* (2), 766–769.
(135) Okuda, T.; Yoshida, T.; Ashida, M.; Yazaki, K. Tannis of *Casuarina* and *Stachyurus* Species. Part 1. Structures of Pendunculagin, Casuarictin, Strictinin, Casuarinin, Casuariin, and Stachyurin. *J Chem Soc Perkin 1* **1983**, 1765. https://doi.org/10.1039/p19830001765.
(136) Nonaka, G. ichiro; Nishioka, I.; Nagasawa, T.; Oura, H. Tannins and Related Compounds. I.1) Rhubarb (1). *Chem Pharm Bull (Tokyo)* **1981**, *29* (10), 2862–2870. https://doi.org/10.1248/cpb.29.2862.
(137) Pfundstein, B.; El Desouky, S. K.; Hull, W. E.; Haubner, R.; Erben, G.; Owen, R. W. Polyphenolic Compounds in the Fruits of Egyptian Medicinal Plants (*Terminalia Bellerica*, *Terminalia Chebula* and *Terminalia Horrida*): Characterization, Quantitation and Determination of Antioxidant Capacities. *Phytochemistry* **2010**, *71* (10), 1132–1148. https://doi.org/10.1016/j.phytochem.2010.03.018.
(138) Tanaka, T.; Tachibana, H.; Nonaka, G.; Nishioka, I.; Hsu, F.-L.; Kohda, H.; Tanaka, O. Tannins and Related Compounds. CXXII. New Dimeric, Trimeric and Tetrameric Ellagitannins, Lambertianins A-D, from *Rubus Lambertianus* SERINGE. *Chem Pharm Bull (Tokyo)* **1993**, *41* (7), 1214–1220. https://doi.org/10.1248/cpb.41.1214.
(139) Tsujita, T.; Matsuo, Y.; Saito, Y.; Tanaka, T. Enzymatic Oxidation of Ellagitannin and a New Ellagitannin Metabolite from *Camellia Japonica* Leaves. *Tetrahedron* **2017**, *73* (5), 500–507. https://doi.org/10.1016/j.tet.2016.12.027.
(140) Wilkins, C. K.; Bohm, B. A. Ellagitannins from *Tellima Grandiflora*. *Phytochemistry* **1976**, *15* (1), 211–214. https://doi.org/10.1016/S0031-9422(00)89087-1.

(141) Tuominen, A.; Toivonen, E.; Mutikainen, P.; Salminen, J. P. Defensive Strategies in *Geranium Sylvaticum*. Part 1: Organ-Specific Distribution of Water-Soluble Tannins, Flavonoids and Phenolic Acids. *Phytochemistry* **2013**, *95*, 394–407. https://doi.org/10.1016/j.phytochem.2013.05.013.

(142) Nishizawa, M.; Yamagishi, T.; Nonaka, G.; Nishioka, I. Tannins and Related Compounds. Part 9. Isolation and Characterization of Polygalloylglucoses from Turkish Galls (*Quercus Infectoria*). *J Chem Soc Perkin 1* **1983**, *2* (9), 961. https://doi.org/10.1039/p19830000961.

(143) Mayer, W.; Gabler, W.; Riester, A.; Korger, H. Über Die Gerbstoffe Aus Dem Holz Der Edelkastanie Und Der Eiche, II. Die Isolierung von Castalagin, Vescalagin, Castalin Und Vescalin. *Justus Liebigs Ann Chem* **1967**, *707* (1), 177–181. https://doi.org/10.1002/jlac.19677070125.

(144) Yoshida, T.; Namba, O.; Lu, C.-F.; Yang, L.-L.; Yen, K.-Y.; Okuda, T. Tannins of Euphorbiaceous Plants. X. Antidesmin A, a New Dimeric Hydrolyzable Tannin from *Antidesma Pentandrum* Var. *Barbatum*. *Chem Pharm Bull (Tokyo)* **1992**, *40* (2), 338–342. https://doi.org/10.1248/cpb.40.338.

(145) Yoshida, T.; Fujii, R.; Okuda, T. Revised Structures of Chebulinic Acid and Chebulagic Acid. *Chem Pharm Bull (Tokyo)* **1980**, *28* (12), 3713–3715. https://doi.org/10.1248/cpb.28.3713.

(146) Klika, K. D.; Saleem, A.; Sinkkonen, J.; Kähkönen, M.; Loponen, J.; Tähtinen, P.; Pihlaja, K. The Structural and Conformational Analyses and Antioxidant Activities of Chebulinic Acid and Its Thrice-Hydrolyzed Derivative, 2,4-Chebuloyl-β-D-Glucopyranoside, Isolated from the Fruit of *Terminalia Chebula*. *Arkivoc* **2004**, *2004* (7), 83–105. https://doi.org/10.3998/ark.5550190.0005.708.

(147) Nonaka, G. I.; Ishimaru, K.; Azuma, R.; Nishioka, I. Tannins and Related Compounds. LXXXV. Structures of Novel C-Glycosidic Ellagitannins, Grandinin and Pterocarinins A and B. *Chemical Pharmaceutical Bulletin* **1989**, *37* (8), 2071–2077.

(148) Hervé Du Penhoat, C. L. M. Michon, V. M. F.; Peng, S.; Viriot, C.; Scalbert, A.; Gage, D. Structural Elucidation of New Dimeric Ellagitannins from *Quercus Robur* L. Roburins A-E. *J Chem Soc Perkin 1* **1991**, *53* (9), 1689–1699. https://doi.org/10.1039/P19910001653.

(149) Kraszni, M.; Marosi, A.; Larive, C. K. NMR Assignments and the Acid-Base Characterization of the Pomegranate Ellagitannin Punicalagin in the Acidic PH-Range. *Anal Bioanal Chem* **2013**, *405* (17), 5807–5816. https://doi.org/10.1007/s00216-013-6987-x.

(150) Nishizawa, M.; Yamagishi, T.; Nonaka, G.; Nishioka, I. Tannins and Related Compounds. Part 5. Isolation and Characterization of Polygalloylglucoses from Chinese Gallotannin. *J Chem Soc Perkin 1* **1982**, 2963. https://doi.org/10.1039/p19820002963.

(151) Mayer, W.; Bilzer, W.; Schilling, G. Über Valoneagerbstoffe, II. Castavaloninsäure, Isolierung Und Strukturermittlung. *Justus Liebigs Ann Chem* **1976**, *1976* (5), 876–881. https://doi.org/10.1002/jlac.197619760510.

(152) Yoshida, T.; Tanaka, K.; Chen, X.-M.; Okuda, T. Tannins from *Hippophae Rhamnoides*. *Phytochemistry* **1991**, *30* (2), 663–666. https://doi.org/10.1016/0031-9422(91)83748-A.

(153) Ito, H.; Miki, K.; Yoshida, T. Elaeagnatins A-G, C-Glucosidic Ellagitannins from *Elaeagnus Umbellata*. *Chem Pharm Bull (Tokyo)* **1999**, *47* (4), 536–542. https://doi.org/10.1248/cpb.47.536.

(154) Suvanto, J.; Tähtinen, P.; Valkamaa, S.; Engström, M. T.; Karonen, M.; Salminen, J. P. Variability in Foliar Ellagitannins of *Hippophaë Rhamnoides* L. and Identification of a New Ellagitannin, Hippophaenin C. *J Agric Food Chem* **2018**, *66* (3), 613–620. https://doi.org/10.1021/acs.jafc.7b04834.

(155) Hatano, T.; Yasuhara, T.; Matsuda, M.; Yazaki, K.; Yoshida, T.; Okuda, T. Oenothein B, a Dimeric, Hydrolysable Tannin with Macrocyclic Structure, and Accompanying Tannins from *Oenothera Erythrosepala*. *J Chem Soc Perkin 1* **1990**, No. 10, 2735. https://doi.org/10.1039/p19900002735.

(156) Yoshida, T.; Feng, W.-S.; Okuda, T. Tannins and Related Polyphenols of Rosaceous Medicinal Plants. XII. Roshenins A-E, Dimeric Hydrolyzable Tannins from *Rosa Henryi* Boul. *Chem Pharm Bull (Tokyo)* **1992**, *40* (8), 1997–2001. https://doi.org/10.1248/cpb.40.1997.
(157) Okuda, T.; Hatano, T.; Ogawa, N. Rugosin D, E, F and G, Dimeric and Trimeric Hydrolyzable Tannins. *Chemical Pharmaceutical Bulletin* **1982**, *30* (11), 4234–4237.
(158) Hatano, T.; Ogawa, N.; Shingu, T.; Okuda, T. Tannins of *Rosaceous* Plants. IX. Rugosins D, E, F and G, Dimeric and Trimeric Hydrolyzable Tannins with Valoneoyl Group(s), from Flower Petals of *Rosa Rugosa* Thunb. *Chem Pharm Bull (Tokyo)* **1990**, *38* (12), 3341–3346. https://doi.org/10.1248/cpb.38.3341.
(159) Piwowarski, J. P.; Kiss, A. K. *C* -Glucosidic Ellagitannins from Lythri Herba (*European Pharmacopoeia*): Chromatographic Profile and Structure Determination. *Phytochemical Analysis* **2013**, *24* (4), 336–348. https://doi.org/10.1002/pca.2415.
(160) Okuda, T.; Yoshida, T.; Kuwahara, M.; Memon, M. U.; Shingu, T. Tannins of *Rosaceous* Medicinal Plants. I. Structures of Potentillin, Agrimonic Acids A and B, and Agrimoniin, a Dimeric Ellagitannin. *Chem Pharm Bull (Tokyo)* **1984**, *32* (6), 2165–2173. https://doi.org/10.1248/cpb.32.2165.
(161) Yoshida, T.; Okuda, T.; Memon, M. U.; Shingu, T. Tannins of *Rosaceous* Medicinal Plants. Part 2. Gemins A, B, and C, New Dimeric Ellagitannins from *Geum Japonicum*. *J Chem Soc Perkin 1* **1985**, 315. https://doi.org/10.1039/p19850000315.

TURUN
YLIOPISTO
UNIVERSITY
OF TURKU

Painosalama Oy, Turku, Finland 2023

ISBN 978-951-29-9430-4 (Print)
ISBN 978-951-29-9431-1 (PDF)
ISSN 0082-7002 (Print)
ISSN 2343-3175 (Online)